STUDIES ON OXIDATIVE DEHYDROGENATION OF n-BUTANE ON MUTH MOLYBDATE-ALUMINIUM PHOSPHATE CATALYSTS

A Thesis Submitted
In Partial Fulfilment of the Requirements
for the Degree of

DOCTOR OF PHILOSOPHY

by

SUBHASH CHANDRA SHENOY

to the

DEPARTMENT OF CHEMICAL ENGINEERING
INDIAN INSTITUTE OF TECHNOLOGY KANPUR

OCTOBER, 1978

BL.

CERTIFICATE

This is to certify that the present work "Studies on Oxidative Dehydrogenation of n-Butane on Bismuth Molybdate-Aluminium Phosphate Catalysts" has been carried out under my supervision and that the work has not been submitted elsewhere for a degree.

M. Someswara Rao

Date: October, 1978.

(Dr.) M. Someswara Rao
Assistant Professor
Department of Chemical Engineering
Indian Institute of Technology
Kanpur 208016, India

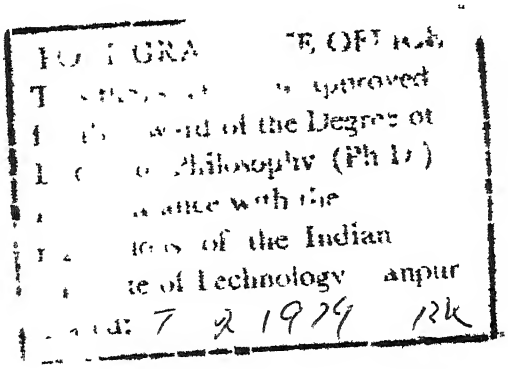

ACKNOWLEDGEMENTS

The author wishes to express his deep sense of gratitude and indebtedness to Dr. M.S. Rao for his able guidance and constant encouragement throughout the course of the work.

The author is grateful to Dr. H. Veeramani for his encouragement and timely help during the course of the work.

The author is grateful to Professor K.V.G.K. Gokhale for his stimulating discussion and critical comments on the work. He is also thankful to Professor Gokhale for reviewing a section of the manuscript.

Dr. G.C. Baral has been a constant source of inspiration and help from the inception of the project. The author is grateful to his friend Dr.R. Sharma for various suggestions and discussion in the early stages of the work. The author is also thankful to Dr. P.K. Bajpai for the help received in recording X-ray diffraction patterns and infrared spectra.

The author is thankful to Mr. Santokh Singh of the Department of Mathematics and Statistics. Discussion on the analysis of response surfaces have been very beneficial.

Messrs A.K. Nayak, Umashankar and S. Bhattacharya have been kind and helpful in the various stages of the work. The author is grateful to all of them.

The author is thankful to Mr. R.N. Srivastava of textbook cell for his excellent typing and Mr. D.S. Panesar for his patience in tracings.

Finally, Senior Research Fellowship awarded to the author by the Council of Scientific and Industrial Research is also acknowledged.

S.C. Shenoy

CONTENTS

CHAPTER

CHAPTER

LIST OF TABLES

LIST OF FIGURES

NOMENCLATURE

a	..	Order of reaction with respect to butane (Chapter 6)
b	..	Order of reaction with respect to butene (Chapter 6)
b_j	..	Regression coefficient of j-th factor (Chapter 5)
b_{ij}	..	Coefficient representing the interaction effect of i-th factor with j-th factor (Chapter 5)
d	..	Interplanar spacing, Å
F	..	Fisher F ratio
hkl	..	Miller indices used in X-ray diffraction
I	..	Relative intensity
k	..	Total number of factors (Chapter 5)
k'	..	Parameter in point selectivity equation (Chapter 6)
K_A, K_B, K_C, K_O, K_W	..	Adsorption constants for butane, butene, butadiene, oxygen and water respectively; bar^{-1}
m	..	Number of responses considered in the regression analysis
n	..	Number of repeated observations (Chapter 5)
n	..	Number of responses in the system of ordinary differential equations describing the model (Chapter 6)
N	..	Total number of experiments (Chapter 5)
p	..	Number of parameters to be estimated (Chapter 5)
p,q	..	Order of reaction with respect to oxygen
p_A, p_B, p_C, p_O, p_W	..	Partial pressures of butane, butene, butadiene, oxygen and water respectively, bar

P	..	Number of parameters to be estimated (Chapter 6)
r_A, r_B, r_C, r_O, r_W	..	Rate of reactions of butane, butene, butadiene, oxygen and water respectively, mol/g(mol/sec)
r_{ox}	..	Rate of oxidation of the catalyst
R	..	Multiple correlation coefficient
s^2_{ad}	..	Variance of adequacy of the model
s^2_y	..	Variance of the optimisation parameter
S	..	Adsorption site
t	..	Time or catalyst to feed ratio, g/(mg mol/sec)
"t"	..	"Student's t" value
u	..	Number of parameters to be estimated(Chapter 6)
u_j	..	Unit vectors in the coordinate directions (Chapter 5)
$\underline{U}$	..	Matrix of eigenvectors (unitary matrix)
v_j	..	Variation interval of j-th factor
x_j	..	Coded value of j-th factor
$\tilde{x}_j$	..	Natural value of the j-th factor
$\tilde{x}_{jo}$	..	Base level of the j-th factor
x'	..	Coordinates of the response surface translated to its 'optimum' point
X	..	Coordinates of the principal axis of the saddle surface
y	..	Response, mol (butenes + butadiene) formed per 100 mol butane fed
$\bar{y}$	..	Average value of y
$\hat{y}$	..	Predicted value of y

Greek Symbols

α	..	Significance level
Δb_j	..	Confidence interval of b_j (Chapter 5)
θ	..	Fraction of catalyst surface not covered by reactants
ϕ	..	Response function
λ	..	Eigenvalues (Chapter 5)
$\underline{A}$	..	Derivative matrix
σ^2	..	Variance

Subscripts

e	..	Extremum
j	..	j-th factor
u	..	u-th trial (Chapter 5)
o	..	Base level
-	..	Notation for matrix

Superscripts

$\wedge$	..	Predicted value
-	..	Average value
T	..	Transpose of the matrix
$\sim$	..	Natural values.

STUDIES ON OXIDATIVE DEHYDROGENATION OF n-BUTANE ON BISMUTH MOLYBDATE-ALUMINIUM PHOSPHATE CATALYSTS

A Thesis Submitted
In Partial Fulfilment of the Requirements
For the Degree of
DOCTOR OF PHILOSOPHY
by
SUBHASH CHANDRA SHENOY
to the
Department of Chemical Engineering
Indian Institute of Technology, Kanpur
October, 1978

SYNOPSIS

Olefins and diolefins are important intermediates in the petrochemical industry, and the future promises further substantial increases in demand. Bismuth molybdate and tin antimonate catalysts are very versatile and are effective in several different processes such as oxidative dehydrogenation of butenes to butadiene, oxidation of propylene to acrolein, ammonoxidation of propylene to acrylonitrile etc.

Several catalysts have been formulated for the abstraction of allylic hydrogen from butenes or propylene. These catalysts, however, are inefficient in the abstraction of first hydrogen from a saturated hydrocarbon molecule like n-butane. Abstraction of first hydrogen atom from n-butane molecule involves the rupture of a strong σ bond between the hydrogen and the carbon atoms. The hydrocarbon molecule thus has a tendency to burn off completely rather than dehydrogenate to yield butenes and butadiene.

The aim of the present work has been to develop a suitable catalyst for the oxidative dehydrogenation of n-butane to butenes and 1, 3-butadiene. Preliminary experiments were carried out on a molybdic oxide-aluminium phosphate catalyst to investigate the feasibility of oxidative dehydrogenation of butane. Experiments were performed at different conditions of temperature, contact time, and catalyst composition. The catalyst showed some activity for the oxidative dehydrogenation of n-butane.

In order to improve the activity of the molybdic oxide-aluminium phosphate catalyst, bismuth was introduced in the catalyst, and the catalyst activity was investigated further. Three types of aluminium phosphate-bismuth molybdate catalysts were chosen, namely,

1. $Bi_2O_3.3MoO_3$ (α-phase) + $AlPO_4$
2. $Bi_2O_3.2MoO_3$ (β-phase or Erman phase) + $AlPO_4$
3. $Bi_2O_3.MoO_3$ (γ-phase or koechlinite) + $AlPO_4$

These catalysts were characterised in terms of chemical compositions, surface areas, characteristic X-ray diffraction reflections, infrared spectra and thermal stabilities (DTA, TGA and DTGA). X-Ray diffraction studies and infrared spectra of $Bi_2O_3.3MoO_3$-$AlPO_4$ catalysts indicated its unsuitability as a catalyst, since it had monoclinic crystal structure with too many edge shared Mo – O octahedra. The other two phases viz. $Bi_2O_3.MoO_3$ and $Bi_2O_3.2MoO_3$ containing corner shared Mo – O

octahedra were investigated to establish the best conditions for oxidative dehydrogenation.

Optimal conditions for oxidative dehydrogenation were established using techniques developed in applied statistics, namely, exploration of response surface using orthogonal and rotatable experimental designs. Various factors, and their region of determination for finding the optimal were

Temperature	400-500°C
Catalyst to feed ratio W/F	0.25-2.5 $\frac{\text{g catalyst}}{\text{mg mol/min}}$ (0.25-2 sec contact time)
Butane to oxygen ratio	0.5-2.0 mol/mol
mol bismuth molybdate per 100 mol aluminium phosphate	0-100
Oxygen to nitrogen ratio	0.5 mol/mol (held constant)
Bismuth molybdate	β- and γ-phases (qualitative variable)

Optimization parameter was chosen as the yield of butene and butadiene. Factorial experiments were designed with temperature, W/F, butane-oxygen ratio and per cent bismuth molybdate as quantitative factors, and the phase of bismuth molybdate as qualitative factor.

To start with, fractional factorial experiments (one-half replication) were designed, and a first order response surface was fitted to the data. Method of steepest ascent was used to move towards the optimum. In the near-optimum region, a central composite design was used, and experimental results were fitted to

a second order model for the response surface. The exact optimal conditions were located using the second order equation, and the second order model was subjected to canonical analysis to examine the exact nature of the response surface.

Mechanistic modelling of the dehydrogenation process was then attempted. Redox, Rideal-Eley and Langmuir-Hinshelwood models were constructed and point selectivity defined as the ratio of rate of formation of butene to that of butadiene was used to identify plausible models. Finally recommendations for future work have been proposed.

CHAPTER 1

INTRODUCTION

1.1. Introduction.

Natural gas and associated gas, presently used as sources of energy can serve as potential feedstocks in the production of petrochemicals like ethylene, propylene, butenes, butadiene, maleic anhydride etc. Use of such a valuable material as a source of energy when other cheaper and abundant energy sources are within easy reach could bring forward a day when such natural resources are extinct. There has been a growing concern in the industrial as well as political circles to utilise these expensive petroleum products very judiciously, with a view to conserve this precious, limited energy source.

1.2. Utilisation of Gaseous Hydrocarbons - Indian Scene.

About 400 million m^3 of associated gas comprising of 75% methane, 8% ethane and 12% propane and butane will be available on the shores of Gujarat and Maharashtra by 1980, from the off-shore oil production platform of Bombay-High [35]. Claims made by the state governments and the industries have led the Indian Government to evaluate the alternatives available for the best use of Bombay-High gas [36]. The methane rich gas from Bombay-High can supply the natural gas requirements for

three urea plants of 1500 tonnes per day capacity, and already there is some thinking regarding the use of Bombay-High gas as a feedstock for the fertiliser plants based in Bombay and Gujarat.

Methane may also be used to produce methanol, acetylene etc., whereas ethane, propane and butane can be used for the production of olefins, butadiene, maleic anhydride and a host of other petrochemicals [61, 114].

The present study is aimed at the utilisation of n-butane. The dehydrogenation route provides a means for the synthesis of other hydrocarbons that yield ultimately various useful products. The dehydrogenation of n-butane has been discussed briefly in the following section.

1.3. n-Butane Dehydrogenation Processes.

Conventionally, n-butane is dehydrogenated to butenes over a chromia-alumina catalyst [34, 41, 42, 55] at temperatures of 500-550°C. The reaction is equilibrium limited [23], and the catalysts tend to loose their activity rapidly due to severe coking of the catalyst pellets.

Halogens and halogen based compounds were used in the reaction in order to alleviate the above difficulties in the dehydrogenation process [42, 61, 98, 115]. In such processes when iodine was the halogen used, butane was dehydrogenated to 1, 3-butadiene in a single step with very good selectivity and

yield. However these processes did not gain much commercial importance due to the prohibitive cost of iodine.

Butane can also be dehydrogenated to butenes and butadiene over various types of solid catalyst [49, 61, 115] using mixtures of butane and air. Such a process appears very attractive since the oxygen present in the reaction media prevents the coking of the catalysts and secondly the dehydrogenation of butane to butadiene can be realized in a single step.

Literature on oxidative dehydrogenation of n-butenes to 1, 3-butadiene [10-21, 45, 61, 104] indicates that the bismuth molybdates catalysts are very active and selective compared to other catalysts. It was generally observed that the molybdic oxide provided the activity in the dehydrogenation while bismuth oxide was responsible for the selectivity.

The feasibility of the one-step oxidative dehydrogenation of n-butane over a molybdic oxide-aluminium phosphate catalyst was established by Gaspar and Pasternak [49]. The activity of the molybdic oxide-aluminium phosphate catalysts could probably be enhanced by the addition of bismuth to molybdic oxide.

1.4. Object of the Present Investigation.

Having looked into the feasibility of the oxidative dehydrogenation reaction over a molybdic oxide-aluminium phosphate catalyst and considering the reported influence of bismuth oxide on the selectivity of the reaction, the present

investigation was directed towards the study of oxidative dehydrogenation of bismuth molybdate-aluminium phosphate catalysts.

The structure of the catalysts were determined first and their thermal stabilities were investigated before actually studying the butane dehydrogenation reaction over them. The results are given in Chapter 4.

The effects of process variables like temperature, contact time, butane to oxygen ratio and catalyst composition on the yield of butenes and butadiene were studied using response surface methodology in order to establish the optimum process conditions. These results are presented in Chapter 5.

Various mechanistic models have been proposed in Chapter 6. Point selectivity (defined as the ratio of rate of formation of butene to that of butadiene) method has been used to identify plausible models. Finally recommendations for future work have been proposed in Chapter 7.

CHAPTER 2

SURVEY OF RELATED WORK AND SELECTION OF CATALYST FOR THE PRESENT WORK

Several processes based on different raw materials have emerged for the production of olefins and diolefins. Due to the relevance and importance, literature on the production of n-butenes and 1, 3-butadiene is reviewed in the following sections.

2.1. Sources of Butenes and Butadiene.

Butenes and butadiene are produced by the following methods:

1. By cracking of hydrocarbons.
2. Manufacture from ethylene, propylene and ethyl alcohol.
3. By thermal dehydrogenation of n-butane and n-butenes.
4. By oxidative dehydrogenation of n-butane and n-butenes.

Various aspects of the above processes have been reviewed by several authors [11, 42, 44, 53, 61, 104, 114, 115, 124].

2.2. Cracking of Hydrocarbons.

In the petroleum industry, naphtha is cracked as a means of obtaining raw materials for the manufacture of organic chemicals. Cracking is directed mostly towards the

production of ethylene and propylene but invariably some butenes and butadiene form as side-products [11, 42]. Cracking is normally done at low pressures with steam as a diluent at a temperature of 700-750°C. Lower hydrocarbons like butane can also be cracked to yield butenes, however the yields are very low [94, 116].

2.3. Manufacture from Ethylene, Propylene and Ethanol.

Commercial processes for the synthesis of butadiene based on ethylene and propylene have been developed, but it is unlikely that these will compete economically with the processes based on butenes and butane. Butadiene can also be obtained from ethanol.

Ethylene dimerization over a Ziegler catalyst such as aluminium triethyl with nickel acetylacetonate yields butenes. Alternatively ethylene may be oxidised to acetaldehyde, which may be further converted to acetaldol by aldol condensation. Further hydrogenation and dehydration yield 1, 3 butadiene [42].

Propylene disproportionation over MoO_3-CoO-Al_2O_3 catalyst at about 200°C and 30 atm pressure yields butene and ethylene as products. Ethyl alcohol dehydration over Al_2O_3-ZnO, MoO-CoO catalyst gives 1, 3-butadiene [39].

2.4. Thermal Dehydrogenation of n-Butane and n-Butenes.

Processes which involve reactions of the type,

$$C_4H_{10} \xrightarrow{\text{Catalyst}} C_4H_8 + H_2 \qquad \Delta H = 28.5 \text{ kcal}$$

$$C_4H_8 \xrightarrow{\text{Catalyst}} C_4H_6 + H_2 \qquad \Delta H = 28 \text{ kcal}$$

are referred to as 'Thermal Dehydrogenation processes'. These reactions are endothermic and the yields of butenes and butadiene are constrained by thermodynamic equilibrium [23].

Practically all operating commercial butadiene processes are based on the thermal dehydrogenation of n-butane or n-butenes or mixtures of these.

1. Thermal Dehydrogenation of n-Butane.

Dehydrogenation of butane to butenes is conveniently carried over a chromia-alumina catalyst [26, 34, 41, 48, 55, 56, 73, 91]. The chromia-alumina catalyst deactivates during dehydrogenation due to coke deposition, and demands frequent regeneration. The summary of the work reported in literature is presented in Table 1.

The most important thermal process using n-butane as the chief raw material for large-scale manufacture of butadiene is the Houdry process [42]. 15-20% chromia on activated alumina is used as a catalyst at a temperature of 620-650°C and a pressure of approximately 0.2 atm without any diluent gas. Several reactors are used in swing operation to tackle the problem of coking.

Table 1. THERMAL DEHYDROGENATION OF n-BUTANE TO n-BUTENES

Catalyst	Temperature °C	Pressure Atms.	Contact Time Seconds	Conversion %
Cr_2O_3 [48]	350	1.0	-	7.5
Al_2O_3-12% Cr_2O_3 [26]	530	1.0	0.5-2.0	-
Al_2O_3-Cr_2O_3 [41]	569	1.1-2.7	0.25-9.0	4-36
Al_2O_3-20% Cr_2O_3 [55, 56]	447-550	0.19-3.331	-	0.1-2.2
Al_2O_3-22% Cr_2O_3 [91]	501	0.06-1.8*	10.0	3-6
Al_2O_3-Cr_2O_3 + Na_2O, LiO_2 [34]	510-550	0.1-0.5	-	-

* Nitrogen diluent.

11. Thermal Dehydrogenation of n-Butenes.

Several processes are in existence differing mainly in their choice of catalyst. The feed-stock used is a C_4 olefin-rich hydrocarbon distillation cut, from which isobutene has been removed by acid treatment. Steam is the most commonly used diluent, and dilution ratios of steam to hydrocarbon upto 20:1 are used. Considerable effort has gone into the development of selective catalysts. Some such catalysts are shown in Table 2.

Catalyst deactivation due to coking is a severe problem in the dehydrogenation of butenes to butadiene. Those catalysts which contain potassium salts are to some extent self-regenerating, in particular the shell 205. Potassium salts have a catalytic effect on the water-gas reaction

$$C + H_2O \rightleftharpoons CO + H_2$$

and in this way coke is removed from the catalyst bed. The Dow catalyst is at a disadvantage since it requires air regeneration and has a short on-stream life. It has the advantage, however, of a significantly higher selectivity.

Dehydrogenation of butenes to butadiene over chromia-alumina catalysts demands temperatures higher than that needed for dehydrogenation of butane over the same catalyst [55, 57, 120]. Coking problems and poor selectivity to butadiene impede their acceptance as a suitable catalyst

Table 2. COMPARISON OF n-BUTENE DEHYDROGENATION (THERMAL) CATALYSTS

	Esso 1707 [22, 103]	Shell 205 [125]	Dow Type B [92]
Chemical composition	18.4 Fe_2O_3, 72.4 MgO, 4.6 CuO, 4.6 K_2O	62.5 Fe_2O_3, 2.2 Cr_2O_3, 33.3 K_2CO_3	$Ca_8Ni(PO_4)_6$ + Cr_2O_3
Temperature °C	625-650	650	625-650
Steam:butane ratio	14:1	18:1	20:1
Conversion %	28-35	37	28-40
Selectivity %*	75-70	76	86

* Selectivity is defined as the ratio of moles of butenes forming butadiene to the total moles of butenes reacted.

OXIDATIVE DEHYDROGENATION

Thermal dehydrogenation of n-butane or n-butenes yields hydrogen as one of the products. Build-up of hydrogen concentration in the product stream imposes a thermodynamic limitation on the equilibrium conversion [23]. If the hydrogen is oxidised during the course of dehydrogenation, the equilibrium of the dehydrogenation reaction can be shifted in a favourable direction. In addition, sufficient heat can be generated for the dehydrogenation reaction which otherwise is endothermic in nature.

Various types of hydrogen acceptors, like – chlorine, bromine, iodine, sulphur and selenium may be used. The dehydrogenation reaction with these hydrogen acceptors is exothermic except for the case of iodine, for which it is endothermic. Suitability of various hydrogen acceptors has been discussed by Vadekar and Pasternak [123]. Extensive reviews of the oxidative dehydrogenation processes have been given by Voge and Adams [124] in 1967, Sittig [114] in 1968, Skarachenko [115] in 1969, Sachtler [104] in 1970 and Hucknall [61] in 1974.

Thus, oxidative dehydrogenation can be effected in two ways. The first is the direct oxidative method, in which the hydrocarbon to be dehydrogenated is mixed with an oxygen containing gas, usually air. This mixture, to which steam may be added, is then passed over a suitable catalyst.

The second method makes use of halogens and sulphur. The gaseous mixture containing hydrocarbon, air and halogen is passed through a catalyst bed. In some process modifications, the halogen may be reacted in a separate stage with the hydrocarbon and at a later stage, the oxygen is used to regenerate the halogen from the resultant halide.

These processes are discussed in detail below for butane and butenes.

2.5. Oxidative Dehydrogenation of n-Butane.

The production of diolefins by the oxidative dehydrogenation of alkanes is generally not successful due to low reactivity of these compounds. At temperatures below 300°C, aldehydes, alcohols and oxides of carbon are formed. At temperatures of 550°C and above cracking of butane dominates. The yield of oxygen containing compounds reduces and the same of ethylene and propylene increases as the reaction temperature is increased from 300°C to 700°C, whilst, the yield of butenes passes through a maximum [115].

The yield of oxygen containing compounds like aldehydes and alcohols decreases when the oxygen to hydrocarbon ratio is reduced. Water is the sole oxygen containing compound at temperature of 500°C and oxygen to hydrocarbon ratio of 0.1 [10].

Levin et al. [81] used a number of oxides in their study and arranged their activities as follows:

$$Ni > Mo > Co > W > Fe > Zn \gg Cu \gg Mn > Cd > Sn > Pb \gg Cr \gg Bi$$

Patent literature on oxidative dehydrogenation of butane is not very extensive. Varied reactor designs have been used for the purpose. McDonald and McIntyre [82] have used fluidised bed reactor whereas Lester [80] designed a reactor in which air and butane streams were separated by a porous concentric tube containing an oxygen transfer agent. The hydrogen generated during butane dehydrogenation diffused across the porous wall, into the air stream, thus reducing the hydrogen partial pressure and increasing the yield of butenes and butadiene. Table 3 provides a glimpse of the results of a few important patents and literature.

Inorganic complexes used as catalysts allow dehydrogenation reaction to be carried out at lower temperatures. Kovaleva and Tulupov [71] used the complex compound $[(CH_3)_2N^+Cl^-]_{21}$ Fe as a catalyst in a melt containing 53% KNO_3, 40% $NaNO_2$ and 7% $NaNO_3$, with a catalyst concentration of 0.1-5%. Oxygen and butane mixture were bubbled through the catalyst containing melt at 170-200°C. The product was only butenes with undetectable side-products.

1. Halogen Based Dehydrogenation.

Iodine can be used for the dehydrogenation of hydrocarbons, especially butane [98]. The endothermic reaction

Table 3. OXIDATIVE DEHYDROGENATION OF n-BUTANE TO n-BUTENES AND 1, 3-BUTADIENE

Catalyst	Temperature °C (secs)	Feed Gas Composition				Selectivity %	Yield %	Ref.
		C_4H_{10}	H_2O	O_2	N_2			
Na-phosphomolybdate	600(1)	1	-	1	-	63	22	[82]
$AlPO_4$ + 2.5 mole % Mo [as Mo_4O_{11}]	593(-)	1	-	1	-	Conversion = 24%		[50]
CoO-MoO_3	550(-)	1	20	1	-	40	12	[113]
KCl coated reactor wall	503(-)	1	-	0.1	-	49	-	[10]
1.25CoO + MoO_3	420(1)	0.88	-	0.1	0.02	-	2.75	[28]

$$C_4H_{10} + 2I_2 \rightleftharpoons C_4H_6 + 4HI$$

proceeds at temperatures above 400°C as studied by Raley et al. [98] and recently by Kuz'michev and Skarachenko [74].

In the presence of a metallic oxide capable of reacting with hydrogen iodide [111], the reaction was found to go to completion with negligible formation of undesirable by-products such as acetylenes. The iodine could be easily regenerated by oxidising the metal iodide with air or oxygen to give metal oxide and free iodine. The two steps can be combined into one by passing hydrocarbon with air and less than stoichiometric amount of iodine over a suitable metal oxide catalyst like PbO, Li_2O [111], and CaO [96]. In this system the elemental iodine is regenerated continuously to carry out the reaction to completion.

Bromine and chlorine can also be employed in place of iodine in the oxidative dehydrogenation process. The reaction is exothermic in the case of chlorine, and mildly exothermic with bromine. These processes use mostly alkali metal halides for catalysing the reaction [118, 119].

Use of mixture of halogens gives better yield and selectivity as compared to the use of a single halogen in the oxidative dehydrogenation. Results of some of the experiments reported in literature are shown in Table 4.

Halogen-based processes offer many advantages over conventional methods, notably high conversions and selectivities,

Table 4. HALOGEN AND SULPHUR BASED DEHYDROGENATION OF n-BUTANE AND n-BUTENES

Catalyst	Feed Gas Composition	Temperature °C	Conversion %	% Yield Butadiene	% Yield Butenes	Ref.
None	$1C_4H_{10}$, $1.87I_2$	575	89.2	25.4	53.8	[98]
None	$1C_4H_{10}$, $1.5I_2$, $0.12O_2$	550	81.1	36.7	41.1	[98]
CaO, CaI_2	$1C_4H_{10}$	570	-	70.0	-	[96]
KCl/Silica gel	$1C_4H_{10}$, 1.3Air, 2.2HCl	580	86.3	36.8	20.8	[119]
CsCl/Silica gel	$1C_4H_{10}$, 1.3Air, 2.2HCl	580	82.6	34.6	27.8	[100]
LiCl, KCl, MnCl Molten bath	$1C_4H_{10}$, $4H_2S$, $2O_2$, 7He	550	89.0	48.3	4.6	[51]
5% CeO_2/Al_2O_3	$1C_4H_8$, 0.4HCl, $10H_2O$, $0.8O_2$, 3He	625	65.2	28.8	-	[93]
5% CeO_2/Al_2O_3	$1C_4H_8$, 0.2HBr, $10H_2O$, $0.8O_2$, 3He	625	80.8	47.4	-	[93]
5% CeO_2/Al_2O_3	$1C_4H_8$, $1.5H_2S$, $10H_2O$, $0.8O_2$, 3He	625	58.7	35.9	-	[93]
5% CeO_2/Al_2O_3	$1C_4H_8$, $1.5H_2S$, 0.2HI, $10H_2O$, $0.8O_2$, 3He	625	85.6	75.2	-	[93]
5% CeO_2/Al_2O_3	$1C_4H_8$, $1.5H_2S$, 0.4HCl, 0.05HBr, $10H_2O$, $0.8O_2$, 3He	625	80.1	64.2	-	[93]

and continuous operation without the need for catalyst regeneration. Iodine offers several advantages over other halogens, especially in the case of butane dehydrogenation. Iodine unlike chlorine and bromine does not react with butadiene at elevated temperatures and there are, thus, no undesirable side reactions.

ii. Sulphur Based Dehydrogenation.

Sulphur vapours were used as hydrogen acceptor by Rasmussen et al. [100] in dehydrogenation of butane, at a temperature range of 650-760°C. Nascent sulphur is an efficient hydrogen acceptor as compared to sulphur vapours. Pasternak and Vadekar [93] have used hydrogen sulphide with a mixture of butane and oxygen to effect oxidative dehydrogenation, where the hydrogen sulphide combined with oxygen to produce nascent sulphur and water. Small quantities of halogens mixed with hydrogen sulphide significantly improved the conversion and selectivity of the dehydrogenation reaction. A molten salt bath of LiCl-KCl-$MnCl_2$ catalysed the reaction equally well when hydrogen sulphide, oxygen and butane were used in the absence of halogens [51]. Table 4 shows some of the results found in the literature.

iii. Other Hydrogen Acceptors.

Ethylene and propylene have been used as hydrogen acceptors in dehydrogenation of butane over Chromia-Alumina catalyst [66, 77-79]. Absence of oxygen in the reaction media leads to coking of the catalyst.

2.6. Oxidative Dehydrogenation of n-Butenes.

Numerous catalysts for oxidative dehydrogenation of butenes have been reported in the literature [44, 53, 69, 114, 115, 124]. The catalysts recommended are generally mixtures of oxides of elements from group V (Bi, Sb, As, P, V) and VI (Cr, Mo, W) of the Periodic Table.

i. Oxide Catalysts.

Pure metal oxides themselves are not very selective and give very poor conversions. The addition of oxides of metals from neighbouring groups often greatly enhances conversion and selectivity of metal oxide catalysts.

Those catalysts based on Bi-Mo, Sb-Sn and Fe-Sb are probably the most useful and have been studied in detail in literature.

Bismuth Oxide-Molybdenum Oxide Catalysts. The oxidation of butenes over bismuth-molybdates has been the subject of considerable study. Over this catalyst, oxidation proceeds with a high selectivity towards butadiene, even at high conversions. Adams et al. [1, 2] and Bleyenberg et al. [25] have reported selectivities of 90-95% at conversions ranging from 20-80% in oxidation of 1-butene at 460°C. Cis-2-butene and trans-2-butene are about 5 times less reactive than 1-butene [2, 63], trans-2-butene being the least reactive of the three.

Over a range of binary catalyst compositions – $Bi_2O_3.3MoO_3$ (α-phase), $Bi_2O_3.2MoO_3$ (β-or Erman phase), $Bi_2O_3.MoO_3$ (γ-phase or koechlinite) and the ternary catalysts based on bismuth molybdate (e.g. Bi_2O_3-MoO_3-Al_2O_3), oxidative dehydrogenation of butenes has been reported to be first order in alkene and zero order with respect to oxygen over a wide range of temperature [2, 122]. Keizer [63] and Bakshi et.al. [12], however, have reported a deviation from zero order with respect to oxygen over koelhlinite catalyst at temperatures in excess of 380°C and high conversions. Appearance of a dependence of rate expression on partial pressure of oxygen was explained by the blocking of active centers [12].

Structure and properties of bismuth molybdates together with the mechanism of oxidative dehydrogenation reactions over these are discussed in detail in Sections 2.7 through 2.9.

Antimony Oxide Containing Catalysts. Many catalysts containing antimony oxide are selective in the oxidation of butenes to butadiene. However they are not as active and selective as bismuth molybdate catalysts.

Of the antimony oxide-containing systems, iron (III) oxide-antimony oxide has been extensively studied by Boreskov and co-workers [27, 108, 110]. These catalyst were found to have a good selectivity to butadiene when they were present in the reduced state.

Catalysts based on antimony oxide-tin (IV) oxide system have also been fairly well investigated [106, 109, 121]. These catalysts give good results when the antimony to tin ratio ranges from 1:16 to 4:1. Antimony oxide-tin oxide catalysts are not very sensitive to the olefin structure of the hydrocarbon being dehydrogenated and with 2-butenes 90% selectivity at 63% conversion has been claimed. This was obtained with steam dilution, the ratio of butene:air:steam being 1:5:4 and a contact time of 4 sec at 440°C.

KINETICS AND REACTION MECHANISM OVER BISMUTH MOLYBDATE CATALYSTS

The oxidative dehydrogenation of butenes over bismuth molybdate catalysts has been a subject of considerable study. A brief review is presented below.

2.7 Kinetics of Dehydrogenation of n-Butene over Bismuth Molybdates.

Over a range of binary catalyst compositions, $Bi_2O_3.3MoO_3$, $Bi_2O_3.2MoO_3$ (Erman phase), $Bi_2O_3.MoO_3$ (koechlinite) and ternary catalysts based on bismuth molybdate (e.g. Bi_2O_3-MoO_3-Al_2O_3), the oxidative dehydrogenation of butenes has been reported to be of the first order in butene, and zero order with respect to oxygen over a wide range of temperatures [2, 63]. These results indicate that the chemisorption of butenes on the catalyst surface is slow and the

chemisorption of oxygen is extremely fast. Detailed studies on the kinetics of dehydrogenation of butenes over bismuth molybdate catalyst have been carried out by Komarovskii et al. [69].

2.8. Mechanism of Oxidative Dehydrogenation.

Two mechanisms were proposed simultaneously by Adams [1] and Sachtler and DeBoer [105] for the oxidative dehydrogenation of 1-butene to 1, 3-butadiene. The mechanism postulated by Adams involved initial adsorption of oxygen on the catalyst surface prior to the occurrence of the reaction while Sachtler and DeBoer showed that the oxidation is a classical example of the Mars-van Krevelen mechanism [85]. Batist et.al. [20] later established the details of the Mars-van Krevelen mechanism for the catalytic oxidation of 1-butene to 1, 3-butadiene over a bismuth molybdate catalyst as follows:

$$C_4H_8 + \square + O^{2-} \rightleftharpoons C_4H_7^- + OH^-$$

$$Mo^{6+} + C_4H_7^- \rightarrow [Mo = C_4H_7]^{5+} \qquad (2.1)$$

$$[Mo = C_4H_7]^{5+} + O^{2-} \rightarrow Mo^{4+} + \square + OH^- + C_4H_6 \qquad (2.2)$$

$$2OH^- \rightleftharpoons O^{2-} + \square + H_2O \qquad (2.3)$$

$$O_2 + 2\square + 2Mo^{4+} \rightarrow 2O^{2-} + 2Mo^{6+} \text{ (fast)} \qquad (2.4)$$

In reaction (2.1) and subsequent steps, $\square$ denotes an anion vacancy and $[Mo = C_4H_7]^{5+}$ represents a π-allyl complex of Mo^{6+} and the allyl carbanion $(C_4H_7)^-$. The kinetics of the reaction were reported to be of the first order in 1-butene and zero order in oxygen, leading to the conclusion that reduction steps (2.1) and (2.2) are rate determining and that reoxidation step (2.4), is comparatively fast. It is of interest that the reverse of reaction (2.1) leads to cis- and trans-2-butenes i.e. double-bond isomerisation, though the isomerisation reaction is slow compared to the oxidation of 1-butene to 1, 3-butadiene.

The validity of the Mars-van Krevelen mechanism was confirmed from the interesting experiments performed by Batist et al. [21] on the reduction and reoxidation of $Bi_2O_3.MoO_3$ catalyst at 470°C. The yellow compound $Bi_2O_3.MoO_3$ was reduced by 1-butene to a blue black compound $Bi_2O_3.MoO_{2.5}$ (i.e. $Bi^{3+} + Mo^{5+}$) which showed an X-ray diffraction pattern similar to that of the original catalyst, implying that the reduction did not affect the position of the metal atoms. The catalyst could not be reduced beyond a state formally described by $Bi_2O_3.MoO_{2.5}$ using 1-butene. However the reduction with hydrogen resulted in a compound containing bismuth metal and molybdenum (IV). The reduction of $Bi_2O_3.3MoO_3$, $Bi_2O_3.2MoO_3$ and $Bi_2O_3.MoO_3$ with hydrogen studied by Beres et al. [24] has also indicated a rapid diffusion of oxygen through the crystal lattice.

From their adsorption studies of butenes, butadiene, water, oxygen etc. over some bismuth molybdates, Matasuura and Schuit [87] have established the existence of two different surface sites. These sites were termed the A-sites and the B-sites. The "A-site" is an O^{2-}-ion in a special position and is associated with a Bismuth ion. The A-sites adsorbed butadiene slowly but strongly, and adsorbed water weakly and reversibly. Oxygen adsorption on the partially reduced catalyst was irreversible. The "B-site" is comprised of an anion vacancy on a Mo^{6+}-ion sorrounded by corner-shared O^{2-}-ions. The adsorption of butadiene on B-sites was found to obey a dual-site mechanism and the same was fast and reversible representing a weak adsorption. The configuration of the oxygen ions in the site is shown below.

$O_B(1)$	$O_B(2)$	MoO_3 layer
	O_A	Bi_2O_3 layer
$O_B(3)$	$O_B(4)$	MoO_3 layer

Matsuura and Schuit [87] proposed the following steps for the formation of butadiene from butene.

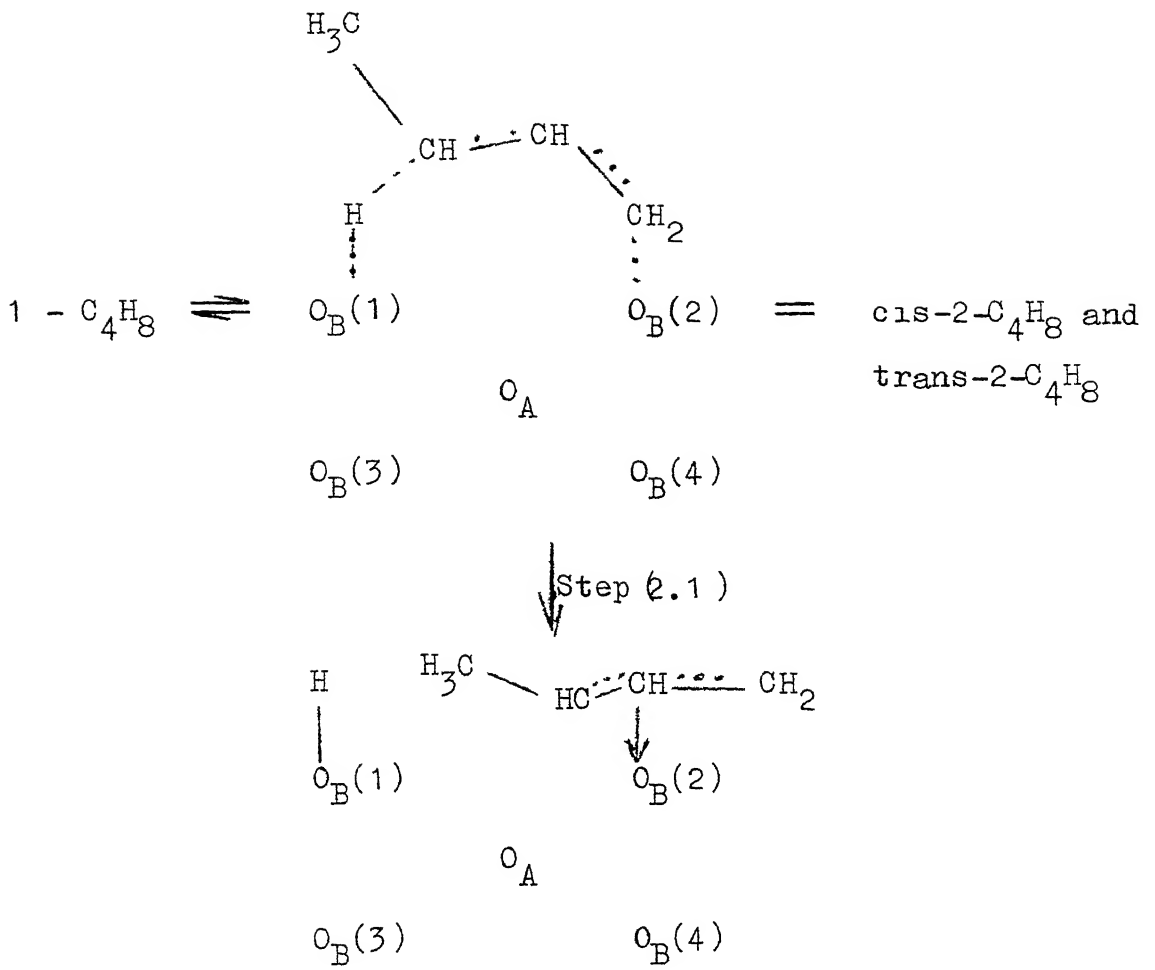

In step (2.1), the adsorption of butene leads to the formation of a hydrogen atom and an allyl group (H-atom located on $O_B(1)$ and allyl group on $O_B(2)$). The dissociation of a second hydrogen atom and the formation of a butadiene weakly attatched to $O_B(2)$ and $O_B(3)$ takes place in the second step.

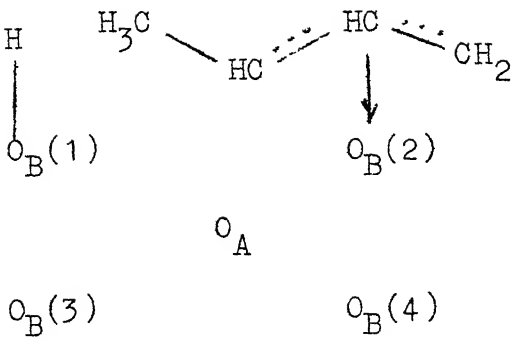

step (2.2) →

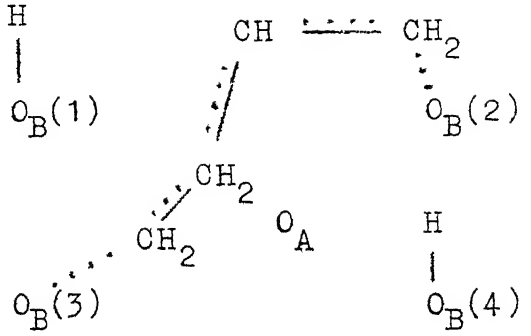

$\longrightarrow$ $C_4H_6 + H_2O$

At this point, there are two alternate steps. In the first one the weakly adsorbed butadiene is desorbed and two hydrogen atoms ($H_{(1)}$ and $H_{(4)}$) migrate to O_A and these are desorbed as a water molecule. In the alternate step the weakly adsorbed butadiene becomes strongly attached at O_A and undergoes further oxidation:

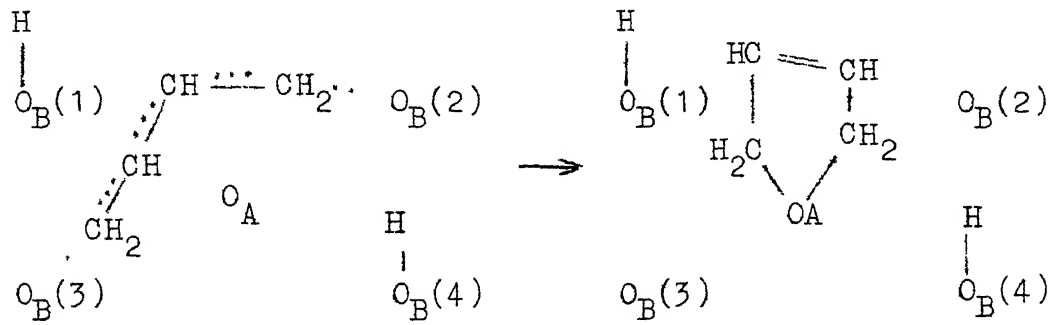

$\longrightarrow$ Furan

The desorption of water and furan results in the reduction of the catalyst. The catalyst is reoxidised at an A-site either by diffusion of an O^{2-} ion from the lattice or by the gas phase oxygen.

Oxidation of propylene to acrolein over $Bi_2O_3.3MoO_3$, $Bi_2O_3.2MoO_3$ and $Bi_2O_3.MoO_3$ showed that activity of the catalyst was insensitive to the type of the molybdate [54]. Configuration of oxygen atoms around molybdenum atoms was different in the three molybdates and thus it was concluded that the O_B sites should be Mo^{6+} and not the oxygen associated with Mo^{6+}. Tracer studies using exchange of O^{36} isotope with partially reduced catalyst confirmed that the A-site is an oxygen ion associated with a bismuth ion [65, 129].

Attempts have been made in the past to relate the activity of the catalyst with the reactivity of the double bond type lattice oxygen $Mo^{6+} = O$ [8, 9, 54]. $Mo^{6+} = O$ bond strengths in bismuth molybdates are in the order $Bi_2O_3.MoO_3 > Bi_2O_3.2MoO_3 > Bi_2O_3.3MoO_3$. However, in the butene oxidative dehydrogenation, the relative bond strengths of $Mo^{6+} = O$ was of no consequence [54].

2.9 Acidity and Activity of the Catalysts.

Ai and co-workers [4-6] have studied the acidity of bismuth molybdate catalysts in relation to their activity for the oxidative dehydrogenation of butenes. Acidity of pure

Bi_2O_3 was found to be lower than that of MoO_3 or MoO_3-P_2O_5, and that with increase in Bi_2O_3 content of the catalyst, the acidity rapidly increases at first, passes through a maximum at a Bi/Mo atomic ratio of 0.2, and then decreases to the value of pure Bi_2O_3 catalyst. Basicity of the catalyst was found to increase with the Bi/Mo ratio. The acidic sites were ascribed to Mo^{6+} cation, since it was more electronegative compared to Bi^{3+}. Anion vacancies proposed by Schuit and co-workers [19, 87] were associated with surface lattice oxygen, O^{2-} which were earlier confirmed by Wragg et al [130].

The activity of the bismuth molybdate catalyst for the oxidation of butenes to butadiene was found to be the best at a Bi/Mo ratio of 0.5-3.0 (medium acidity). At lower Bi/Mo ratios (high acidity), acidic products like maleic anhydride were formed in preference to butadiene.

2.10. Choice of Catalyst for the Present Work.

The dehydrogenation of butane involves abstraction of hydrogen atoms from the parent molecule. Paraffinic hydrocarbons act upon the metal oxide catalysts more or less as electron donating agents; this tendency being very weak, in butane, its dehydrogenation activity will be governed by the activity of the surface sites. Therefore, an efficient catalyst will be the one which has either active Lewis acid-sites that can abstract hydrogen atoms from butane as hydride-ions, or

has suitable Bronsted basic sites which can abstract protons from butane molecule or both. Acidic sites consisting of metal cations are then necessary for adsorbing the remainder of the butane molecule. Thus the dehydrogenation of butane can proceed by stepwise abstraction of hydrogen over these centers.

Molybdenum oxide on aluminium phosphate has been used in the past as a catalyst for the dehydrogenation of butane in the presence of oxygen [50]. Mo^{6+} ions provide good active centers for the adsorption of olefins. However, the oxygen, O^{2-} ions associated with the molybdenum tetrahedra are not mobile, and hence are not efficient in oxidising the hydrogen abstracted from the butane molecule. Lattice oxygen, O^{2-} associated with Bi^{3+} has been proven to be very mobile, and can oxidise the abstracted hydrogen easily.

The aim of the present work was to obtain dehydrogenation products like butenes and butadiene from butane using oxygen, as the hydrogen acceptor with as little oxygenated products (aldehydes, alcohols etc.) as possible. The molybdic oxide-aluminium phosphate is an acidic catalyst and hence may have a good selectivity for oxygenated products.

Bismuth molybdate-aluminium phosphate catalyst was chosen for the present work from the above considerations. Bismuth oxide helps not only in reducing the acidity of the catalyst but also provides mobile lattice oxygen. This should make the bismuth molybdate-aluminium phosphate catalyst more

active and selective than the molybdic oxide-aluminium phosphate catalyst in the oxidative dehydrogenation of n-butane.

$Bi_2O_3.MoO_3$ (koechlinite or γ-phase),

$Bi_2O_3.2MoO_3$ (Erman or β-phase),

and $Bi_2O_3.3MoO_3$ (α-phase)

were chosen as the different phases of catalyst for the study. These three phases give catalysts with different Bi/Mo ratios.

CHAPTER 3

MATERIALS, EQUIPMENT AND EXPERIMENTAL PROCEDURES

3.1. Feed Gases.

n-Butane. C.P. grade n-butane obtained from Matheson Gas Company was used in all the experiments. Typical composition of C.P. grade n-butane is as follows:

Minimum purity	99 vol % with small amounts of isobutane and 2-2, dimethylpropane as impurities.
Sulphur content	less than 0.005 wt %
Moisture	about 100 p.p.m.

Oxygen. Industrial grade oxygen was supplied by Indian Oxygen Ltd., Kanpur. Oxygen gas had a minimum purity of 99 vol %,

Nitrogen. Technical grade nitrogen (99.5% pure) supplied by Indian Oxygen Ltd., Kanpur, was used in the present study.

Air. An oil-free rotary compressor with teflon seal was used to compress air. The compressed air was passed over a bed of calcium chloride and activated charcoal in order to remove moisture, carbon dioxide and any other impurities.

PREPARATION OF CATALYSTS

Effect of preparation of catalyst on the activity of bismuth molybdate catalyst has been investigated by Batist et al. [17] and Grzybowska et al. [52]. Procedures suggested by Batist and co-workers [17, 70] have been used in the preparation of bismuth molybdates in the present study. Aluminium phosphate was prepared according to the procedure of Gaspar and Pasternak [50]. Reagents used in the preparation of catalysts are as follows:

Bismuth Nitrate. ($Bi(NO_3)_3.5H_2O$). BDH Analar grade bismuth nitrate was used in most of the catalyst preparations. Bismuth nitrate was analysed by EDTA titration with xylenol orange indicator (see Appendix I) and was found to be 98.97% pure.

Bismuthyl Nitrate. ($BiONO_3.H_2O$). Bismuthyl nitrate was prepared in the laboratory as follows· 500 g of bismuth nitrate were placed in a 4-litre beaker to which 2.5 litre of distilled water were added and stirred vigorously for 5 minutes. The bismuthyl nitrate slurry was filtered and the unwashed cake was dried at 80°C [89] for 24 hours in an oven. Bismuthyl nitrate was analysed by EDTA titration with xylenol orange indicator (see Appendix I for details) and was found to contain 81.09% Bi_2O_3 by weight.

Molybdic Acid. (H_2MoO_4). Pure grade molybdic acid was obtained from Reachim, U.S.S.R. It was analysed using oxine

reagent and was found to contain 86.934% MoO_3 by weight. Details of the analysis are given in Appendix I.

Ammonium para Molybdate. $((NH_4)_6\ Mo_7O_{24}.4H_2O)$. J.T. Baker Analysed Reagent. Analysis certificate indicated that it contains 82.5% MoO_3 by weight.

Aluminium Nitrate. $(Al(NO_3)_3.9H_2O)$. Sarabhai Chemicals G.R. grade and J.T. Baker Aralyzed Reagent grade aluminium nitrate were used.

Ortho-Phosphoric Acid. (H_3PO_4). G.R. grade o-phosphoric acid (85% H_3PO_4 by weight), supplied by E. Merck (India) Ltd. was used.

Ammonia Solution. G.R. grade ammonia solution (Sarabhai Chemicals), containing 25 weight percent ammonia - sp. gr. 0.91 was used in the present study.

Nitric Acid. (HNO_3). BDH Analar grade, and Pfeizer Certified Reagent containing 69 wt % HNO_3 were used.

3.2. Bismuth Molybdates.

1. γ-Bismuth Molybdate ($Bi_2O_3.MoO_3$).

Procedure suggested by Konings et al. [71] was used in the preparation of γ-bismuth molybdate. 114.9403 g (0.4 mol) of bismuthyl nitrate were added to 34.686 g (0.2 mol) of molybdic acid suspended in 2 l of boiling water. A white slurry, with a pH of 2.5, was formed which slowly started

changing its colour after about half an hour. It was lemon yellow after 3 hours. The suspension was stirred vigorously for 20 hours under boiling conditions. The mass was then cooled and filtered. The filtered cake was washed with water and then dried at 110°C for 24 hours in an oven. The filtrate from the unwashed cake was analysed and was found to contain very little bismuth molybdate in it.

Dried bismuth molybdate cake was ground to a fine powder and calcined in a muffle furnace at 500 ± 10°C. Chemical composition of the compound was verified by chemical analysis (see Appendix I).

ii. β-Bismuth Molybdate ($Bi_2O_3.2MoO_3$).

0.5 mol of catalyst was prepared according to the method suggested by Batist et al. [17].

490.075 g (1 mol) of bismuth nitrate were dissolved in 180 cm^3 of nitric acid and 2 litres of water.

174.49 g of ammonium para molybdate were dissolved in 2 litres water and 50 cm^3 of 0.91 sp. gr. ammonia solution.

Ammonium molybdate solution was added to bismuth nitrate solution resulting in a white precipitate. Dilute ammonia solution was added to the slurry to adjust the initial pH of 1 to 6.5. It was then filtered and the residue was dried at 110°C for 24 hours to obtain a faint yellow coloured product. The powdered sample was calcined at 500 ± 10°C for 3 hours and then further kept at 450 ± 10°C for 90 hours

during which time the colour of the sample turned yellow. The composition of the compound was checked by chemical analysis (see Appendix I).

iii. α-Bismuth Molybdate ($Bi_2O_3.3MoO_3$).

0.5 mol of catalyst was prepared by using the procedure suggested by Batist et al. [17].

490.075 g (1 mol) of bismuth nitrate were dissolved in 180 cm^3 of nitric acid and 2 litres of water.

261.735 g ammonium para molybdate were dissolved in 2 litres of water and 50 cm^3 of ammonia solution of specific gravity 0.91.

Ammonium molybdate was added dropwise to the bismuth nitrate solution and a white precipitate was obtained. The solution was kept well stirred and was heated to evaporate the water. Later it was dried in an oven at 110°C for 24 hours and calcined at 500 ± 10°C for 4 hours.

3.3. Ortho-Aluminium Phosphate (o-$AlPO_4$).

The procedure suggested by Gaspar and Pasternak [50] was used in the preparation of o-$AlPO_4$.

472.7 g (1.26 mol) of aluminium nitrate were dissolved in 3.8 litres of water. 145.3 g of ortho-phosphoric acid were then added and the contents were mixed. An ammonia solution of 0.91 specific gravity was added slowly to the well stirred aluminium nitrate-phosphoric acid solution till the pH

of the slurry reached 7.0-7.1. The white coloured aluminium phosphate slurry was then filtered and the cake was washed with water and dried in an oven at 110°C for 48 hours.

Aluminium phosphate was prepared in six batches. To avoid the batch to batch variations, aluminium phosphate prepared in different batches were mixed together, crushed and ground to a fine powder in a stainless steel ball mill with stainless steel balls.

Aluminium phosphate thus prepared contains ammonium nitrate and some ammonium phosphate as impurities. Three samples of aluminium phosphate were ignited separately at 700°C in silica crucibles. The ignited residue was cooled in a desiccator and weighed. The percent o-$AlPO_4$ in aluminium phosphate was computed. The samples contained 73.156 wt %. o-$AlPO_4$ in the prepared aluminium phosphate. The aluminium phosphate was stored in the unignited condition and was ignited prior to its use.

3.4. Molybdic Oxide-Aluminium Phosphate Catalyst.

Molybdic oxide-aluminium phosphate catalysts with various $MoO_3/AlPO_4$ ratios were prepared according to the procedure described below for the preparation of a typical catalyst with a weight ratio of $MoO_3/AlPO_4$ of 0,1.

41.676 g (0.25 mol) of aluminium phosphate were ignited at 600 ± 10°C for 3 hours in a muffle furnace. The

ignited sample was ground to a fine powder and then dry mixed with 4.13694 g (0.025 mol) of molybdic acid. Dry grinding was continued for 15 minutes. About 60 cm^3 of water were then added before wet grinding. Later it was dried in an oven at 110°C for 12 hours. The dried catalyst was crushed to 1-2 mm fraction and calcined at 600 ± 10°C for 4 hours in a muffle furnace. The catalyst was cooled and stored in a desiccator.

3.5. Bismuth Molybdate-Aluminium Phosphate Catalyst.

Bismuth molybdate-aluminium phosphate catalysts were prepared for varied bismuth molybdate to aluminium phosphate ratios and different phases of bismuth molybdates (α, β and γ). Methods of preparation of these catalysts are identical. A typical preparation is described below for the case of a catalyst with $Bi_2O_3.2MoO_3$:$AlPO_4$ ratio of 0.05.

41.676 g (0.25 mol) of aluminium phosphate were ignited at 600 ± 10°C for 3 hours in a muffle furnace. Ignited aluminium phosphate was ground to a fine powder and then mixed with 9.424 g (0.0125 mol) of $Bi_2O_3.2MoO_3$. The mixture was ground for 15 minutes. About 55 cm^3 of water were then added and wet grinding was carried out. Later it was dried in an oven at 110°C for 12 hours. The dried catalyst was broken into 1-2 mm fraction and activated at 500 ± 10°C for 10 hours in a muffle furnace. The catalyst was cooled and stored in a desiccator.

EXPERIMENTAL SETUP AND PROCEDURES

3.6. Description of the Experimental Setup.

A schematic diagram of the experimental setup is shown in Fig. 1. Three capillary flowmeters (5) were used to meter butane (1), nitrogen (2) and oxygen (3) separately. Manometers were provided to measure the differential pressure across the capillary as well as the absolute downstream pressure. Water was used as manometric fluid. Needle valves V1 and V2 were provided to control the flow rates of gases. The valve V1 was a fine control needle valve. Drying tubes containing calcium chloride (7), were provided in the flow-loop to remove moisture if any, from the gases. A separate air line (4, 6, 7) was also provided for use.

The reactor was made from a 15.1 mm I.D., 625 mm long 1/2 inch schedule - 40 tube of type 304 stainless steel (Cr 19%, Ni 9%, C 0.08% max). Out of the total 625 mm length, 280 mm long section was used for packing the reactor with catalyst and inerts (9, 10). The remaining 325 mm length was used for the preheating of the feed gases. A nitrogen-oxygen mixture was heated in the annular space formed by the reactor tube and a 12.5 mm O.D. stainless steel tube. Butane was heated separately inside the 12.5 mm O.D. tube, and was mixed with nitrogen-oxygen stream just before entering the catalyst bed to avoid any pre-catalyst bed reactions. Two chromel-alumel thermocouples, TC1 and TC2 in 6 mm O.D. stainless steel sheaths,

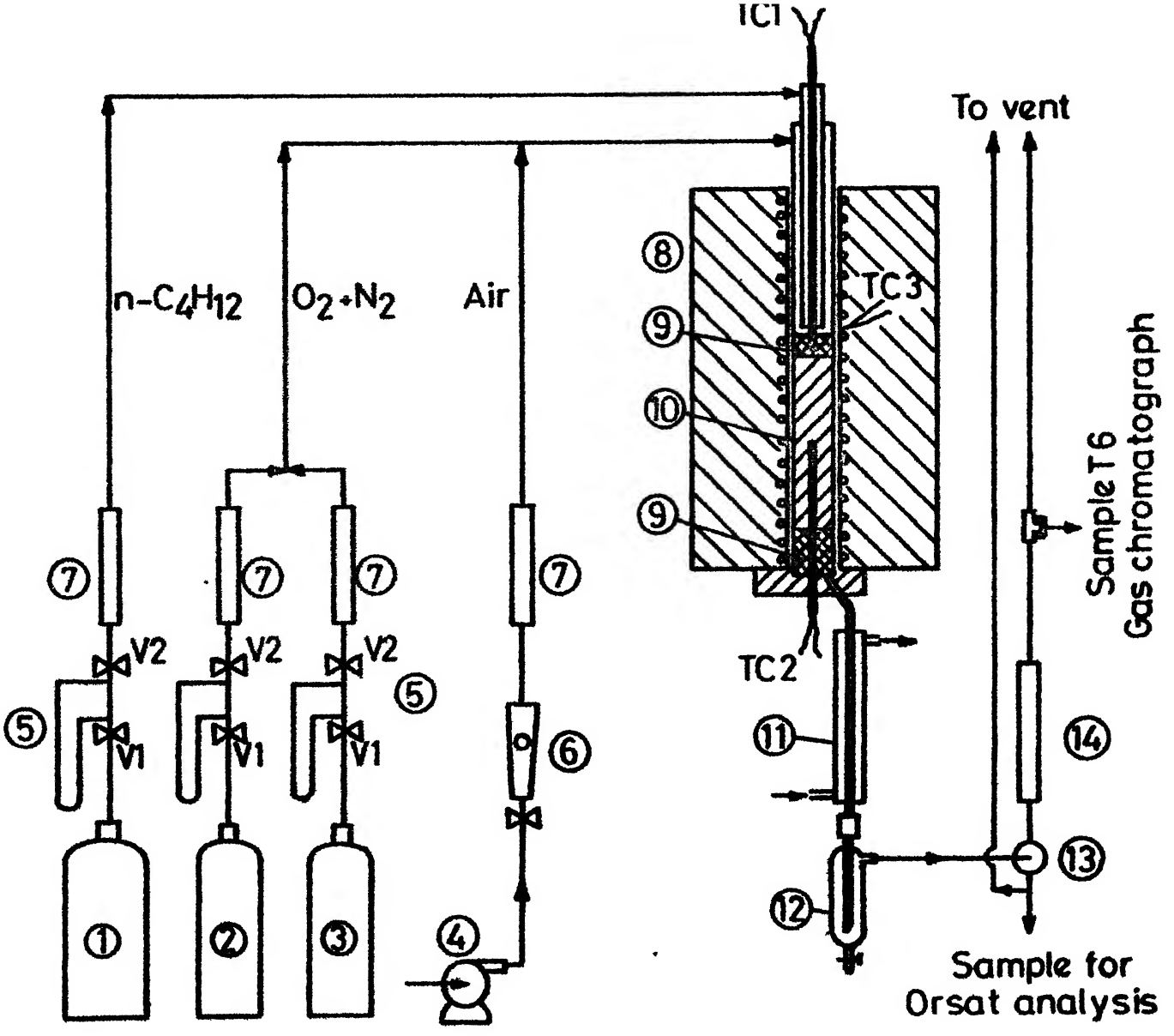

Legend

1. Butane cylinder
2. Nitrogen cylinder
3. Oxygen cylinder
4. Air compressor
5. Capillary flowmeter
6. Rotameter
7. $CaCl_2$ drying tubes
8. Furnace
9. Inert packing
10. Catalyst bed
11. Cooler-condenser
12. Separator
13. Three-way-stopcock
14. Pottassium hydroxide on asbestos

TC1, TC2, TC3-Thermocoupl

V1, V2-Needle valves

Fig. 1 : Experimental setup.

coaxial with the reactor tube, were provided for measuring the temperatures at the entry and middle of the catalyst bed.

The reactor was placed in a 42 mm I.D., vertical tubular furnace (8). The reactor temperature was controlled using "Alnor" type N-15 temperature controller, 0-880°C range, supplied by Alnor Instrument Company. Thermocouple TC3 was used as the temperature sensing element for the controller. A cooler-condenser (11), fabricated from a 6 mm O.D. stainless steel tube was provided for rapid cooling of the reactor effluents. Trap (12), separated condensates if any, from the reactor product stream. A three-way stopcock (13), allowed the sampling of the product gases, which were passed over a column containing potassium hydroxide on asbestos for chromatographic analysis.

Chromatographic Assembly. The chromatographic analysis of the reactor effluents, namely, ethylene, propylene, n-butane, 1-, trans-, cis-2-butenes and butadiene required a column temperature of 21°C. This necessitated a chromatograph with a refrigeration facility for the column oven since the average room temperature in the city of Kanpur is usually above the desired temperature of 21°C. A chromatograph was, therefore, constructed in the laboratory, the details of which are shown in Fig. 2.

The chromatographic assembly consisted of an injector (11), a column (7), and a detector block (8) placed in a

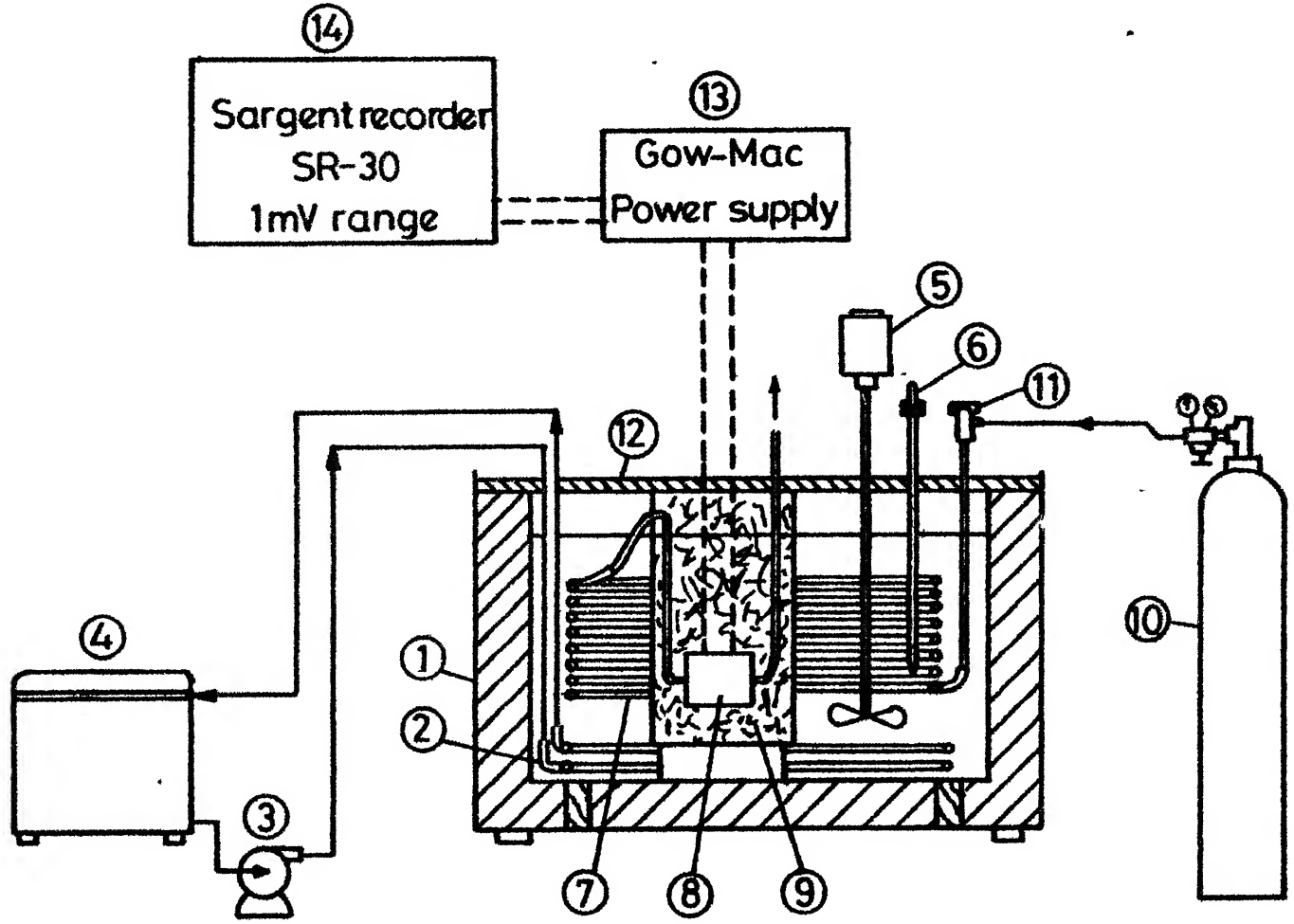

Legend

1. Insulated water bath
2. Water circulation coil
3. Circulation pump
4. Ice box
5. Stirrer
6. Jumo contact thermo-meter
7. Chromatographic colur
8. Detector block assemb
9. Glass wool insulation
10. Nitrogen cylinder
11. Injector block
12. Insulation cover
13. Gow-Mac power supp
14. Sargent recorder

Fig. 2 : Chromatographic assembly.

water-bath (1). The injector had a rubber septum to facilitate the injection of gases to be analysed into the column. Along with the carrier gas, these gases were passed into the column in which they were separated before entering the thermal conductivity detector (8).

The chromatographic column and the detector block were placed in an insulated water bath, the temperature of which was controlled within an accuracy of $\pm$ 0.1°C by circulating chilled water (2, 3, 4). The chilled water circulation pump (3) was connected to a Jumo mercury contact thermometer (6) via a 15 ampere contactor.

The detector block was essentially the same as the one used in Varian Chromatograph Model Aerograph 90-P3. A matched quad of Gow-Mac WX-type 9225 tungsten-rhenium filaments with 12 inch long kovar leads were fitted in the detector block. The detector block assembly was placed in a 150 mm x 150 mm x 220 mm aluminium container and was insulated with glass-wool.

A Gow-Mac power supply (13), Model 9999-C:1, 220 V, 50 Hz was used to supply current to the detector filaments. The ripple of the power supply was measured to be 0.7 mV. A Sargent recorder (14), Model SR-30, fitted with a Model 204 Disc chart integrator, was used to record the chromatographic signals. High purity nitrogen (oxygen content less than 0.001 vol %) was used as the carrier gas.

3.7. Process Measurements.

Chromel-alumel thermocouples protected in stainless steel sheaths were used to measure temperatures of the reactor and the furnace. The standardization procedure for the thermocouples is discussed in Appendix II. A Honeywell, Model 2720, portable calibrating potentiometer test set was used to measure the voltage across the thermocouple junction. The accuracy of the potentiometer was $\pm$ 0.01 mV.

Butane, oxygen and nitrogen flow rates were measured with capillary flow meters. Air flow rate was measured with a rotameter. The gas flow rates were calibrated at a down stream pressure of 50 cm water using a soap bubble flow meter of 200 cm^3 volume.

3.8. Experimental Procedure.

The reactor tube was assembled and the threaded joints which were in contact with high temperatures were sealed with a high-alumina/sodium silicate cement. The refractory cement was allowed to set for at least 6 hours.

The reactor tube was later packed with about 40 cm^3 of catalyst (1-2 mm), sandwiched between 10 cm^3 and 5 cm^3 of porcelein packing (inert) on the exit and inlet sections respectively. Air was passed through the reactor at a flow rate of about 200 cm^3 per minute and the reactor furnace was switched on. When the required temperature reached, nitrogen

and oxygen were supplied to the reactor and subsequently the air supply was stopped.

When the catalyst bed temperature was steady, butane was introduced into the reactor. The flow rates of butane, oxygen and nitrogen were adjusted to the required values using the valves V1 and V2 (Fig. 1). When the measured temperatures at the inlet and the middle of the catalyst bed registered steady values, it was assumed that steady state has been achieved. Two reactor effluent samples were drawn out separately, one of which was taken into an Orsat apparatus to estimate carbon dioxide, oxygen and carbon monoxide and the other was used for chromatographic analysis. The latter sample was passed over a bed containing potassium hydroxide on asbestos before analysis in order to remove the carbon dioxide from the product stream which interfere with the analysis (see Section 3.9). About 10-15 cm^3 of this gas sample was injected into the gas chromatograph for analysis. The rate of formation of the condensate, which contained small quantities of oxygenated compounds, was negligible.

When the experimental conditions were altered for the next experiments, care was taken to change the partial pressures of butane and oxygen very gradually. A sudden change in the partial pressure of butane was found to increase the temperature of the catalyst bed catastrophically.

After the desired experiments were completed, air was again introduced into the reactor and the nitrogen and oxygen streams were shut-off. Butane partial pressure was tapered off to avoid sudden increases in the catalyst bed temperature.

The oxide coating formed on the reactor wall was frequently removed by pickling the reactor tube in an acid bath containing 3% HCl, 3% H_2SO_4 and 94% water, at a temperature of about 70°C [58]. The reactor tube was thoroughly washed with distilled water after such a treatment and dried before placing in situ.

ANALYTICAL METHODS

3.9. Methods of Analysis.

Chromatographic as well as Orsat analyses were employed to establish the composition of the reactor effluents.

The Orsat analysis of the product gases was carried out to determine the percentage of carbon dioxide, oxygen and carbon monoxide in the product stream. Details of the reagents used in the Orsat analysis are given in Appendix III.

The chromatograph used for the analysis of the hydrocarbon mixture has been described in Section 3.6. The chromatographic column was a coil of copper tubing, 15.4 m length and 5.2 mm I.D., packed with 30/44 mesh Chromosorb P (obtained from Chromatography and Instruments Co., Baroda, Gujarat, India) coated with propylene carbonate (35% by weight).

Prosynth grade propylene carbonate was obtained from Riedel, Germany. Dichloromethane (G.R. grade, E. Merck, Germany) was used as a solvent to deposit propylene carbonate on Chromosorb P.

The above column could completely separate methane, ethane, ethylene, propane, propylene, n-butane, 1-butene, trans-2-butene, cis-2-butene and 1, 3-butadiene. However, the carbon dioxide peak interfer with the propylene peak and methane, oxygen and carbon monoxide emerged as a single peak which warranted a separate method of analysis for estimating these components. Orsat analysis as described above was, therefore, used in addition to the chromatographic analysis for determining CO, CO_2 and O_2.

The separating power of the column depends upon a number of factors [47, 64]. Experiments were conducted to find the best conditions. The following operating conditions were arrived at based on minimum H.E.T.P. (height equivalent of a theoretical plate) for n-butane separation:

Column temperature : 21°C

Carrier gas flow rate : 36 cm^3/minute

Fig. 3 shows a typical chromatogram.

3.10. Calibration.

In order to interpret the chromatogram in quantitative terms, the thermal conductivity detector of the chromatograph was calibrated using pure gas samples. The method of absolute

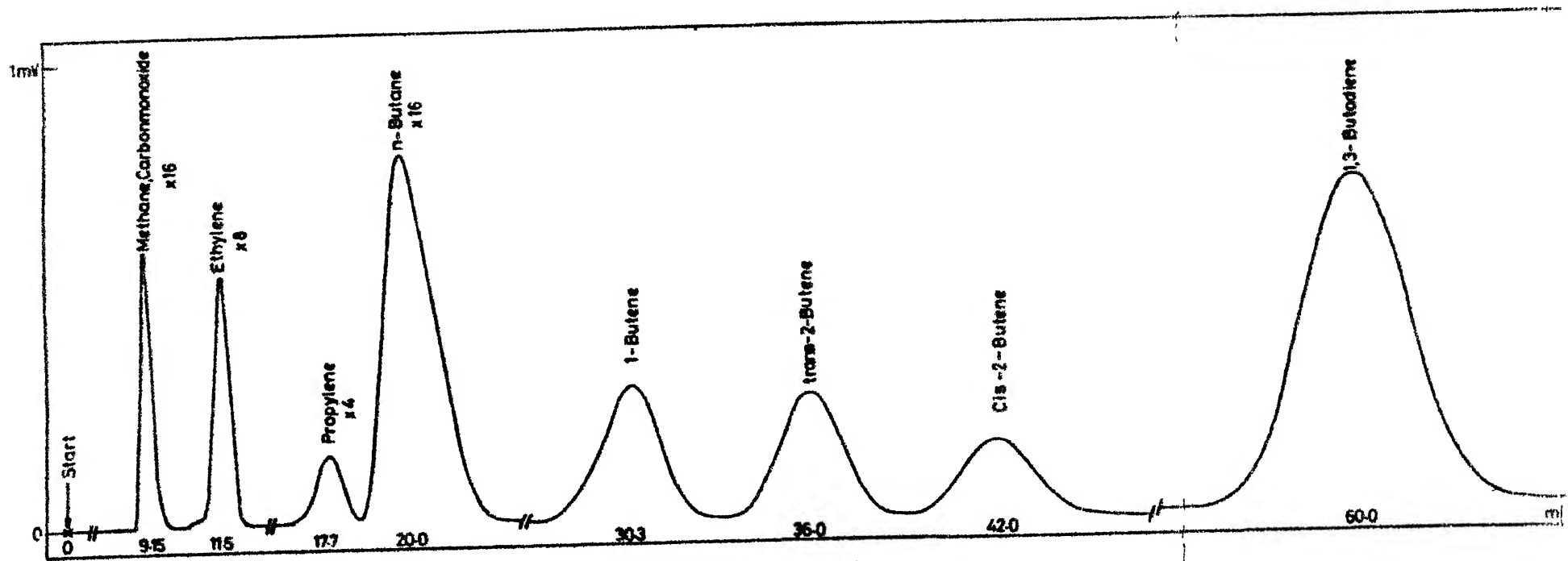

Fig. 3. Sample chromatogram.

Column · 35% Propylene Carbonate on Chromosorb-P, 5·2mm I.D, 15·4m long
Carrier gas · Nitrogen, 36cm^3/min
Temperature : 21°C
Detector T.C.D

standardisation was used to calibrate the detector response [47, 64, 83]. The volume of gas handled being large, the errors involved in the accurate measurement of gas volumes was small.

During calibration, pure gas samples (C.P. grade), obtained from Matheson Gas Company, were injected into the column using 100 µl, 250 µl and 500 µl Hamilton gas-tight microliter syringes. A Sargent Recorder (fitted with a disc integrator) with a 1 mV range was used to record the chromatograms. The retention times and the response factors were calculated by injecting various volumes of the same gas and averaging the peak area per unit volume of the gas injected. Reproducibility of the peak area was checked by injecting identical volumes of the gas at different times. The response factors thus calculated are given in Table 5. The specific volume data of the hydrocarbon gases, used in the calculation of the response factors, were taken from Matheson Gas Data Book [86].

The retention times of hydrocarbons changed with the operation of the column over a period of several months. No efforts were made either to change or repack the column during the investigation since the separation was always complete.

Table 5. RETENTION TIMES AND RESPONSE FACTORS FOR HYDROCARBONS

Component	Retention Time minutes	Response Factor x 10^6 mol/integrator count
Ethane	10.6	0.1655
Ethylene	11.5	0.202
Propane	13.6	0.1626
Propylene	17.7	0.216
n-Butane	20.0	0.2297
1-Butene	30.3	0.2172
trans-2-Butene	36.0	0.2424
cis-2-Butene	42.0	0.2464
1, 3-Butadiene	60.0	0.2483

3.11. Process Calculations.

Quantities like conversion, yield etc. were calculated by a material balance of carbon, hydrogen and oxygen. The details of this procedure is presented in Appendix IV.

CHAPTER 4

CHARACTERISATION OF BISMUTH MOLYBDATE-ALUMINIUM PHOSPHATE CATALYSTS

4.1. Introduction.

The activity of a catalyst is related to its solid state properties like surface area, crystal structure, phase composition and thermal stability. Such properties aid in understanding the catalytic behaviour of the solid and elucidating the reaction mechanism.

The catalysts used in present study were characterised in terms of chemical compositions, characteristic X-ray diffraction reflections and thermal stability. The various properties studied and their implications are listed below.

4.2. Chemical Composition.

Bismuth molybdates used in the present investigations, were prepared in three stoichiometric compositions, with varying bismuth to molybdenum ratios. The γ-phase ($Bi_2O_3.MoO_3$) has been obtained by slurry reaction while the β-phase ($Bi_2O_3.2MoO_3$) was prepared by the precipitation method. The α-phase ($Bi_2O_3.3MoO_3$) has been prepared by evaporating the slurry obtained from the precipitation reaction between bismuth nitrate and ammonium molybdate and since the reagents involved

are of known purity, the product has not been analysed for its chemical composition.

The bismuth molybdate suspensions of γ- and β-phases were separated from their mother liquor and the chemical composition of the same in the dry form confirmed that the compositions are essentially that of the γ- and β-phases ($Bi_2O_3.MoO_3$ and $Bi_2O_3.2MoO_3$). This confirmation at this stage was necessary since any possible losses in the filtrate would have considerably affected the chemical compositions of the bismuth molybdates prepared. The molybdenum contents in these two bismuth molybdates were analysed using oxine reagent. EDTA was used as a masking agent to prevent the interference by bismuth ion [43, 97]. Experimental details for the same are indicated in Appendix I. The β- and γ-phases contained 38.35% MoO_3 and 23.89% MoO_3 (by weight) respectively and these closely correspond to the calculated percentages.

4.3. Bulk Density.

Various catalysts were prepared using bismuth molybdates (i.e. the α-, β- and γ-phases) in different proportions with ortho-aluminium phosphate. On characterisation, since the α-phase has been found to be unsuitable as a catalyst (on the basis of X-ray diffraction patterns and infrared spectra; detailed in Section 4.5 and 4.6 respectively), it was not used in the present study. As such only the catalysts involving

the β- and γ-phases of the bismuth molybdate were adopted.

Typical bulk density values for the catalysts containing β- and γ-phases are presented in Table 6. It was observed that the bulk density of the prepared ortho-aluminium phosphate was around 0.27 g/cm^3, which is very low compared to the reported value around 2.57 g/cm^3 of the crystalline ortho-aluminium phosphate [127]. The aluminium phosphate in the present case was amorphous as evidenced by the X-ray diffraction data.

The bulk densities of $Bi_2O_3.MoO_3$-$AlPO_4$ and $Bi_2O_3.2MoO_3$-$AlPO_4$ catalysts were found to increase with the increase in the proportions of the active components. This is expected since the densities of the constituent bismuth molybdates were high (3-6 g/cm^3). The bulk densities of both types of bismuth molybdates were comparable at equal ratios of bismuth molybdate to aluminium phosphate.

4.4. Surface Area Measurements.

The surface area determinations were made using liquid nitrogen adsorption isotherms (adopting a standard value of 16.2 $Å^2$ for nitrogen molecule) with a static apparatus. The typical results for the catalysts involved are presented in Table 7.

It has been observed that the addition of bismuth

Table 6. BULK DENSITIES OF BISMUTH MOLYBDATE-ALUMINIUM PHOSPHATE CATALYSTS

S.No.	Catalyst Composition mol/100 mol o-$AlPO_4$	Bulk Density g/cm^3	
		$Bi_2O_3 \cdot MoO_3$	$Bi_2O_3 \cdot 2MoO_3$
1	0.0 (o-$AlPO_4$)	0.26	0.26
2	1.0	-	0.25
3	3.0	-	0.27
4	5.0	-	0.29
5	7.0	0.32	0.32
6	9.0	-	0.34
7	15.0	0.41	0.40
8	21.0	-	0.47
9	23.0	0.46	-
10	25.0	0.49	0.49

Table 7. SURFACE AREA VALUES OF THE CATALYST SAMPLES

S.No.	Catalyst	Specific Surface Area m^2/g
1	$AlPO_4$, calcined	49.2
2	$Bi_2O_3.MoO_3$, calcined	9.3
3	$Bi_2O_3.2MoO_3$, calcined	3.8
4	0.1 MoO_3 : 1 $AlPO_4$, calcined	37.8
5	0.07($Bi_2O_3.MoO_3$) : 1 $AlPO_4$, calcined	21.1
6	0.05($Bi_2O_3.2MoO_3$) : 1 $AlPO_4$, dried, uncalcined	83.0
7	0.05($Bi_2O_3.2MoO_3$) : 1 $AlPO_4$ calcined	11.1

molybdate or molybdic oxide to aluminium phosphate reduces the specific surface areas of the catalysts. The uncalcined $Bi_2O_3.2MoO_3$-$AlPO_4$ catalyst (with around 12% of water as indicated by the TGA data) has a surface area higher than that of calcined $Bi_2O_3.2MoO_3$-$AlPO_4$ as also the calcined $AlPO_4$ base.

4.5. X-Ray Diffraction Studies.

X-ray diffraction studies enable the determination of the nature and the extent of the individual constituents present in any material, while the chemical analyses indicate the overall chemical composition taking into consideration all the constituents within the material. In the present investigations this technique was adopted to ascertain the crystallinity of the starting materials prepared as also to observe any possible changes in the starting materials on calcination to around 500°C.

The X-ray diffraction analyses have been carried out on General Electric XRD-5 diffractometer using Ni-filtered Cuk$_\alpha$ radiation. The samples were scanned between 10° and 60° (2θ) on a scale of 2° (2θ) to an inch. The 'd' spacings were calculated for various reflections obtained in each case using the standard Bragg's equation.

X-Ray Diffraction Results:

1. Ortho-Aluminium Phosphate (o-$AlPO_4$).

The characteristic diffraction pattern (Fig. 4) for this material has indicated only a very broad hump in the range

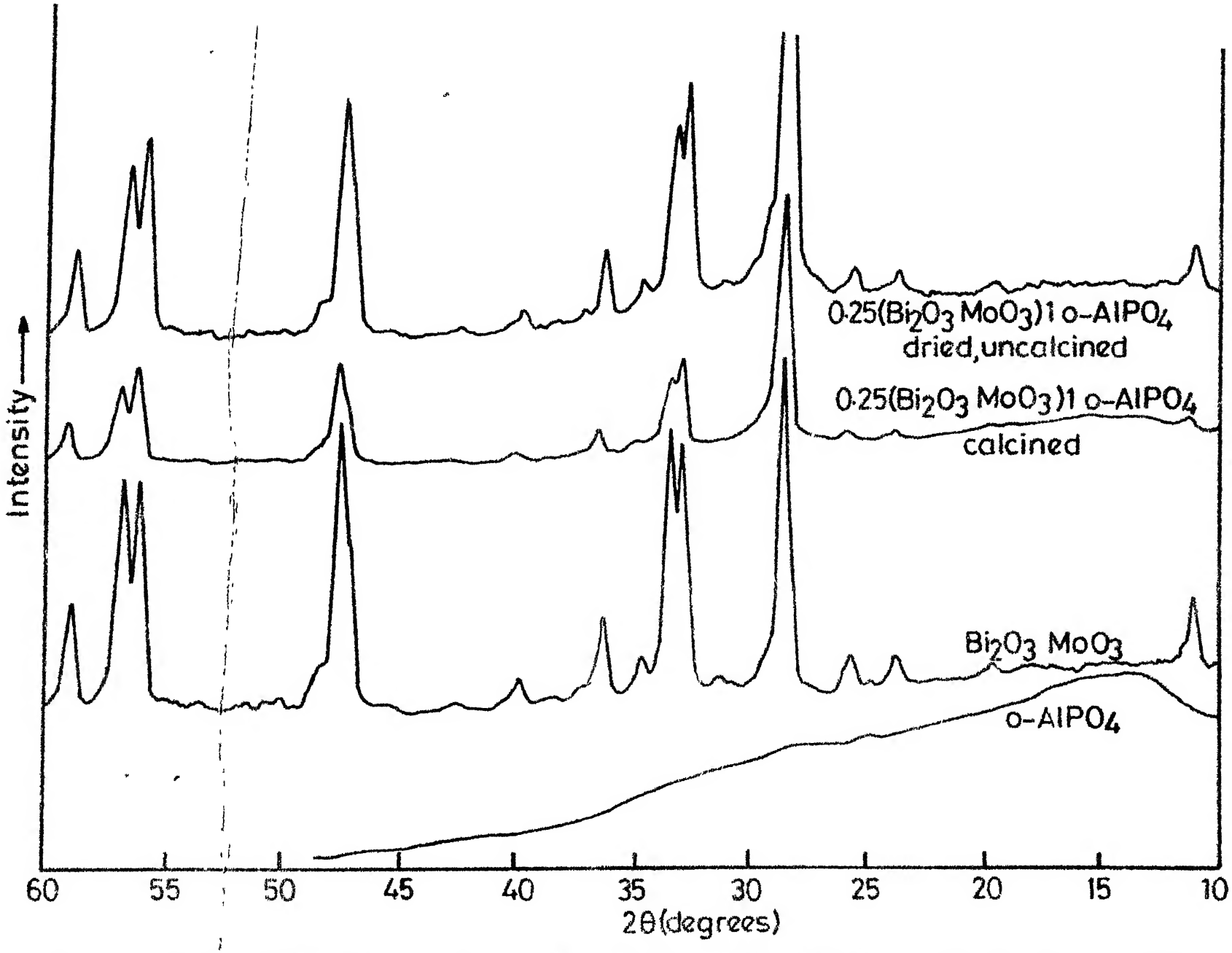

Fig 4 X-Ray diffraction pattern of o-$AlPO_4$, Bi_2O_3. MoO_3 and Bi_2O_3. MoO_3-$AlPO_4$ catalysts.

of 12° to 18° (2θ). No other reflections could be noticed. Several peaks reported in the literature [75] for a crystalline phase of this material are absent here, thus indicative of its amorphous nature.

11. Bismuth Molybdates.

In the present case, diffraction patterns of the α-, β- and γ-phases were studied. Typical diffraction pattern for $Bi_2O_3.MoO_3$ sample is indicated in Fig. 4 with the corresponding 'd' spacings and the peak intensities are presented in Table 8. The 'd' spacings in the present case are in close agreement with the values reported by Frondel [49] for the bismuth molybdate (mineral koechlinite) with composition $Bi_2O_3.MoO_3$ (Table 8). On the basis of the 'd' spacings for 200, 002 and 060 reflections, the cell parameters have been computed to be a = b = 5.46 Å and b = 16.08 Å. These are also in agreement with the reported values [45, 49].

The results of the X-ray measurements of $Bi_2O_3.3MoO_3$ are shown in Fig. 5. The corresponding 'd' spaeings are given in Table 9. The X-ray diffraction data of the prepared $Bi_2O_3.3MoO_3$ closely resemble those given by Erman et.al. [45] (Table 9). Thus the $Bi_2O_3.3MoO_3$ prepared in the laboratory has the monoclinic structure as reported by Erman et.al.

In Fig. 6 the characteristic X-ray diffraction reflections for the prepared -bismuth molybdate ($Bi_2O_3.2MoO_3$) are indicated. The 'd' spacings for the reflections (Table 10)

Table 8. X-RAY DIFFRACTION DATA FOR $Bi_2O_3.MoO_3$. 'd' SPACINGS AND PEAK INTENSITIES (I).

Present Work		Frondel [49]		
d, Å	I*	d, Å	I	hkl
3.26	3			
3.15	100	3.13	100	131
2.87	4			
2.73	74	2.73	60	200, 002
2.69	79	2.68	50	060
2.60	11	2.59	10	220, 022
2.478	25	2.473	30	151
2.265	8	2.263	20	240, 042
2.006	2			
1.938	49	1.936	60	202
1.926	86	1.918	80	260, 062
1.888	13	1.879	10	222
1.652	69	1.647	90	331, 133
1.632	70	1.628	70	191, 280
1.575	32	1.570	60	260

* Arbitrary units indicating the line intensities.

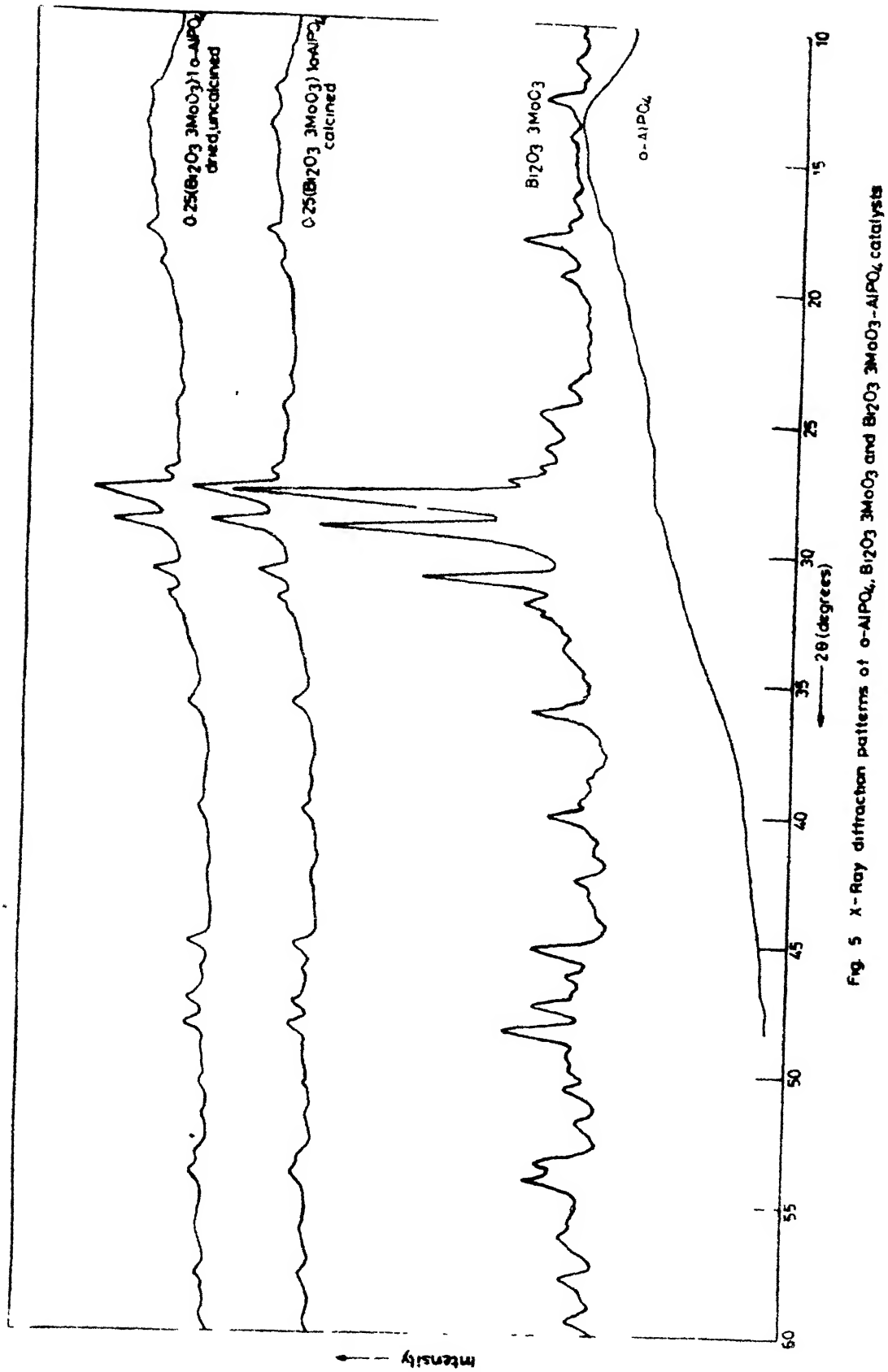

Fig. 5 X-Ray diffraction patterns of o-$AlPO_4$, Bi_2O_3 $3MoO_3$ and Bi_2O_3 $3MoO_3$-$AlPO_4$ catalysts

Table 9. X-RAY DIFFRACTION DATA OF $Bi_2O_3.3MoO_3$. 'd' SPACINGS AND PEAK INTENSITIES (I).

Present Work		Erman et.al. [46]		
d, Å	I**	d, Å	I*	hkl
4.87	26	4.83	w.	012
3.59	16	3.60	w.	102
3.41	8	3.42	w.	210, 112
3.18	138	3.18	s.	032
3.05	100	3.05	s.	131
2.87	59	2.84	s.	204, 133
2.481	28	2.477	w.	024
2.243	24	2.248	w.	240, 034
2.001	28	2.002	med.	330, 044, 106
1.914	20	1.914	w.	061, 035, 226, 404
1.877	31	1.878	med.	160, 316, 321
1.806	11	1.805	w.	320
1.760	9	1.764	w.	400, 045
1.713	23	1.715	med. w.	336
1.692	26	1.691	med. w.	435, 431
1.592	14	1.589	w.	064
1.554	14	1.550	v. w.	337

** Arbitrary units indicating the line intensities.

* s. = strong; med. = medium; med. w. = medium weak; w. = weak; v.w. = very weak.

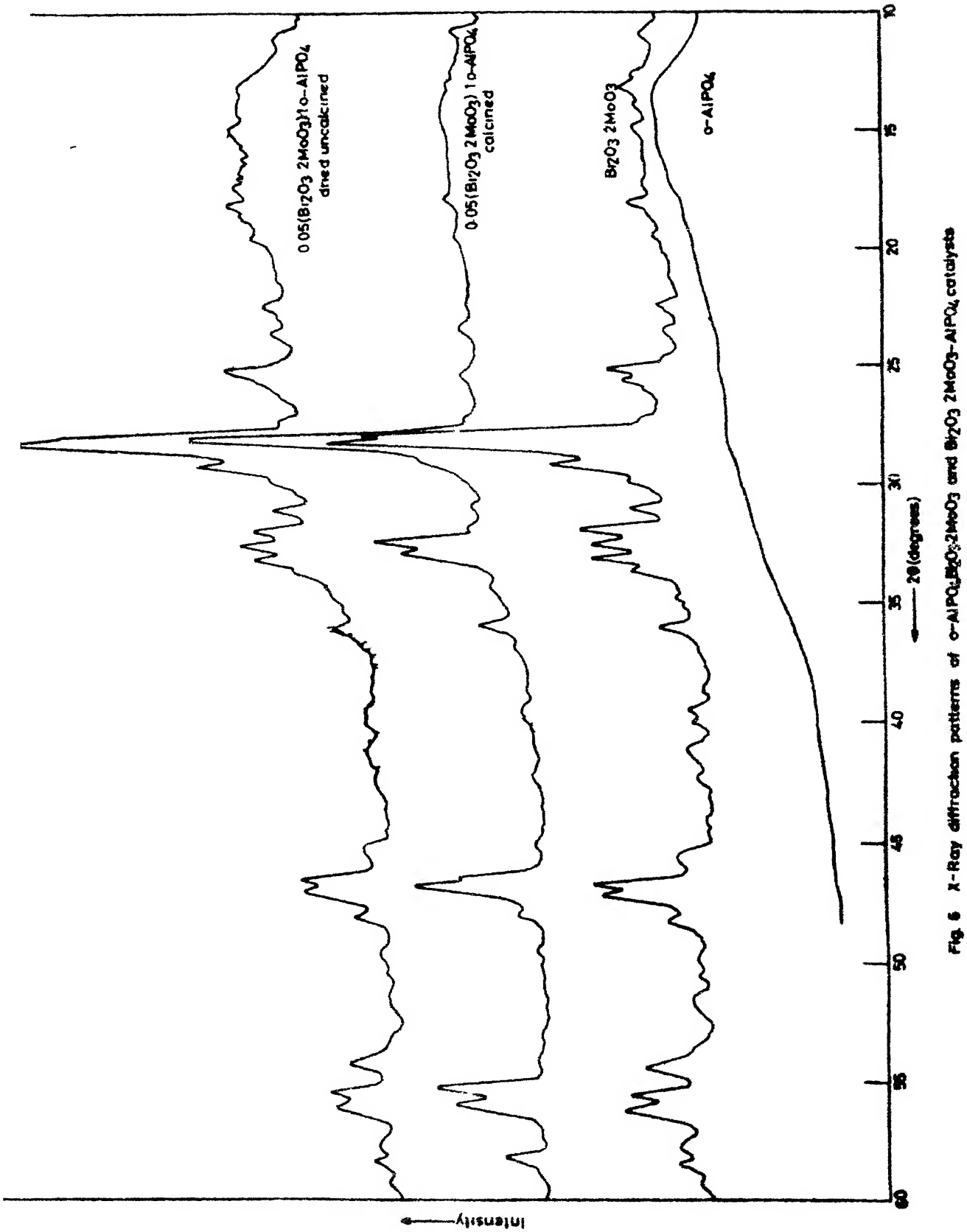

Fig. 6 X-Ray diffraction patterns of o-$AlPO_4$, Bi_2O_3·2MoO_3 and Bi_2O_3 2MoO_3–$AlPO_4$ catalysts

Table 10. X-RAY DIFFRACTION DATA OF $Bi_2O_3.2MoO_3$. 'd' SPACINGS AND PEAK INTENSITIES (I).

Present Work		Batist et.al. [17]		
d, Å	I**	d, Å	I	hkl*
8.04	18	8.01	20	
4.90	33	4.92	70	
3.55	78	3.44	5	
3.20	362	3.20	600	301
3.15	402	3.15	400	
3.05	136	3.06	40	
2.99	44	2.98	20	
2.88	42	2.87	20	
2.80	107	2.81	100	321, 330
2.75	96	2.73	30	
2.70	100			002
2.491	42	2.486	12	
4.987	44	1.986	65	402, 600
1.941	133	1.945	100	
1.924	122	1.928	30	
1.884	42	1.883	20	
1.687	80	1.687	100	
1.653	98	1.650	30	303
1.634	107	1.641	95	
1.598	42	1.592	65	602

** Arbitrary units indicating the line intensities.

* From the data of Erman et.al. [46].

are compared with the values reported by Batist et.al. [17]. The prepared $Bi_2O_3.2MoO_3$ corresponds to β-bismuth molybdate as identified from the characteristic reflections at 5.95, 4.90, 2.80, 1.987, 1.941, 1.634 and 1.598 Å (2θ = 14.85°, 18.1°, 32.0°, 45.8°, 46.85°, 56.3° and 57.7°). However the presence, to a restricted extent, of the α-phase (as identified by its characteristic line at 3.05 Å at a 2θ value of 29.2°) and γ-phase (as inferred from its characteristic lines at 8.04, 1.924 and 1.653 Å at 2θ values of 10.94°, 47.25° and 55.6°) has also been evidenced in the X-ray diffraction patterns. The coexistence of these two phases in minor proportions with the β-phase is due to the partial decomposition of the latter at room temperature according to the following reaction

$$Bi_2O_3.2MoO_3(\beta) \longrightarrow Bi_2O_3.MoO_3(\gamma) + Bi_2O_3.3MoO_3(\alpha) \qquad (4.1)$$

iii. $Bi_2O_3.MoO_3$-$AlPO_4$ Catalyst.

The X-ray diffraction patterns for the uncalcined and the calcined $Bi_2O_3.MoO_3$-$AlPO_4$ catalysts are shown in Fig. 4. Typical 'd' spacings are presented in Table 11. As can be evidenced from the Fig. 4, the uncalcined and calcined specimens of the $Bi_2O_3.MoO_3$-$AlPO_4$ catalysts have similar 'd' spacings indicating that they have not undergone any noticeable modification in crystal structure. However, an interesting feature is apparent in the diffraction patterns. A comparison

Table 11. X-RAY DIFFRACTION DATA OF $Bi_2O_3.MoO_3$-$AlPO_4$ CATALYST.
$Bi_2O_3.MoO_3/AlPO_4$ = 0.25 mol/mol.
'd' SPACINGS AND PEAK INTENSITIES (I).

Uncalcined		Calcined	
d, Å	I*	d, Å	I*
8.04	8	8.05	5
3.26	4		
3.15	100	3.15	100
2.88	2		
2.74	42	2.74	36
2.68	34	2.69	29
2.60	6	2.60	50
2.50	13	2.49	10
2.27	4	2.276	4
1.941	28	1.939	24
1.926	50	1.927	41
1.892	7	1.891	6
1.653	38	1.653	38
1.635	33	1.633	30
1.578	17	1.578	17

* Arbitrary units indicating the line intensities.

of certain reflections for $Bi_2O_3.MoO_3$-$AlPO_4$ with those of pure $Bi_2O_3.MoO_3$ specimens indicated modifications in the relative intensities (Fig. 4). For example, the intensities for the reflections at 2.73 and 1.652 Å corresponding to 2θ values of 32.75° and 55.65° have increased compared to their doublet peaks at 2.69 and 1.632 Å corresponding to 2θ values of 33.5° and 56.35°. Since the reflections at 2.73 and 1.652 Å are for 002 and 331 planes respectively, it may be inferred in the present case that a tendency for preferred orientations of the planes in these directions for $Bi_2O_3.MoO_3$ exists in the presence of $AlPO_4$. This appears to be also the case for $Bi_2O_3.2MoO_3$ in the presence of $AlPO_4$ (discussed below).

iv. $Bi_2O_3.3MoO_3$-$AlPO_4$ Catalyst.

The X-ray diffraction pattern for this catalyst is shown in Fig. 5 and the data are presented in Table 12. It can be seen from the figure that the relative peak shapes are not affected significantly. The peaks of the calcined and the uncalcined catalysts appeared in the same 2θ ranges. Thus the presence of $AlPO_4$ or calcination of $Bi_2O_3.3MoO_3$ together with $AlPO_4$ did not bring any modifications.

v. $Bi_2O_3.2MoO_3$-$AlPO_4$ Catalyst.

The X-ray diffraction patterns of the uncalcined and the calcined $Bi_2O_3.2MoO_3$-$AlPO_4$ catalysts are shown in Fig. 6 and the data are presented in Table 13. A comparison of peaks in

Table 12. X-RAY DIFFRACTION DATA OF $Bi_2O_3.3MoO_3$-$AlPO_4$ CATALYST.

$Bi_2O_3.3MoO_3/AlPO_4$ = 0.25 mol/mol.

'd' SPACINGS AND PEAK INTENSITIES (I).

Uncalcined		Calcined	
d(Å)	I*	d(Å)	I*
4.88	28	4.89	26
3.59	12	3.60	13
3.18	143	3.19	127
3.05	100	3.06	100
2.87	45	2.88	41
2.481	28	2.483	25
2.244	18	2.245	21
2.003	39	2.003	30
1.916	35	1.918	24
1.879	34	1.880	27
1.804	15	1.807	10
1.762	11	1.764	9
1.714	21	1.716	18
1.694	29	1.695	25
1.592	18	1.593	17
1.556	11	1.556	9

* Arbitrary units indicating the line intensities.

Table 13. X-RAY DIFFRACTION DATA OF $Bi_2O_3.2MoO_3$-$AlPO_4$ CATALYST.

$Bi_2O_3.2MoO_3/AlPO_4$ = 0.05 mol/mol.

'd' SPACINGS AND PEAK INTENSITIES (I).

Uncalcined		Calcined	
d, Å	I*	d, Å	I*
7.97	16	8.19	20
4.90	26	4.95	12
3.55	95	3.53	48
3.20	347	3.18	375
3.15	429		
3.06	155	3.06	59
2.99	50	2.90	12
2.87	53		
2.80	87	2.81	23
2.75	113	2.77	124
2.70	100	2.73	100
2.488	37	2.501	39
1.991	42	2.008	10
1.943	129	1.949	88
1.926	124	1.934	135
1.884	55	1.890	27
1.687	76	1.691	14
1.653	100	1.659	118
1.635	96	1.638	98
1.595	21	1.600	9
1.576	42	1.580	47

* Arbitrary units indicating the line intensities.

$Bi_2O_3.2MoO_3$-$AlPO_4$ catalyst does not show any changes in the positions of the peaks for the two substances except that some of the relative peak intensities have increased slightly. This is indicative of the preferred orientation of certain crystal planes of $Bi_2O_3.2MoO_3$ in the presence of $AlPO_4$ which has already been explained earlier. This feature was observed in the case of $Bi_2O_3.MoO_3$-$AlPO_4$ catalyst also (see Section 4.5, v).

In addition, a comparison of the intensities for the peaks of calcined $Bi_2O_3.2MoO_3$-$AlPO_4$ catalyst with the corresponding peak intensities for the uncalcined $Bi_2O_3.2MoO_3$-$AlPO_4$ catalyst indicates certain structural changes pertaining to $Bi_2O_3.2MoO_3$ compound. The reduction in the relative intensities in the peaks of α-bismuth molybdate at 'd' spacings of 3.53, 3.06 (most characteristic) and 2.008 Å at 2θ values of 25.1°, 29.2° and 45.15° respectively in the calcined catalyst reveals the reduced presence of α-bismuth molybdate in the same. It may be inferred that the calcination of $Bi_2O_3.2MoO_3$ sample together with $AlPO_4$ results in inhibiting its decomposition into α- and γ-phases.

4.6. Infrared Measurements.

Having established the overall structure of the bismuth molybdates and bismuth molybdate-aluminium phosphate catalysts through X-ray diffraction studies, their infrared spectra were obtained in order to understand the nature of the bond between

molybdenum and oxygen atoms and the influence of aluminium phosphate on it. The X-ray diffraction pattern was of no use in establishing the structure of aluminium phosphate due to its amorphous nature. Accordingly, an attempt has been made to determine its structure using infrared technique.

The infrared spectra were recorded on a Perkin-Elmer Model 521 spectrometer in the range 4000-250 cm^{-1}. The samples were prepared in the form of KBr discs.

Results of Infrared Analyses:

1. Ortho-Aluminium Phosphate ($-AlPO_4$).

The ir spectrum in the range 250-1200 cm^{-1} for $o-AlPO_4$ (Fig. 7d) exhibited two broad and intense bands at 1070 and 500 cm^{-1}. The former band has been ascribed to the triply degenerate stretching vibrations (ν_3 mode, Nakamoto [90b]) of tetrahedral $(PO_4)^{3-}$. The band at 500 cm^{-1} was attributed to the triply degenerate bending vibrations (ν_4 mode, Nakamoto [90b]) of $(PO_4)^{-}$ tetrahedra. Thus in the prepared aluminium phosphate, the phosphorous atom is surrounded by a tetrahedron of oxygen atoms. It is also known that in the ortho-aluminium phosphates, the network of aluminium and phosphorous atoms is analogous to a $Si(SiO_4)$ network, with both aluminium and phosphorous surrounded by a tetrahedron of oxygen atoms [127]. In addition, two bands (not indicated in the figure) around 1614 cm^{-1} (intense) and 3410 cm^{-1} (wide and intense) were ascribed to O-H in-plane-bending vibrations and -OH stretching vibrations respectively.

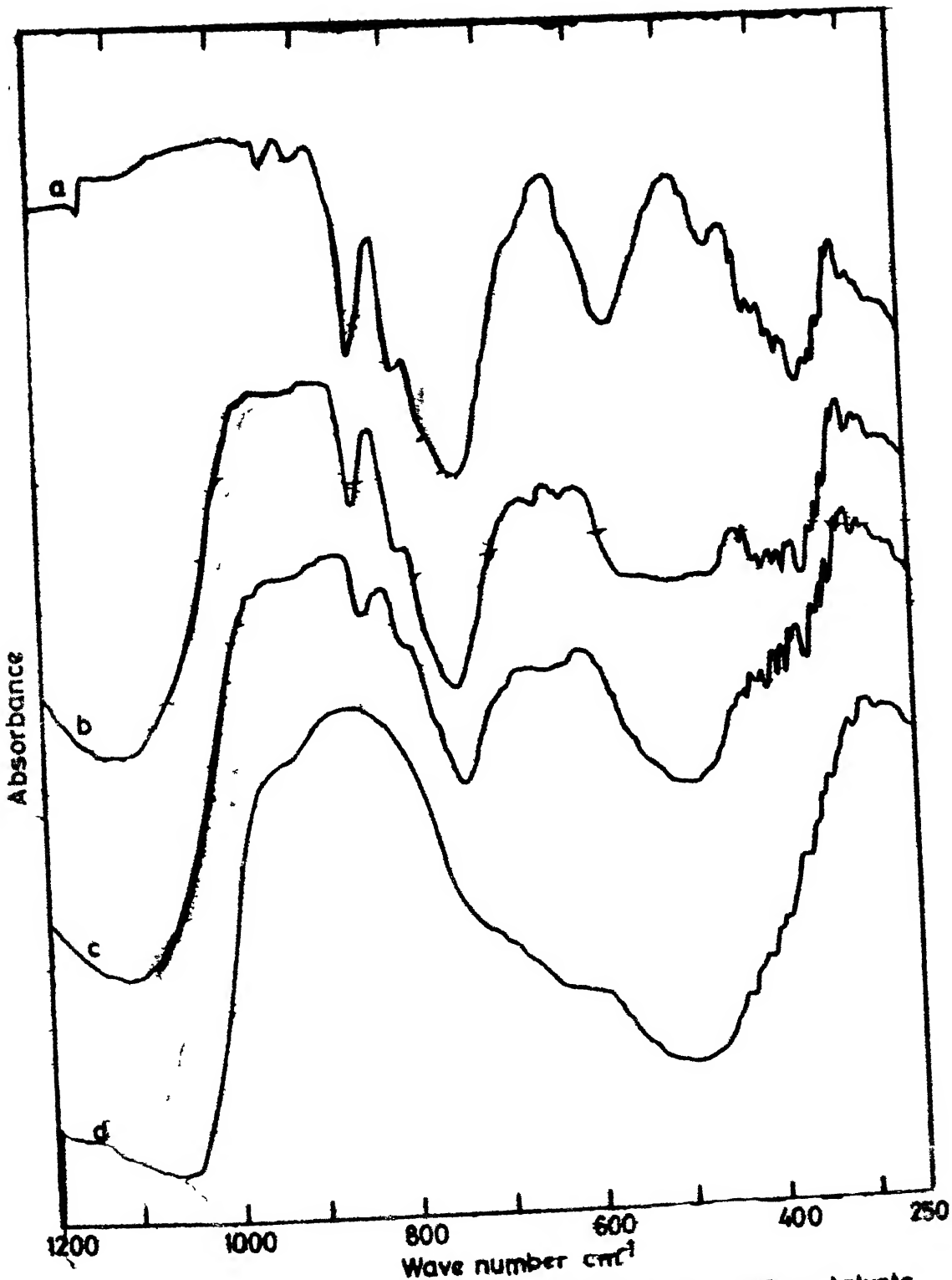

Fig. 7 : Infrared spectra of $Bi_2O_3.MoO_3$ and $Bi_2O_3.MoO_3$-$AlPO_4$ catalysts. (a) $Bi_2O_3.MoO_3$; (b) Catalyst 0.25mol $Bi_2O_3.MoO_3$/mol o-$AlPO_4$; (c) Catalyst 0.05mol $Bi_2O_3.MoO_3$/ mol o-$AlPO_4$; (d) o-$AlPO_4$.

The broad band observed in the range of 300-800 cm^{-1} also contains the absorption band due to O-H out-of-plane bending vibrations.

ii. Bismuth Molybdates.

In the bismuth molybdates, the molybdenum atoms are in octahedral configuration with corner-sharing or edge-sharing of the oxygen atoms [18]. Hence, at the surface we can have either a terminal oxygen O_t, which is bonded to only one molybdenum atom or bridging oxygen that is bonded to two molybdenum atoms. These bonds are represented as $Mo-O_t$ and $Mo-O_b$ respectively. Mitchell and Trifiro [90a] have assigned infrared frequencies to the various vibrational modes of the octahedral molybdenum identified by Clark and Doyle [37]. The ir spectra of various bismuth molybdates prepared in the present study are interpreted below.

The ir spectrum of $Bi_2O_3.MoO_3$ indicated in Fig. 7a exhibits bands at 950 (weak), 940 (weak), 910 (weak), 850 (sharp + shoulder at 870), 800 (sharp), 740 (broad and intense with a shoulder at 780), 570 (intense with shoulders at 600 and 520) cm^{-1}. The bands observed at 740 and 850 cm^{-1} were assigned to $Mo-O_b$ and $Mo-O_t$ stretching vibrations. A prominent shoulder band of $Mo-O_t$ at 800 cm^{-1} is indicative of the tetrahedral molybdenum.

The spectra for $Bi_2O_3.3MoO_3$ and $Bi_2O_3.2MoO_3$ are presented in Figs. 8a and 8b. The band pattern in the region 600-900 cm^{-1} has undergone modification in the present cases

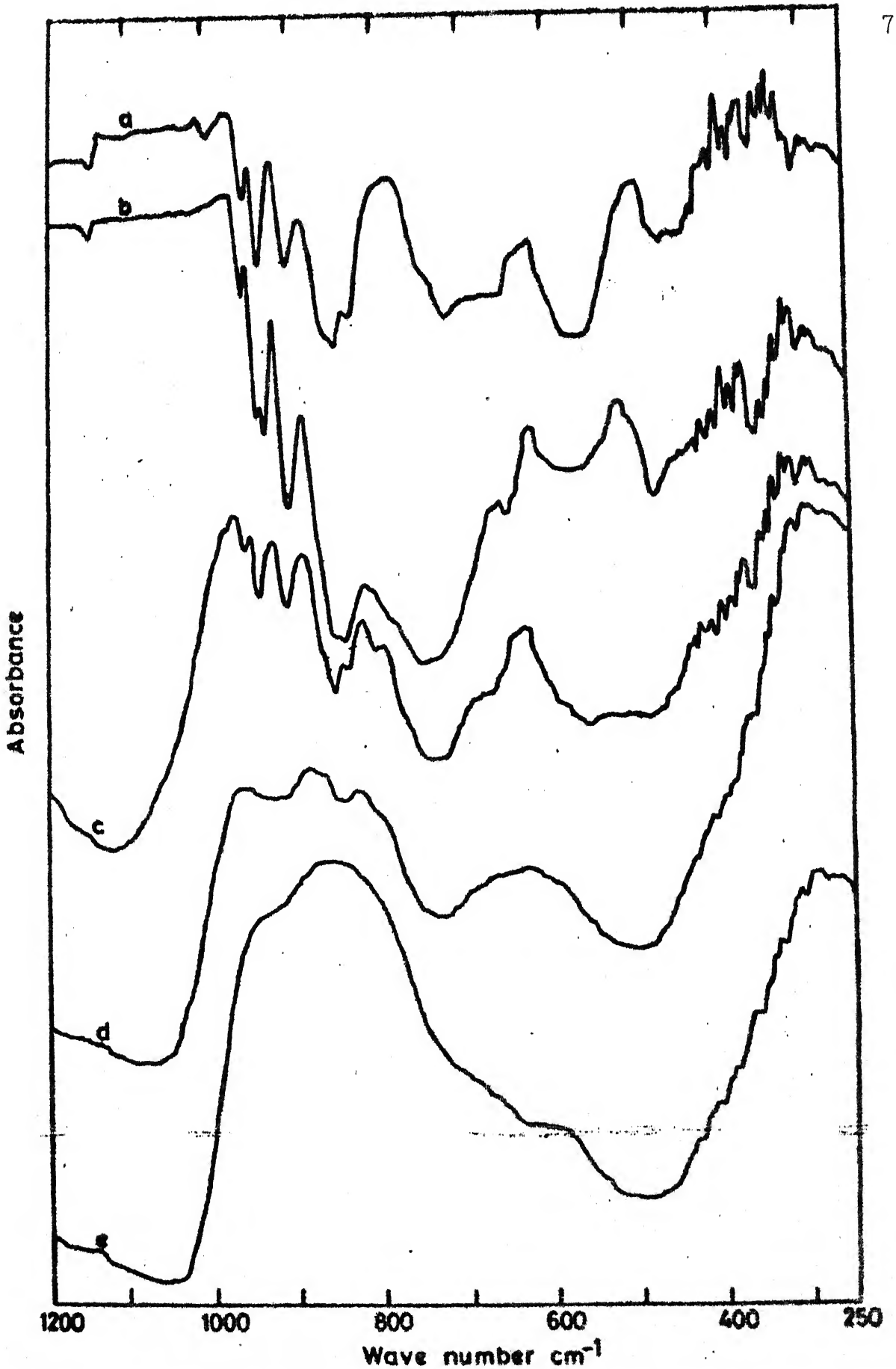

Fig. 8 : Infrared spectra of $Bi_2O_3.3MoO_3$, $Bi_2O_3.2MoO_3$ and $Bi_2O_3.2MoO_3$-$AlPO_4$ catalysts. (a) $Bi_2O_3.3MoO_3$; (b) $Bi_2O_3.2MoO_3$; (c) Catalyst 0·25 mol $Bi_2O_3.2MoO_3$ / mol o-$AlPO_4$; (d) Catalyst 0·05 mol Bi_2O_3. $Bi_2O_3.2MoO_3$ / mol o-$AlPO_4$; (e) o-$AlPO_4$.

compared to the patterns observed for $Bi_2O_3.MoO_3$ sample. Intense bands are observed 850, 725, 570 and 460 cm^{-1}. The bands occurring at 740 and 850 cm^{-1} are relegated to the stretching vibrations of $Mo-O_b$ and $Mo-O_t$ bonds. The presence of edge-shared molybdenum octahedra in the two bismuth molybdates is evidenced from the sharp bands observed in the range 900-950 cm^{-1}. A weak band observed around 995 cm^{-1} in the case of $Bi_2O_3.3MoO_3$ was due to the $Mo-O_t$ stretching vibrations of free MoO_3.

The broad bands noticed in all the bismuth molybdates in the range 400-500 cm^{-1} are attributed to the absorption by Bi_2O_3.

iii. $Bi_2O_3.MoO_3$-$AlPO_4$ Catalysts.

Figs. 7b and 7c show the ir spectra of the two catalysts with compositions 0.25 mol $Bi_2O_3.MoO_3$/mol $AlPO_4$ and 0.05 $Bi_2O_3.MoO_3$/mol $AlPO_4$ respectively. The ir spectra for these catalysts exhibit the general features of the $Bi_2O_3.MoO_3$ compound (Fig. 7a). The bands due to adsorbed water as in the case of o-$AlPO_4$ were also observed (not shown in the figure) around 1615 and 3410 cm^{-1} in the present case.

iv. $Bi_2O_3.2MoO_3$-$AlPO_4$ Catalysts.

The ir spectra of these catalysts are shown in Figs. 8c and 8d. Both spectra exhibit the general features observed in ir spectrum of $Bi_2O_3.2MoO_3$ (Fig. 8a). The absorption bands due to adsorbed moisture were also indicated at 1615 cm^{-1} and 3410 cm^{-1}.

4.7. Thermal Characteristics.

The differential thermal analyses (DTA), the thermogravimetric analyses (TGA) and the differential thermogravimetric analyses (DTGA) were carried out in order to understand the thermal stability and possible phase transitions taking place in the individual starting materials used in the preparation of the catalysts. These patterns enable 1) the location of the phase changes at different temperatures 2) determination of the transformation energies involved and 3) the modifications in the sample weights during the transformations.

The DTA, TGA and DTGA of the samples were recorded simultaneously using MOM Derivatograph (Hungary) with platinum-platinum rhodium thermocouple as the temperature sensing element. The samples were heated in an alumina crucible using $-Al_2O_3$ as the reference. The furnace heating rate was maintained constant at 5°/minute.

Differential thermal analysis has also been carried out on DUPONT 900 DTA unit fitted with 1200°C furnace assembly using Pt-Pt 13% Rh thermocouples with heating rate maintained at 12°C/minute. This has been conducted to obtain the DTA pattern on cooling, recording the curves corresponding to the reactions in the transformation region. This operation was not possible with MOM derivatograph and enables a clear understanding on the nature of the reversibility of transformations.

Results of Thermal Analyses:

1. Ortho-Aluminium Phosphate ($o\text{-}AlPO_4$).

The DTA, TGA and DTGA curves are shown in Fig. 9. The DTA curve exhibited an endotherm commencing at 60°C attaining a maximum around 120°C. This endotherm was attributed to the dehydration of aluminium phosphate. Between 120°C and 810°C, phosphate does not show any transitions [129]. The TGA and DTGA curves exhibited a weight-loss of 10 per cent in the dehydration range.

11. Bismuth Molybdates.

The DTA, TGA and DTGA curves for $Bi_2O_3.MoO_3$ are indicated in Fig. 10a. The DTA curve shows well defined endotherms with peaks at 630, 705 and 720°C in addition to the initial endothermic slope. These endotherms correspond to the structural transformation, $\gamma \rightarrow \gamma'$ where γ' is the high temperature modification of γ-bismuth molybdate. It appears from the DTA pattern that the $\gamma \rightarrow \gamma'$ transformation takes place in several steps as could be seen from these individual endotherms occurring within the temperature range of the transformation.

Heating and cooling curves indicated in Fig. 10b were obtained to understand the nature of reversibility of these transformations. It is seen from the figure that upon first heating, a large peak is observed at 686°C with a shoulder at 680°C undergoes a reduction in its area on first

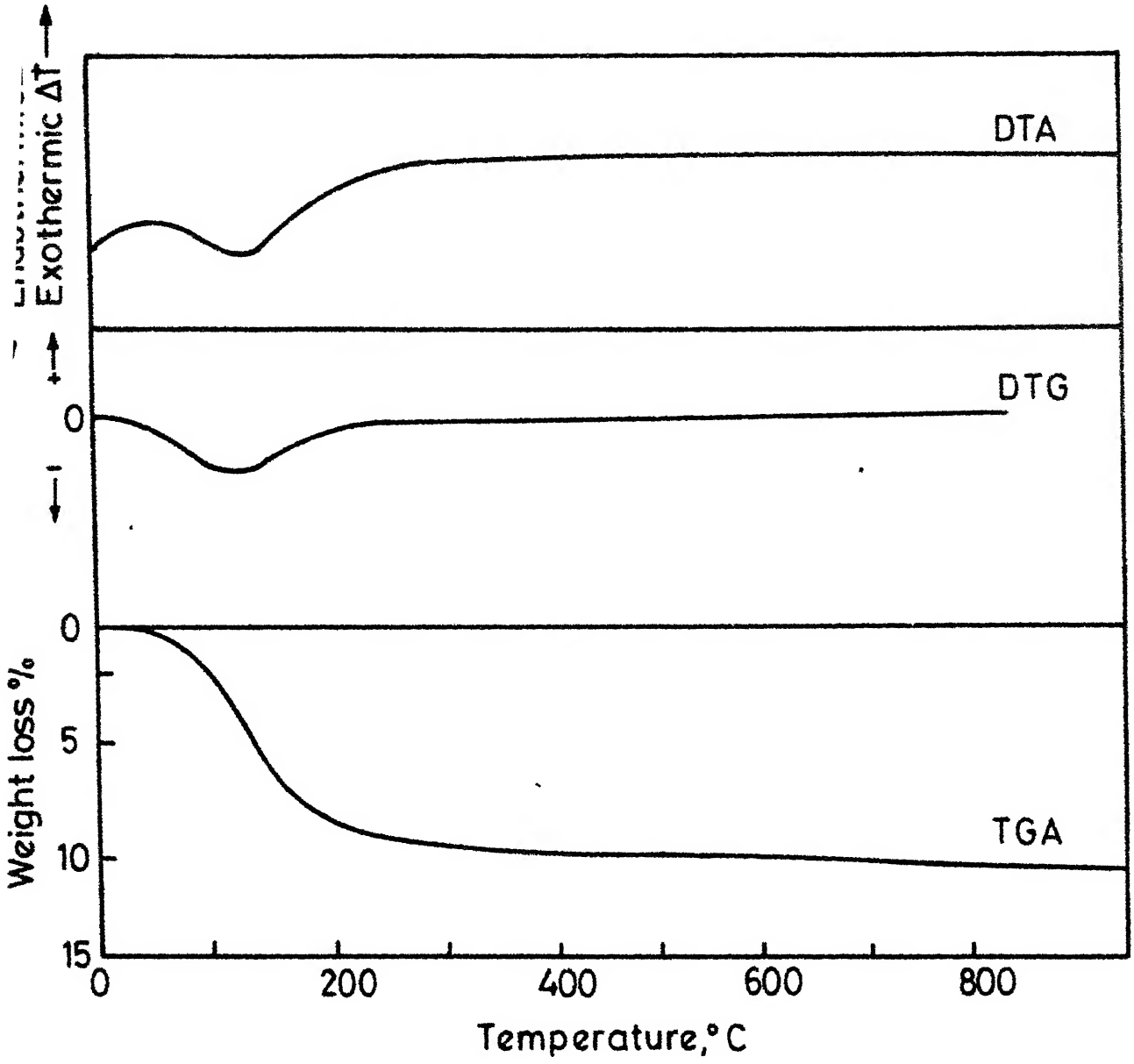

Fig. 9 : TGA, DTG and DTA curves for o-$AlPO_4$. Sample weight 356mg, heating rate 5°C/min. Reference: α-Al_2O_3.

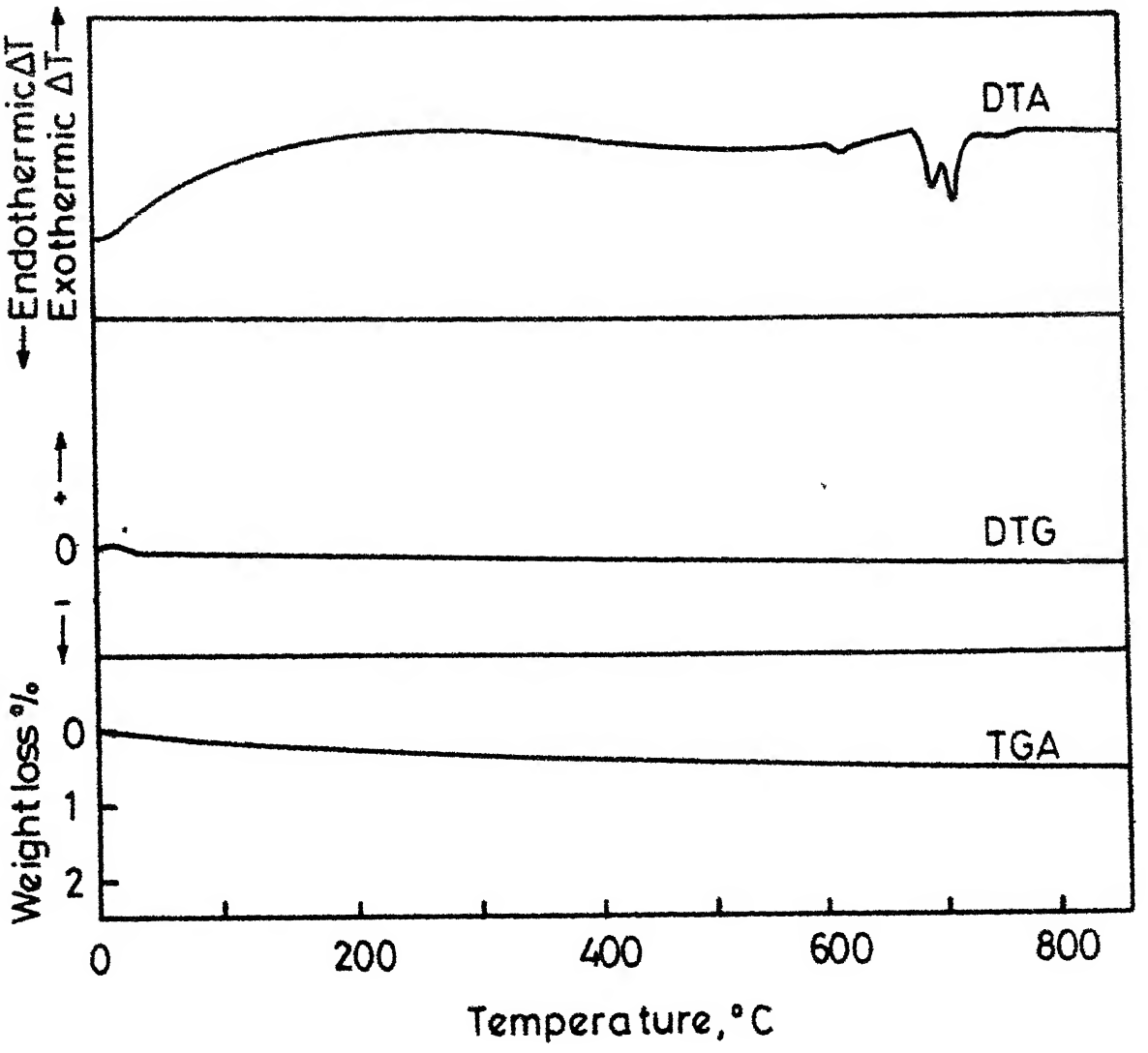

Fig. 10a: TGA, DTG and DTA curves for $Bi_2O_3.MoO_3$. Sample weight 1056 mg, heating rate 5°C/min. Reference: α-Al_2O_3.

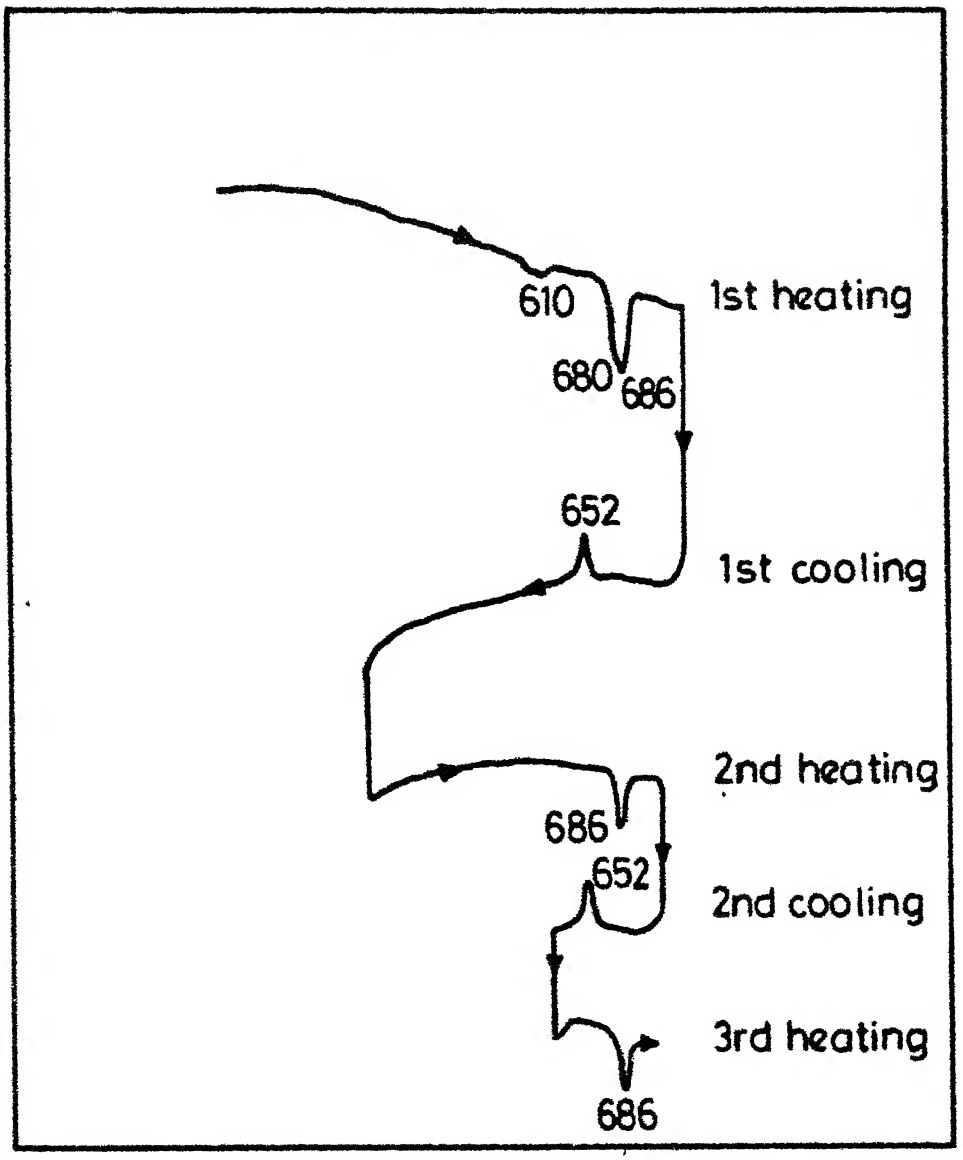

Fig. 10 b : Differential thermal pattern for $Bi_2O_3.MoO_3$ indicating the forward and backward transformations (arrows indicate heating and cooling cycles).

cooling, thus, indicating that some of the transitions observed in the first heating curve are irreversible. Repeated heating and cooling of the same sample (second heating - second cooling - third heating) showed that the areas under the peaks remained unchanged. Hence, it can be inferred that the peak at 610°C and the shoulder at 680°C are associated with the irreversible $\gamma \rightarrow \gamma'$ transition, while the peak observed at 686°C is due to the melting of γ' phase.

The TGA and DTGA curves (Fig. 10a) indicated minimal weight-loss (around 0.6%) for the sample when heated upto 800°C.

The DTA curve for the β-bismuth molybdate ($Bi_2O_3.2MoO_3$) (Fig. 11a) exhibits two endotherms. The shallow endotherm observed at 550°C is relegated to the solid-state reaction (Equation (4.1)) between α- and γ-phases present in the $Bi_2O_3.2MoO_3$ sample. An exothermic hump developing at about 650°C immediately followed by an intense endothermic peak attaining a maximum around 700°C were due to the decomposition of β-phase into α- and γ'-phases (650°C) and subsequent melting of these two phases (700°C).

The DTA pattern indicated in Fig. 11b clearly brings out the reversibility of $\alpha \rightarrow \beta + \gamma'$ transformations. In the forward run, the intense endothermic peak attained a maximum at 700°C while the corresponding cooling curve was split into two peaks with maxima at 656°C and 630°C. The 656°C peak represents solidification of α- and γ'-phases, the peak at 630°C indicates

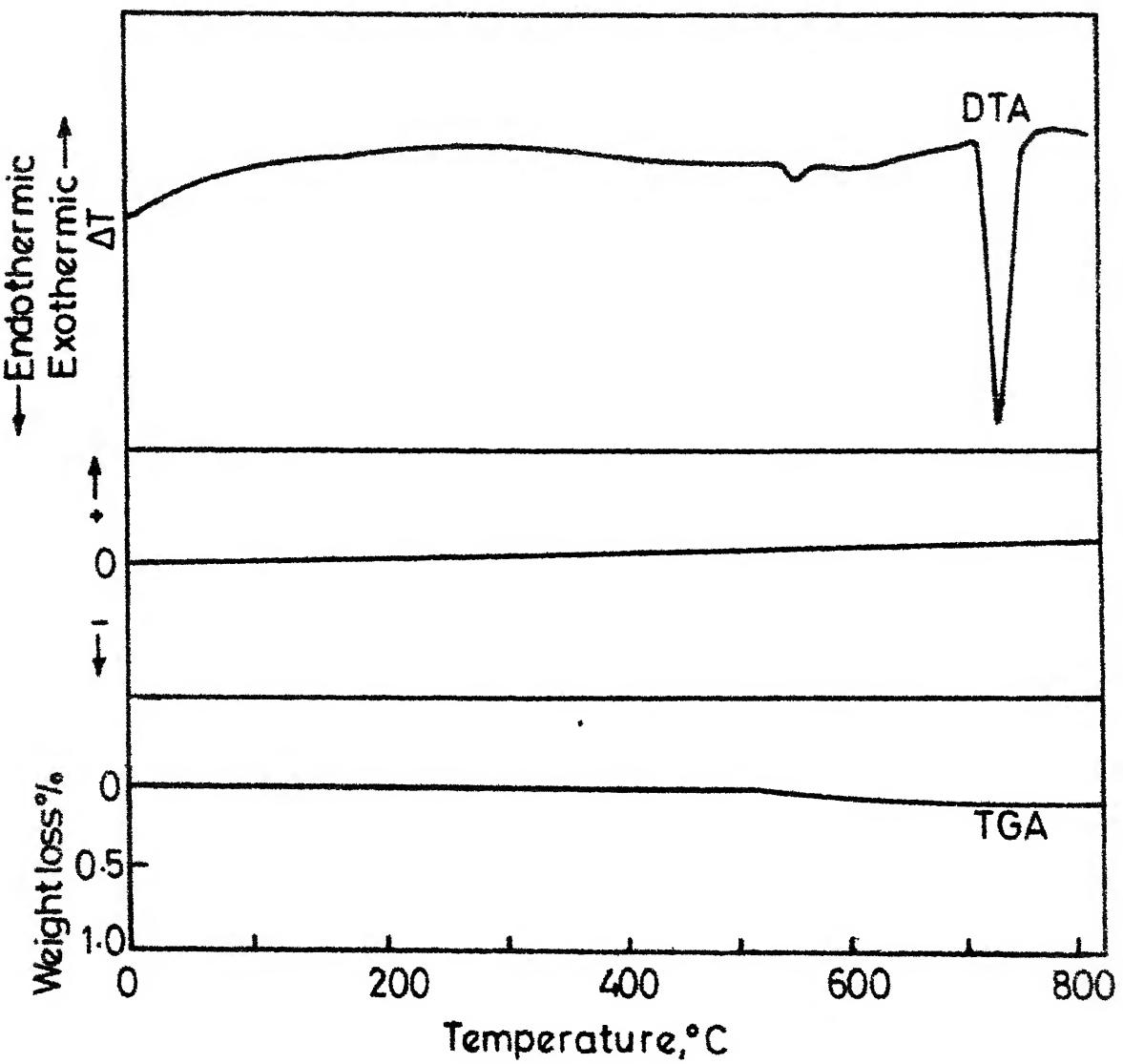

Fig. 11a : TGA, DTG and DTA curves for $Bi_2O_3.2MoO_3$. Sample weight 1130 mg, heating rate 5°C/min. Reference. α-Al_2O_3.

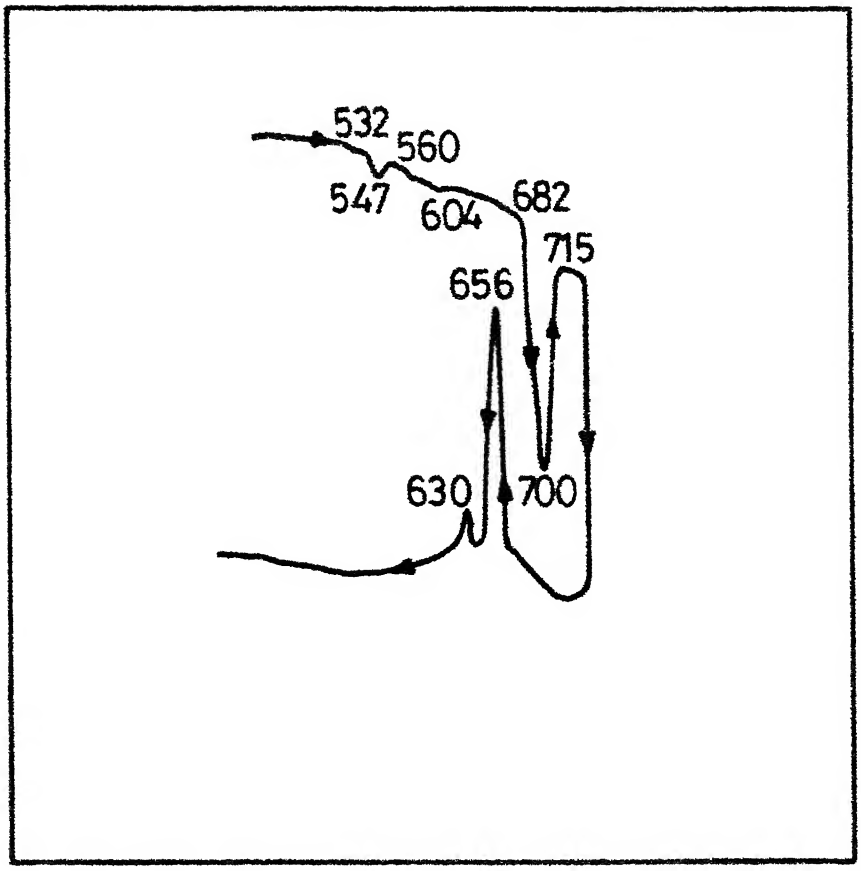

Fig.11b : Differential thermal pattern for $Bi_2O_3.2MoO_3$ indicating the forward and backward transformations (arrows indicate heating and cooling cycle).

the reversible reaction, $\alpha + \gamma' \rightarrow \beta$. Thus it can be concluded that the β-phase is not stable beyond 630°C. One conclusion is apparent at this stage, i.e., the structural transitions observed in the present case are reversible, while the same were irreversible in the case of γ-bismuth molybdate.

The TGA and DTGA indicate minimal weight-loss around 0.1% for the sample upto a temperature of 800°C (Fig. 11a). This could be due to the sublimation of molybdic oxide occluded in $Bi_2O_3.2MoO_3$ during its preparation.

iii. $Bi_2O_3.2MoO_3$-$AlPO_4$ Catalyst.

In order to understand the nature of the phase transitions undergone by the individual starting materials during calcination, the thermograms of uncalcined and calcined $Bi_2O_3.2MoO_3$-$AlPO_4$ catalysts were obtained (Figs. 12 and 13).

The DTA curves for the uncalcined as also the calcined catalysts are identical. The endothermic peak first observed at 110°C is due to dehydration. The identical nature of the two thermograms with no noticeable peaks beyond the dehydration range confirms the absence of any chemical reaction between the two starting materials, namely, $Bi_2O_3.2MoO_3$ and $AlPO_4$. It may be mentioned here that the endothermic peaks as observed in the pure bismuth molybdate sample (Fig. 11a) are not evidenced in this case since the amount of bismuth molybdate present together with $AlPO_4$ is only 4.76 per cent. As such the energies involved in the transformations would be correspondingly low with the peaks smaller than that could be noticed.

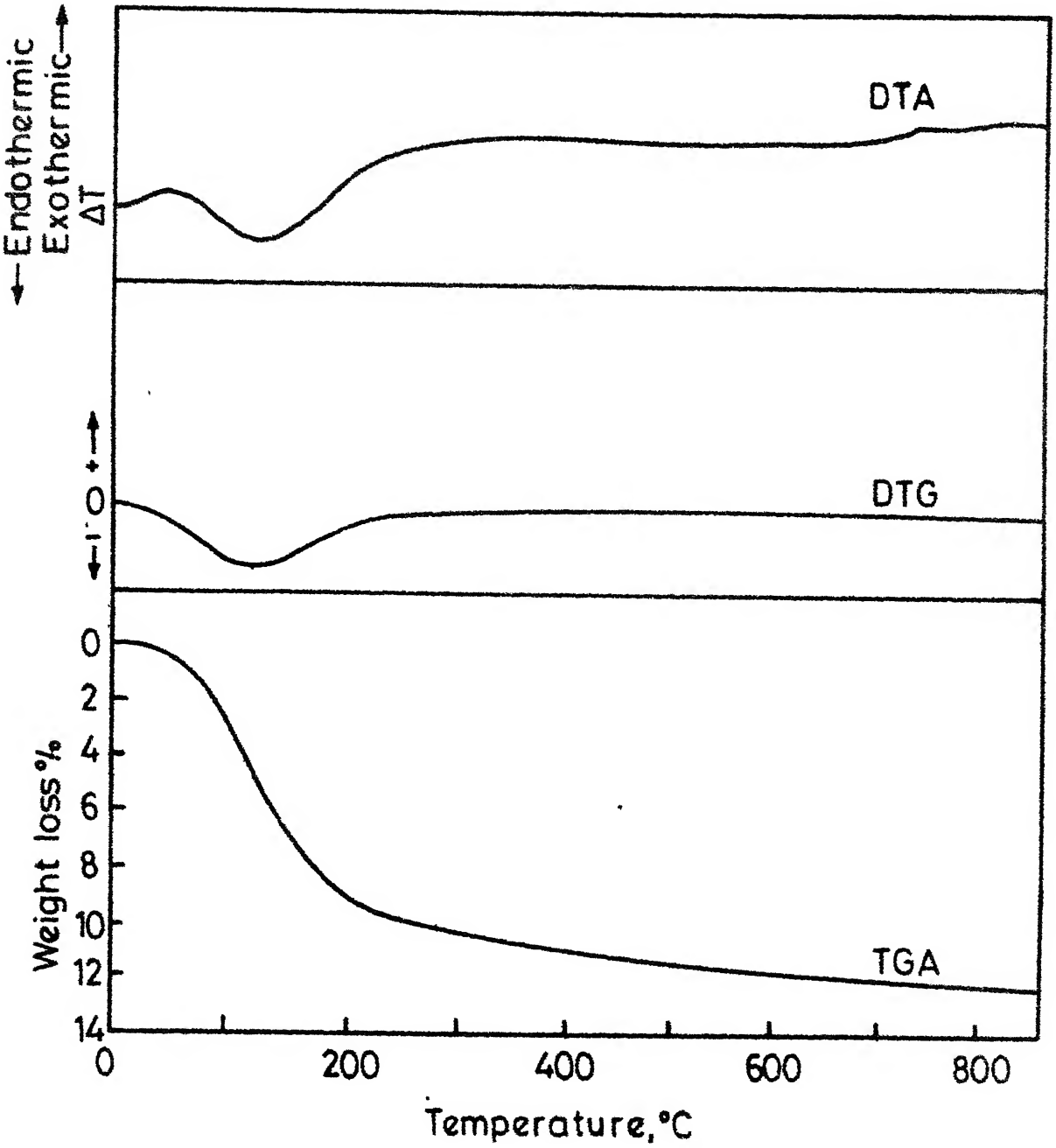

Fig. 12 : TGA, DTG and DTA curves for uncalcined Bi_2O_3. $2MoO_3$ - $AlPO_4$ catalyst. Catalyst composition 0.05 mol $Bi_2O_3 2MoO_3$ per mol o-$AlPO_4$. Sample weight 422 mg, heating rate 5°C/min. Reference : α-Al_2O_3.

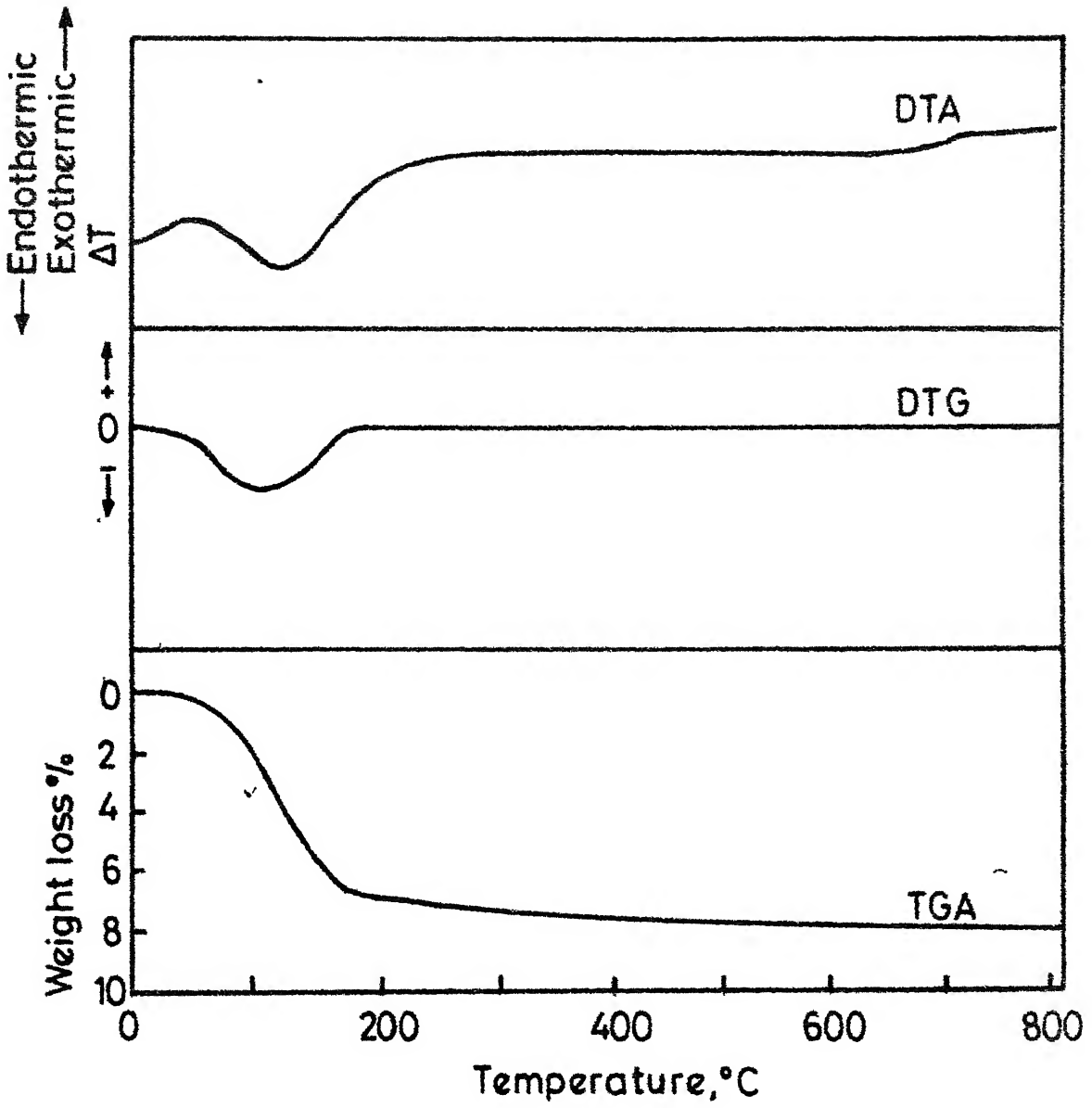

Fig. 13 : TGA, DTG and DTA curves for calcined Bi_2O_3. $2MoO_3$-$AlPO_4$ catalyst. Catalyst composition 0.05 mol $Bi_2O_3.2MoO_3$ per mol o-$AlPO_4$. Sample weight 424 mg, heating rate 5°C/min. Reference : α-Al_2O_3.

The TGA and DTGA curves indicated a weight-loss of about 12% in the case of uncalcined catalyst sample. This loss corresponds to the dehydration of the aluminium phosphate present in the sample. The patterns for the TGA and DTGA curves in the case of calcined samples, although similar in trend to the corresponding uncalcined samples, exhibited relatively lower weight-loss (8%).

4.8. Discussions and Conclusions.

Aluminium phosphate, bismuth molybdates and the bismuth molybdate-aluminium phosphate catalysts have been characterised in detail using X-ray diffraction, infrared spectra and thermal analysis techniques. The bulk density and the surface area measurements have been carried out on the starting materials as also the catalysts.

The X-ray diffraction studies for ortho-aluminium phosphate indicated its amorphous nature, making it difficult to establish its structure. However, the infrared spectra revealed that the phosphorous in the same was tetrahedrally coordinated to the surrounding oxygen atoms. Considering the fact that aluminium phosphates are iso-structurals with silica [127] it can be stated that the prepared aluminium phosphate had a network structure similar to that of $Si(SiO_4)$ network with both aluminium and phosphorous surrounded by tetrahedra of oxygen atoms.

X-ray diffraction studies for γ-bismuth molybdate ($Bi_2O_3.MoO_3$) established that its structure was analogous to the structure of mineral koechlinite. The infrared spectra of the same indicated the presence of corner-shared molybdenum octahedra with terminal oxygen bonded to only one molybdenum atom (inferred from the band at 850 cm^{-1}). Such oxygen sites are indicative of an active dehydrogenation catalyst [18, 90a]. X-Ray diffraction and infrared studies of $Bi_2O_3.MoO_3$-$AlPO_4$ catalysts indicated that the calcination of $Bi_2O_3.MoO_3$ together with $AlPO_4$ did not bring about any changes in its structure. However, the thermal analyses revealed that the $Bi_2O_3.MoO_3$ undergoes a phase transition, $\gamma \rightarrow \gamma'$, at temperatures of 630°C and above. This phase transition is irreversible and results in a loss of catalytic activity [18, 90a].

X-Ray diffraction studies for the β-bismuth molybdate ($Bi_2O_3.2MoO_3$) indicated the presence, in restricted quantities, of α- and β-bismuth molybdates. The infrared spectra also confirmed the presence of α-phase in the prepared $Bi_2O_3.2MoO_3$ from the occurrence of sharp bands in the range of 900-950 cm^{-1} (characteristic of α-bismuth molybdate). The DTA analysis indicated that these α- and γ-bismuth molybdates recombined at a temperature of 550°C. The DTA analysis also indicated that the thermal decomposition experienced by β-bismuth molybdate above 630°C was of reversible nature.

The X-ray diffraction studies evidenced that the calcination of $Bi_2O_3.2MoO_3$ with o-$AlPO_4$ resulted in the inhibition of the decomposition of γ-bismuth molybdate into α- and γ-phases. Similar observations were reported by Batist et.al. [16] in the case of $Bi_2O_3.2MoO_3$/silica gel catalysts. It may be stated that the ortho-aluminium phosphates are iso-structurals with one or more forms of silica having a direct parallelism between all crystalline modifications of $AlPO_4$ and SiO_2 [127]. The DTA analyses of the uncalcined and the calcined $Bi_2O_3.2MoO_3$-$AlPO_4$ indicated no reaction between the two constituents. This was also confirmed in the infrared analyses.

In the case of α-bismuth molybdate ($Bi_2O_3.3MoO_3$) the X-ray diffraction data indicated that the compound has a monoclinic structure. In addition, the X-ray results have also revealed that the calcination of $Bi_2O_3.3MoO_3$ together with $AlPO_4$ did not bring about any changes in its structure. Since the monoclinic structure of $Bi_2O_3.3MoO_3$ results in edge-sharing molybdenum octahedra, this compound was not considered as a good dehydrogenation catalyst [18].

The absence of any thermal transition in the normal temperature range (400-500°C) experienced in the oxidative dehydrogenation of butane and butenes suggests that both $Bi_2O_3.MoO_3$-$AlPO_4$ are potential catalysts for the oxidative dehydrogenation of butane.

CHAPTER 5

STUDIES ON BISMUTH MOLYBDATE-ALUMINIUM PHOSPHATE CATALYSTS USING RESPONSE SURFACE METHODOLOGY

5.1. Introduction.

Meagre information seems to be available in literature on the oxidative dehydrogenation of butane. In the present investigation, in which the suitability of Bismuth Molybdate-Aluminium Phosphate as a catalyst has been studied, the chemical process has been treated as a black box and its input-output relationships were studied using response surface methodology. The inputs to the black box were the experimental variables like the temperature of reaction, contact time, butane-oxygen ratio, oxygen-nitrogen ratio, composition of catalyst, method of catalyst preparation etc. The output of the black box could be the selectivity or the yield of any particular product and the like. Choice of the response and the independent variables has been discussed in Section 5.5. An introduction to the response surface methodology is given below.

5.2. Response Surface Methodology.

Let y be the response of a chemical process dependent on the levels of k quantitative factors or process variables x_1, x_2, ..., x_k which can be precisely measured and controlled.

The model for the u^{th} combination of factor levels is given by,

$$y_u = \phi(x_{1u}, x_{2u}, \ldots, x_{ku}) \qquad u = 1, 2, \ldots, N \qquad (5.1)$$

where N is the number of experiments and ϕ is the functional relationship. It is further assumed that the response y_u has a mean $\bar{y}_u$ and variance σ^2.

A geometrical portrait of the response function in the factor space is called a response surface.

The experimental region R, is a bounded subspace of the whole factor space. R is bounded because of practical limitations. The response surface methodology deals with the problem of locating a point $(x_1^o, x_2^o, \ldots, x_k^o)$ within R at which y is an extremum [3, 29, 31, 32, 38, 40, 59]. The response surface methodology, originally introduced by Box and Wilson [31], is essentially applied in two stages in order to find the optimum conditions. The two stages are termed the first-order strategy and the second order strategy respectively. The methodology is applied as follows:

After conducting preliminary experiments using any suitable experimental design, a hyper-planar surface is fitted to the response data, and the adequacy of the model is tested. The direction of steepest ascent/descent is established and the factor level combinations lying along this direction are computed. Experiments will have to be performed at these factor levels to verify the predicted value of the response. One of these factor level combinations is chosen as a base level

for the next experimental design and then the experiments are performed around these chosen base levels. The whole procedure is repeated till a near-stationary region is reached where the hyper-planar approximation of the response surface is no more valid (i.e. the first order strategy fails). Thereupon, a second order strategy is employed in which the interactions and the higher order effects of the various factors (i.e. non-linearity) are determined by augmenting the experimental design.

The traditional one factor-at-a-time method, where the experiments are carried out holding all the factors constant except the one under consideration, often fails to locate the true optimum [31].

The response surface methodology cuts down experimental efforts by making use of experimental designs which permit the experimenter to assess the strength of the interactions between the various factors while varying them simultaneously [38]. In the following section, the results of the feasibility studies of the oxidative dehydrogenation of butane are presented.

5.3. Molybdic Oxide-Aluminium Phosphate Catalyst – A Feasibility Study.

Exploratory work of Gaspar and Pasternak [50] indicated that molybdic oxide-aluminium phosphate catalysts could dehydrogenate n-butane to 1, 3-butadiene in the presence of oxygen. Since the aim of the present investigation was to dehydrogenate n-butane to 1, 3-butadiene in one step,

experiments were first conducted using the molybdic oxide-aluminium phosphate (MoO_3-$AlPO_4$) catalyst prepared in the laboratory. This gave an estimate of the molybdic oxide content of the bismuth molybdate-aluminium phosphate catalysts subsequently tested.

MoO_3-$AlPO_4$ catalysts prepared according to the procedure of Section 3.4 were used in the preliminary experiments. The catalyst composition was varied from 0 to 0.3 mol MoO_3/mol $AlPO_4$. The experiments were conducted at the following levels of the variables:

Temperature	...	550, 600°C
Catalyst-feed ratio	...	0.75, 1.25 g/(mgmol/minute)
Butane-oxygen ratio	...	1:1
Diluent	...	Nil

Experimental data are presented in Appendix VII, for runs numbered 1 through 21. The results are shown graphically in Figs. 14 through 21.

The overall conversion of n-butane over varying catalyst composition is shown in Fig. 14. Catalyst compositions of 0.15 mol MoO_3/mol $AlPO_4$ and above seem to have very little influence on the overall conversion of butane. The effect of the molybdic oxide-aluminium phosphate ratio on the yields of 1, 3-butadiene, 1-butene, propylene and ethylene are shown in Figs. 15 through 18. These figures show that the individual yields of olefins and diolefins pass through a maximum at a

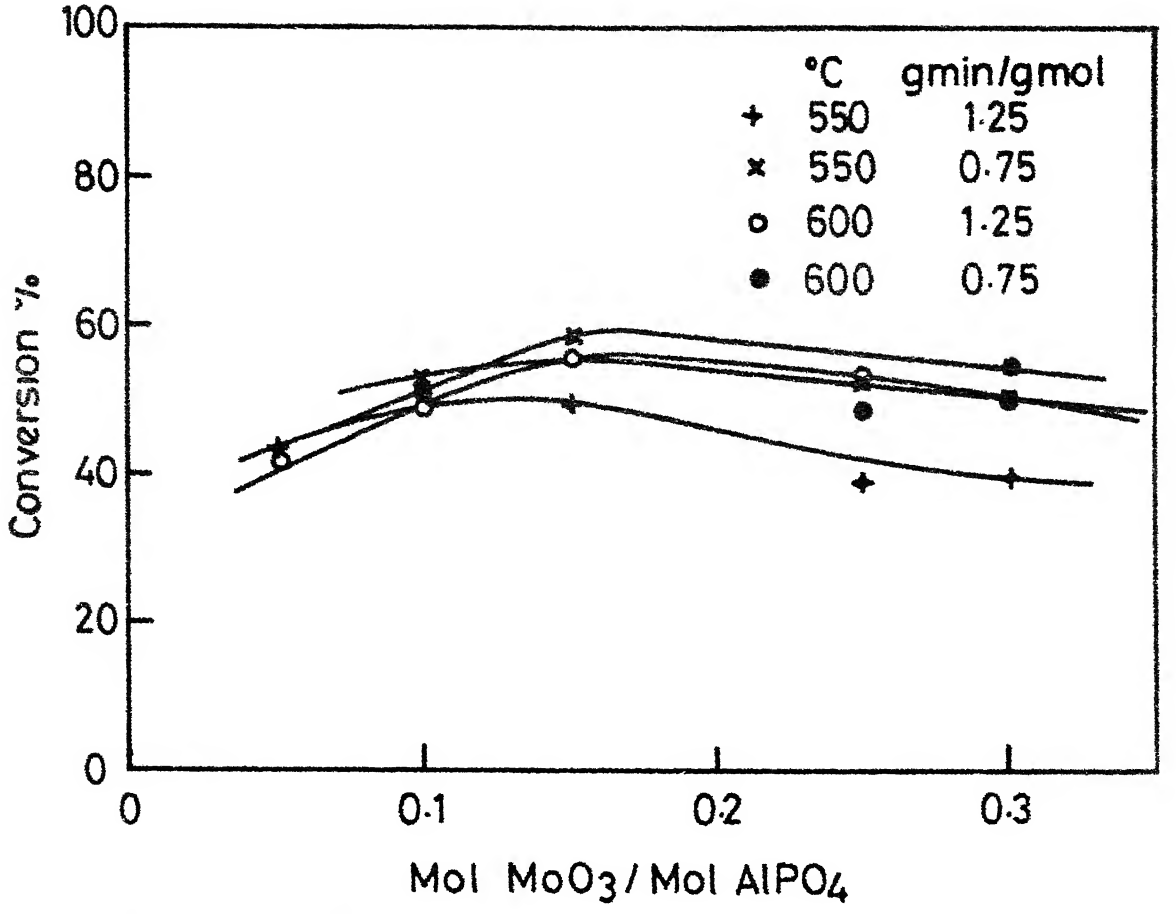

Fig. 14 : Molybdic oxide-aluminium phosphate catalyst: overall conversion.

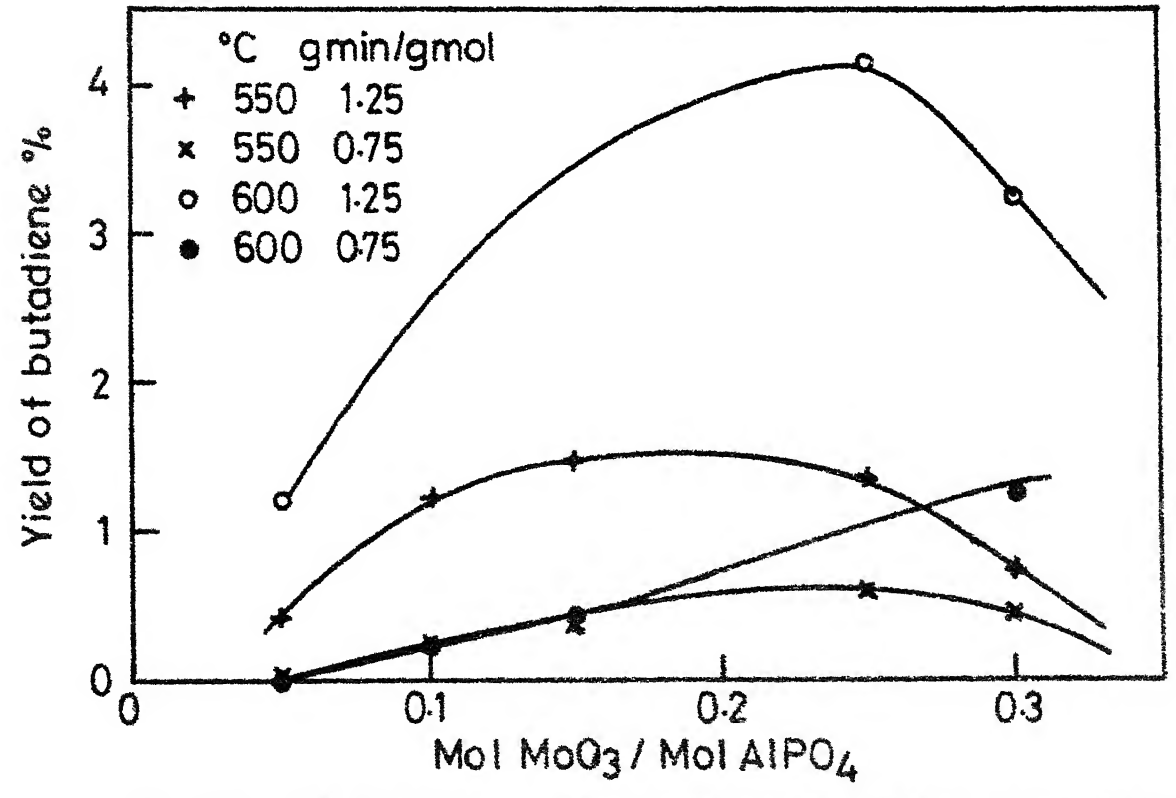

Fig. 15 : Molybdic oxide-aluminium phosphate catalyst;

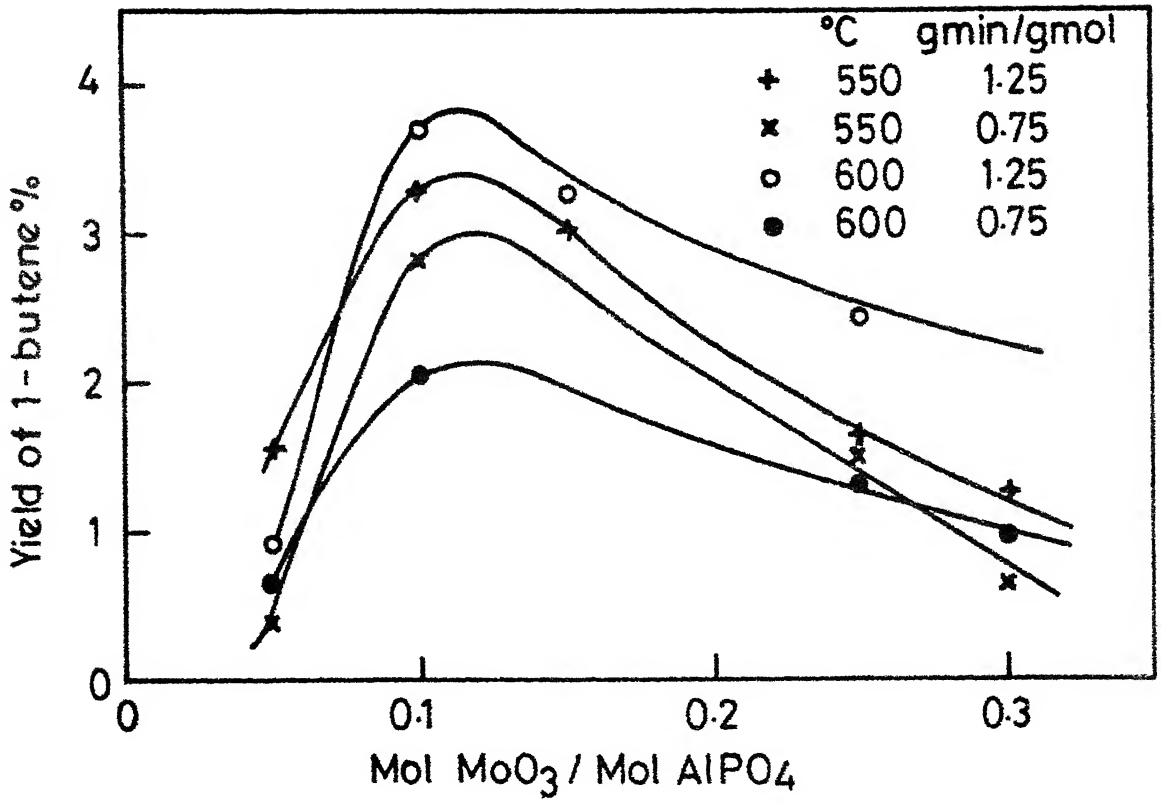

Fig. 16 : Molybdic oxide-aluminium phosphate catalyst: 1-Butene yield.

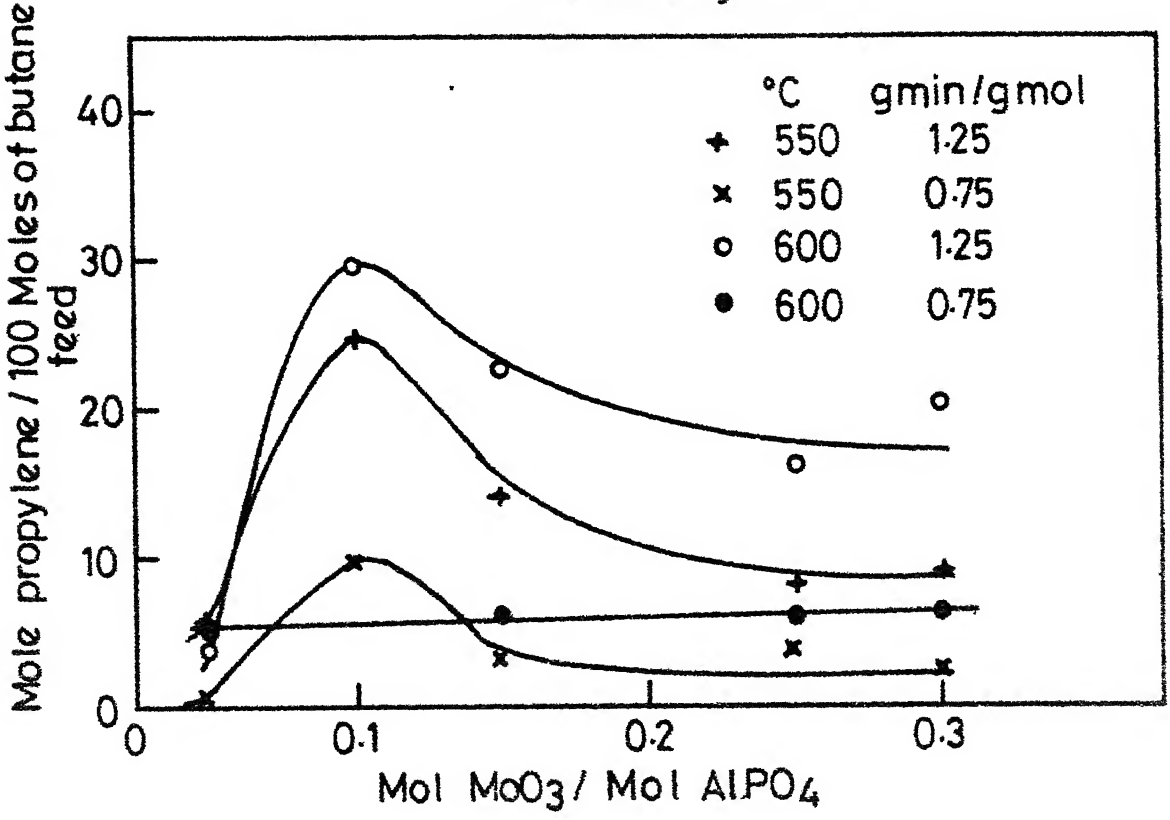

Fig. 17 : Molybdic oxide-aluminium phosphate catalyst· Propylene yield.

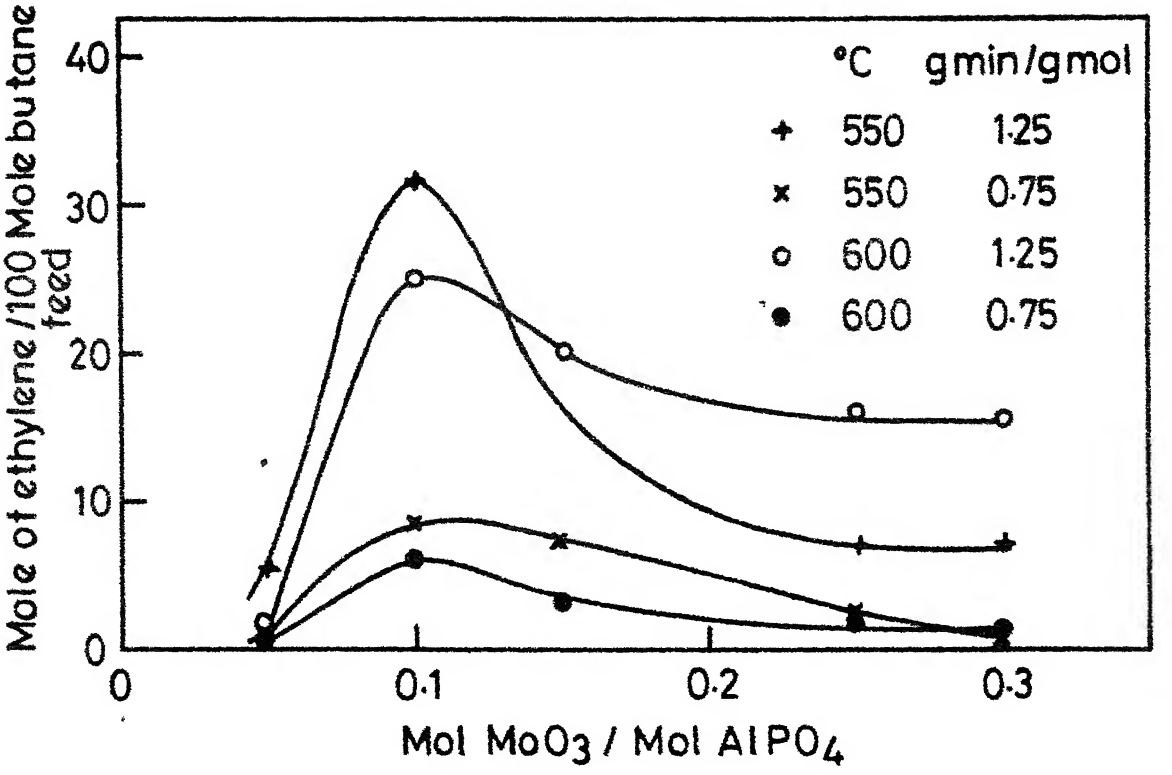

Fig. 18 : Molybdic oxide-aluminium phosphate catalyst: Ethylene yield.

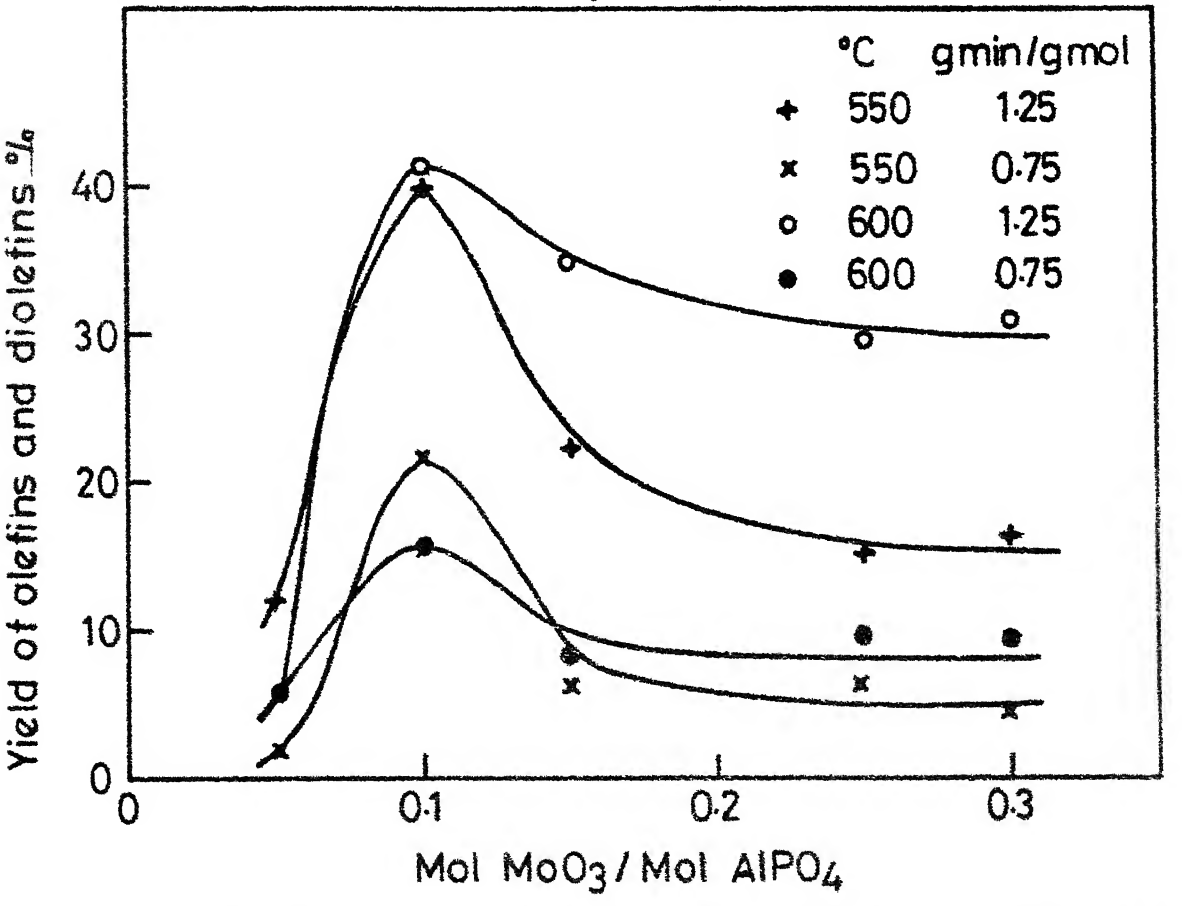

Fig. 19 : Molybdic oxide-aluminium phosphate catalyst:

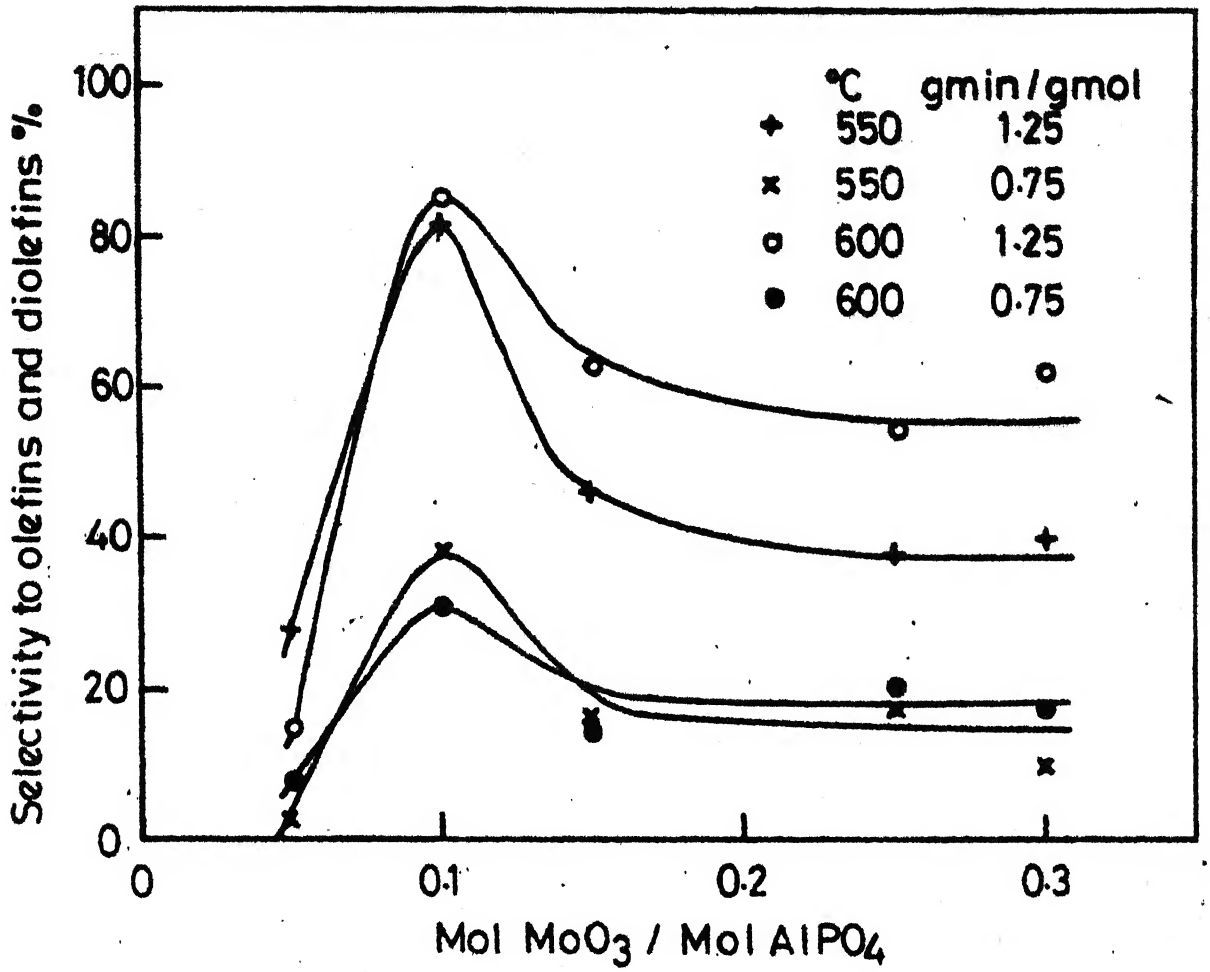

Fig. 20 : Molybdic oxide-aluminium phosphate catalyst: Selectivity to olefins and diolefins.

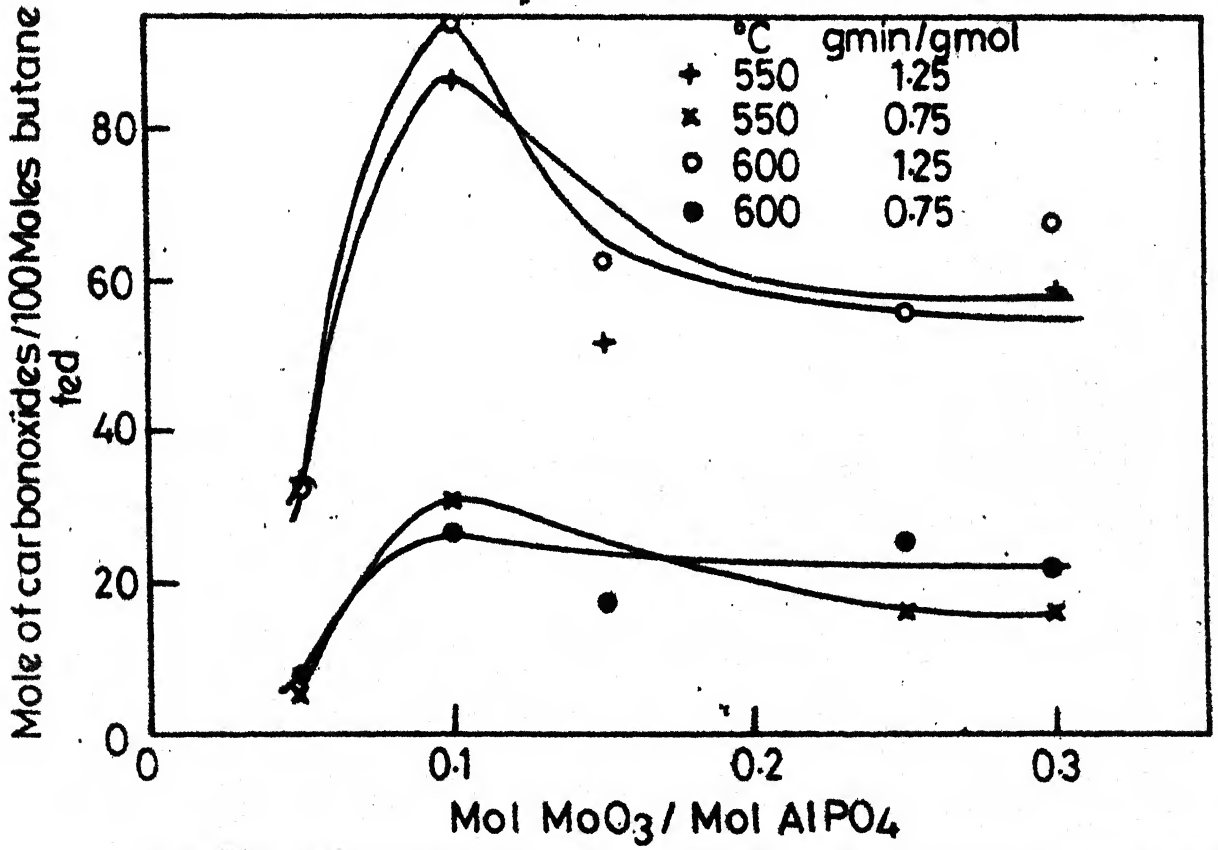

Fig. 21 : Molybdic oxide-aluminium phosphate catalyst: Formation of carbon oxides.

catalyst composition of about 0.1 mol MoO_3/mol $AlPO_4$. Figs. 19 and 20 show that the peak selectivity to total olefins and diolefins together with their peak yield occurs around the same catalyst composition.

These results show that the best catalytic activity in the case of MoO_3-$AlPO_4$ catalyst occurred at a catalyst composition of 0.1 mol MoO_3/mol $AlPO_4$. However, the activity of the catalyst for the formation of undesired products like CO and CO_2 (shown in Fig. 11) is also the highest at the same catalyst composition.

The following sections are devoted to the enhancement of (butene + butadiene)yield by experimenting on the constituent elements of the catalyst and the process variables affecting the oxidative dehydrogenation.

5.4. Studies on Bismuth Molybdate-Aluminium Phosphate Catalysts.

Having established the feasibility of the one-step oxidative dehydrogenation of n-butane to 1, 3-butadiene, attempts were made to improve the gross yield of butenes and butadiene by incorporating bismuth in the catalyst. Bismuth oxide when present together with molybdic oxide enhances the selectivity of butene to butadiene reaction. Hence the oxidative dehydrogenation of butane was further investigated over bismuth molybdate-aluminium phosphate catalysts. Bismuth molybdate catalysts were prepared according to the procedures

outlined in Section 3.5. The different factors affecting the oxidative dehydrogenation process are analysed in the following section.

5.4.1. Identification of Factors and the Experimental Region.

Preliminary experiments (not reported herein) showed that for the reactor diameter used and the operating conditions chosen, catalyst dilution was not necessary. A catalyst particle size range of 1-2 mm was used throughout the investigation.

Preliminary experiments also indicated that air enriched in oxygen was needed to get enhanced yield of butadiene. Further, in order to reduce the experimental effort, the oxygen-nitrogen ratio was kept constant at 0.5.

Of the numerous factors affecting the process, the following four were considered to be the most important:

1. Reaction temperature.
2. Catalyst-feed ratio.
3. Butane-oxygen ratio.
4. Composition of the catalyst.

The range of experimentation is chosen based on the following considerations:

(1) Reaction Temperature: The lower limit of the reaction temperature was fixed at 400°C, since at temperatures of 350°C and below, oxygenated products like alcohols are reported to be formed in preference to dehydrogenated products [53].

The upper limit was set at 500°C since the bismuth molybdate catalysts tend to loose their activity above 500°C [53].

(2) Catalyst-Feed Ratio: The catalyst-feed ratio (W/F) was chosen in the range of 0.3-2.6 g catalyst/(mgmol/minute). This was equivalent to a contact time of about 0.25-2 seconds, a range normally used in practice.

(3) Butane Oxygen Ratio: The choice of butane-oxygen ratio was governed by the explosion range of the butane-air mixture. The explosition range of butane is 1.9-8.5 vol % in air [86]. Therefore, any butane-air mixture having a butane to oxygen ratio between 0.092 and 0.445 is explosive and hence cannot be used in the experiments.

At butane to oxygen ratios of 0.09 and less, oxygenated compounds tend to dominate the product stream [53, 61]. The upper limit of butane to oxygen ratio was fixed at 2.0 since at very low oxygen concentrations, bismuth molybdate tends to deactivate rapidly due to the loss of lattice oxygen.

(4) Composition of the Catalyst: The bismuth molybdate-aluminium phosphate catalysts were prepared with different proportions of bismuth molybdate to aluminium phosphate. The composition of bismuth molybdate was also treated as a variable, since bismuth molybdates of different phase compositions show good activity for the oxidation dehydrogenation of butanes [53, 61, 104, 115].

Two phases of bismuth molybdates, namely, β- and γ- with compositions $Bi_2O_3.2MoO_3$ and $Bi_2O_3.MoO_3$ respectively were used in the present experiments. Structural studies of the bismuth molybdates discussed in Chapter 4 concluded that α-bismuth molybdate ($Bi_2O_3.3MoO_3$) with its edge shared MoO_6 octahedra structure was likely to be less active compared to the β- and γ-phases. Moreover, the catalyst grannules of $Bi_2O_3.3MoO_3$-$AlPO_4$ catalyst were very friable. Hence this catalyst was not used in the present study.

The β- and γ-phases of bismuth molybdates were treated as qualitative variables in the present response surface strategy. The nature of the qualitative variable demands that the strategy has to be applied in parallel for these two phases. Therefore, experiments were conducted side-by-side on these two phases in the linear region of the response surface in order to locate the best possible values of the optimisation factor (to be defined in the following section) obtainable on them. Once the approximate extrema were located, a decision was taken, as to which of the qualitative factors should be used in the second order strategy.

The ranges of experimentation for the various factors used in the present study are summarised in Table 14. The choice of the optimisation parameter is discussed in the following section.

Table 14. EXPERIMENTAL REGION OF FACTORS USED IN THE STUDY OF OXIDATIVE DEHYDROGENATION OF BUTANE

S.No.	Factor	Code Name	Experimental Region
1.	Temperature	x_1	400-500°C
2.	Catalyst-feed ratio, W/F	x_2	0.3-2.6 g-minute/mol
3.	Butane-oxygen ratio	x_3	0.5-2.0
4.	Catalyst composition (mol bismuth molybdate per 100 mol aluminium phosphate)	x_4	0.0 and above
5.	Phase of bismuth molybdate	-	β-bismuth molybdate ($Bi_2O_3.2MoO_3$) γ-bismuth molybdate ($Bi_2O_3.MoO_3$)

Oxygen consumption was an important variable as it would determine the total volume of gases to be handled in the up-stream and down-stream units of an actual chemical plant. In the present study, it was observed that the oxygen consumption was always almost complete and hence it could not be considered as an optimisation parameter.

Based on the above considerations, the total yield of (butenes + butadiene)was chosen as the optimisation parameter (response) in the present investigation.

5.4.3. Selection of an Experimental Design.

A 2^{k-1} fractional factorial design was used in the present study. According to this design, 8 experiments had to be performed for each qualitative variable. The fractional factorial design reduces the amount of experimentation without loosing at the same time the advantages of symmetry, orthogonality, normalisation and rotatability required of a good experimental design [38]. The details regarding the fractional factorial design are given in the following sections.

5.5. First Order Response Surface Strategy: Application of Steepest Ascent to Move to a Near-Stationary Region.

Having defined the factors governing the process and the process response to be optimised, a base level had to be chosen within the experimental region of the factor space, R. This experimental region has already been given in Table 14.

The base level should be the combination of factor levels corresponding to the best conditions determined from an analysis of the a-priori information.

Further, the variation interval for each factor had to be chosen. The variation interval of a factor when added or subtracted from the base level gives the upper or the lower level of the factor respectively.

To simplify the recording conditions of an experiment, and the processing of the experimental data the values of the factors were coded as follows:

$$x_j = \frac{\tilde{x}_j - \tilde{x}_{j0}}{v_j} \qquad j = 1, 2, \ldots, k \qquad (5.2)$$

where

x_j is the coded value of the j-th factor.

$\tilde{x}_j$ is the natural value of the j-th factor.

$\tilde{x}_{j0}$ is the natural value of the base level.

v_j is the variation interval of the j-th factor.

Conventionally, the coded value of the upper level corresponds to +1, the lower level to -1 and the base level to 0.

The first order approximation of the response surface resulted in the simplification of the functional form of ϕ in Equation (5.1) to the linear form,

$$y = b_0 + b_1x_1 + b_2x_2 + b_3x_3 + b_4x_4 \qquad (5.3)$$

where b_1, b_2, b_3 and b_4 are the coefficients associated with the factors x_1, x_2, x_3 and x_4 respectively. The above

coefficients together with b_o were evaluated experimentally. The experiments were performed according to a 2^{4-1} fractional factorial design [38] shown in Table 15.

In this design, the experimental levels of factor x_4 were generated using the relation,

$$x_4 = x_1x_2x_3 \tag{5.4}$$

Such a design gave the product $x_1x_2x_3x_4 = +1$. This product is called the defining contrast. Which effect is confounded with which interaction, was calculated from the defining contrast [38]. For the above design the confounding pattern may be seen to be,

$$\begin{aligned} \underline{1} &= \underline{234} \\ \underline{2} &= \underline{134} \\ \underline{3} &= \underline{124} \\ \underline{4} &= \underline{123} \\ \underline{12} &= \underline{34} \\ \underline{13} &= \underline{24} \\ \underline{23} &= \underline{14} \end{aligned} \tag{5.5}$$

This means that the main effect of variable x_1 was confounded with the interaction of the variables 2, 3 and 4 (i.e. $x_2x_3x_4$) and so on. The estimates b_1, b_2, b_3 and b_4 will be the estimates of their true values provided the third order interactions of the effects are negligible.

The coefficients b_o, b_1, b_2, b_3 and b_4 can be estimated in the least squares sense as,

Table 15. DESIGN MATRIX FOR 2^{4-1} FRACTIONAL FACTORIAL EXPERIMENT

Design Trial No.	x_o *	x_1	x_2	x_3	x_4 ($= x_1x_2x_3$)	Response y
1	+1	-1	-1	-1	-1	y_1
2	+1	+1	-1	-1	+1	y_2
3	+1	-1	+1	-1	+1	y_3
4	+1	+1	+1	-1	-1	y_4
5	+1	-1	-1	+1	+1	y_5
6	+1	+1	-1	+1	-1	y_6
7	+1	-1	+1	+1	-1	y_7
8	+1	+1	+1	+1	+1	y_8

* x_o is a dummy variable bearing a constant value of +1.

$$\hat{\underline{b}} = (\underline{x}^T \underline{x})^{-1} \underline{x}^T \underline{y} \qquad (5.6)$$

where $\underline{x}$ is the design matrix, $\underline{y}$ is the vector of observed yields and $\hat{\underline{b}}$ is the vector of coefficients. In the case of present experimental design, $\hat{\underline{b}}$ can be alternatively calculated from the equation,

$$\hat{b}_j = \frac{\sum_{i=1}^{N} x_{ij} y_i}{\sum_{i=1}^{N} x_{ij}^2}, \qquad j = 1, 2, \ldots, k \qquad (5.7)$$

The first-order strategy was applied till such time the Equation (5.3) described the yield-response surface within experimental errors. This was verified by testing the adequacy of the model and the significance of coefficients describing the model.

Adequacy of the Model: The experimental variance of the optimisation factor, s_y^2 was compared with the variance of adequacy of the model, s_{ad}^2 (defined below) by constructing an F test [60]. The test is described below.

The experimental error variance of the optimisation parameter was calculated using the formula,

$$s_y^2 = \frac{\sum_{q=1}^{n} (y_q - \bar{y})^2}{n - 1} \qquad (5.8)$$

where,

s_y^2 is the variance of the optimisation parameter; n is the number of repeat observations, $\bar{y}$ is the mean value of the repeat observation. The variance of adequacy of the model s_{ad}^2 was calculated as,

$$s_{ad}^2 = \frac{\sum_{i=1}^{N} (\hat{y}_i - y_i)^2}{N - (k + 1)} \qquad (5.9)$$

where,

s_{ad}^2 is the variance of adequacy of the model

$\hat{y}_i$ is the predicted value of the optimisation parameter.

Equation (5.3) was used to calculate the predicted values of the total yield of (butene + butadiene). The adequacy of the model represented by Equation (5.3) was tested by constructing the Fisher ratio (F test) as,

$$F_{calc} = \frac{s_{ad}^2}{s_y^2} \qquad (5.10)$$

The model was deemed inadequate if,

$$F_{calc} > F_{0.05}(N - (k+1), n - 1)$$

where,

$F_{0.05}(N - (k+1), n - 1)$ is the tabulated value of F at a significance level of 0.05 with N - (k+1) degrees of freedom (d.f.) in the numerator and n-1 degrees of freedom in the denominator. The tabulated values of F are found in most books on statistics [60].

Significance of the Coefficients: Significance of each coefficient was tested by constructing the confidence intervals [3, 129]. First the variance $s^2_{b_j}$ of the regression coefficient b_j was calculated as,

$$s^2_{b_j} = \frac{s^2_y}{N} \tag{5.11}$$

The confidence interval, Δb_j was then calculated as,

$$\Delta b_j = \pm t_{0.05}\, s_{b_j} \tag{5.12}$$

where,

s_{b_j} is the standard deviation of the regression coefficient.

$t_{0.05}$ is the tabulated value of the "student's t" at 5% significance level and n-1 degrees of freedom [60].

When some coefficients of a model were not significant, the variation intervals of the factors associated with these coefficients are increased in order to test whether these coefficients are really not significant. If they are still found to be not significant, then the terms associated with these coefficients are deleted from the model and again the adequacy of the model is tested.

Once the model fitted to Equation (5.3) was found to be adequate the steepest ascent technique was applied to locate the combination of factor levels which improve the yield.

Steepest Ascent Along the Response Surface: The direction of steepest ascent was determined using the relation,

$$\nabla \phi = \frac{\partial \phi}{\partial x_1} \vec{u}_1 + \frac{\partial \phi}{\partial x_2} \vec{u}_2 + \ldots + \frac{\partial \phi}{\partial x_k} \vec{u}_k \qquad (5.13)$$

where,

ϕ is the function describing the response surface.

$\nabla \phi$ is the gradient of the response function.

$\frac{\partial \phi}{\partial x_j}$ is the partial derivative of the function with respect to the j^{th} factor.

$\vec{u}_1, \vec{u}_2, \ldots, \vec{u}_k$ are the unit vectors in the direction of the coordinate axes.

It can be easily verified that the components of the gradient $\nabla \phi$ i.e., $\frac{\partial \phi}{\partial x_j}$, $j = 1, 2, \ldots, k$ are the same as the regression coefficients in Equation (5.3). The details regarding the numerical evaluation of the direction of the steepest ascent are found in Sections 5.5.1 and 5.5.2.

The steepest ascent calculations were used to locate the possible combination of factor levels along the steepest ascent direction which predicted increasing yields of (butenes + butadiene). The predicted yields of (butenes + butadiene) were not experimentally verified, since the experimental range in the present investigation was narrow. Moreover, the step sizes chosen were small, so that the predicted responses were bound to be observed experimentally.

One of the above combination of factor levels was used as the base level for the next experimental design. This above procedure was repeated. This iteration process was discontinued when the response surface was no more describable by Equation (5.3). This indicated that the factor levels were now close to the stationary region of the response surface.

The strategy was applied in parallel to the two qualitative factors namely, β- and γ-phases of bismuth molybdates as described in Section 5.4.1. Once the best possible yields of (butenes + butadiene) attainable with these two factors were known, one of these factors was eliminated based on the values of the best yields obtained and the process conditions at which these best yields were realised. The second order response surface strategy was then applied only to this qualitative factor.

A base level of quantitative factors will have to be chosen to begin the search for the optimum yield. A discussion on the choice of initial base levels is presented in the following section. The first order strategy as applied to the two qualitative factors is described in Sections 5.5.2 and 5.5.3. The two qualitative factors are discriminated against each other in Section 5.6 where the second order response surface strategy adopted has also been discussed.

5.5.1. Choice of a Base Level.

Having chosen the factors and the experimental region of the factor space, the optimisation parameter and the experimental design (Section 5.4), experiments were conducted to search for an optimum yield of (butenes + butadiene).

The search was initiated by choosing a base level of factors, and setting up a 2^{4-1} fractional factorial design around this base level. This base level of factors was chosen on the basis of a-priori knowledge. The levels of temperature, the butane to oxygen ratio and the catalyst to feed ratio, were chosen close to the best values reported in literature for the butene oxidation dehydrogenation process [53, 61, 104, 115].

The proportion of bismuth molybdate to aluminium phosphate was chosen as follows: Experiments on MoO_3-$AlPO_4$ catalysts had showed an optimum ratio of molybdic oxide to aluminium phosphate to be in the range of 0.1-0.15 mol per mol. The bismuth molybdate-aluminium phosphate catalyst should contain about 0.1-0.15 mol of bismuth molybdate per mol of aluminium phosphate. The composition of the bismuth molybdate was, therefore, fixed at 20.0 mol bismuth molybdate/100 mol aluminium phosphate.

The variation interval of temperature was chosen to be 25°C, large enough to take care of the non-isothermal effects in the catalyst bed. The variation intervals of other

factors were chosen rather arbitrarily.

Table 16 lists the base levels and the variation intervals of the various factors used for the first move on the response surface. A fractional factorial design was set up using these values and the response surface methodology was initiated using the experimental data obtained. Experiments conducted on $Bi_2O_3.2MoO_3$-$AlPO_4$ and $Bi_2O_3.MoO_3$-$AlPO_4$ are found in Sections 5.5.2 and 5.5.3 respectively.

5.5.2. Optimisation of Butenes + Butadiene Yield Using $Bi_2O_3.2MoO_3$-$AlPO_4$ Catalyst.

In the present section, experiments performed on $Bi_2O_3.2MoO_3$-$AlPO_4$ catalysts are dealt with. The response surface methodology was initiated by choosing the base level of the factors and their variation intervals at the values shown in Table 16.

Fractional factorial design used in the experiments is shown in Table 17. The experimental trials were run in a random manner to avoid any possible bias on the part of the experimenter. The randomisation sequence is shown in column 3 of the table. The experimental results are given in Appendix VII for runs numbered 22 through 31. The yield of (butenes + butadiene) was calculated as the moles of total butenes and butadiene formed per 100 moles of butane fed.

Equation (5.3) was fitted to the experimental data, and the coefficients b_o, b_1, b_2, b_3 and b_4 were estimated

Table 16. FIRST ORDER RESPONSE SURFACE STRATEGY.

INITIAL BASE LEVELS AND VARIATION INTERVALS OF FACTORS.

Factor	Code	Base Level	Variation Interval	Factor Level -1	+1
Temperature °C	x_1	450	25	425	475
W/F g-min/mg mol	x_2	1.3	0.3	0.7	1.6
Butane/oxygen ratio	x_3	1.0	0.25	0.75	1.25
Moles of bismuth molybdate/100 mol aluminium phosphate	x_4	20	5	15	25
Type of bismuth molybdate	Qualitative Factor; β- and γ-phases.				

Table 17. FIRST ORDER RESPONSE SURFACE STRATEGY. FIRST MOVE ON THE RESPONSE SURFACE

$Bi_2O_3.2MoO_3$-$AlPO_4$ CATALYST. DESIGN MATRIX, EXPERIMENTAL RESULTS AND TEST FOR MODEL ADEQUACY.

Run No.	Design Trial No.	Randomised Sequence	Factor Levels x_o*	x_1	x_2	x_3	x_4	Yield** Expt. y	Pred. y
22	1	10	+1	-1	-1	-1	-1	5.751	5.903
23	2	5	+1	+1	-1	-1	+1	0.503	1.042
24	3	1	+1	-1	+1	-1	+1	2.029	2.719
25	4	7	+1	+1	+1	-1	-1	1.152	0.656
26	5	4	+1	-1	-1	+1	+1	4.346	6.712
27	6	8	+1	+1	-1	+1	-1	1.746	2.649
28	7	9	+1	-1	+1	+1	-1	8.649	6.326
29	8	2	+1	+1	+1	+1	+1	4.171	1.463
Repeat Trials									
30	9	3	+1	-1	+1	-1	+1	2.707	
31	10	6	+1	-1	+1	-1	+1	3.298	

$$s^2_{ad} = \frac{\sum_{i=1}^{N} (y_1 - y_1)^2}{N - (k+1)} = \frac{20.4461}{8-(4+1)} = 6.815, \quad d.f. = 3$$

$$s^2_y = 0.4065, \quad d.f. = 2$$

$$F_{calc} = \frac{6.815}{0.4065} = 16.56$$

$$F_{0.05}(3, 2) = 19.164$$

$$F_{calc} < F_{0.05}(3, 2)$$

$$t_{0.05} = 2.92, \quad \text{at} \quad d.f. = 2$$

$$\Delta b_j = \pm t_{0.05} \sqrt{\frac{s^2_y}{N}} = 0.6565$$

$\therefore$ Model is adequate.

* x_o is a dummy variable having a constant value of +1.

** mol (butenes + butadiene) formed per 100 mol. of butane fed.

using Equation (5.7). The yields of the repeat trials 3, 9 and 10 were averaged before making the calculations. The yield of (butenes + butadiene) was represented by the following equation:

$$\hat{y} = 3.6245 - 1.7315\, x_1 - 0.893\, x_2 + 1.035\, x_3 - 0.700\, x_4 \qquad (5.14)$$

The above model was tested for the adequacy of fit and the significance of the regression coefficients. These calculations described below are summarised in Table 17.

The yield values reported in trials 3, 9 and 10 were used to calculate the error variance of the yield of (butenes + butadiene), s_y^2, employing Equation (5.8). The error variance was found to be 0.4065 at a degrees of freedom of 2.

The adequacy of the model represented by Equation (5.14) was tested next. The predicted values of the yields were calculated using Equation (5.14) and s_{ad}^2, the variance of adequacy of the said model, estimated using Equation (5.9), was 6.815 at a degrees of freedom of 3.

The F ratio, calculated using Equation (5.10), was found to be 16.56. The tabulated value of F [60] at a significance level of 0.05 and degrees of freedom (3, 2) is 19.164. This value is denoted as $F_{0.05}(3, 2)$ in Table 17. Since F_{calc} was less than $F_{0.05}(3, 2)$, Equation (5.14) represents the response surface of yield adequately at 5% significance level.

Having established the adequacy of the model, the significance of the estimated coefficients was tested. The "t" value at a significance level of 0.05 and degrees of freedom of 2 was found to be equal to 2.92 [60]. The confidence interval, $\triangle b_j$ of the regression coefficients was calculated to be $\pm$ 0.6565, using Equation (5.12). All the coefficients of Equation (5.14) were found significant since their absolute values were larger than their confidence intervals.

The adequacy of the linear model indicated that the subregion in which the response surface was explored, was away from its near-stationery region. Hence the steepest ascent technique described in the previous section was applied to the yield surface represented by Equation (5.14) to locate possible combination of factor levels which enhance the yield. The direction of the steepest ascent was located using Equation (5.13), in which the components of the gradient (the partial derivatives of response function $\emptyset$ represented by Equation (5.14)) are the regression coefficients in Equation (5.14). Thus by changing the independent variables x_1, x_2, x_3 and x_4 in proportion to the values of their regression coefficients, the movement along the steepest path may be realised. From the fitted model, it will be now interesting to compute these factor level combinations which predict an increase in the yield of (butenes + butadiene). These calculations, summarised in Table 18, are described below.

Table 18. CALCULATION OF STEEPEST ASCENT. FIRST MOVE ON THE RESPONSE SURFACE.

$Bi_2O_3 \cdot 2MoO_3$-$AlPO_4$ CATALYST.

		x_1 °C	x_2 $\frac{gmin}{mg\ mol}$	x_3 $\frac{mol}{mol}$	x_4 $\frac{mol}{100\ mol}$	Calculated Yield y
1. Base level		450	1.3	1.0	20	
2. Variation interval (unit)		25	0.3	0.25	5	
3. Estimated slope $\hat{b}_j$ (change in yield per unit change in x)		-1.732	-0.893	1.104	-0.700	
4. Unit X $\hat{b}_j$		-43.3	-0.268	0.276	-3.5	
5. Step when x_1 changes by 22		-22	-0.134	0.14	-1.8	
6. The direction of steepest ascent represented by a series of possible trials on it	1	428	1.17	1.14	18.2	6.42
	2	406	1.03	1.38	16.4	9.22
	3	428*	1.03	1.38	16.4	8.70
	4	428*	0.90	1.42	14.6	8.95
	5	428*	0.76	1.56	12.8	10.24

* Temperature level was held at this level so that it may be used as basic level in the next step.

The base levels and the variation intervals of the factors are shown in the first two rows respectively of the table. In the third row, the regression coefficients of the response surface model (Equation (5.14)) are given. These coefficients also represent the gradient of the yield in their respective directions.

In order to follow the path of the steepest ascent, the factor levels were changed in proportion to their slopes (i.e. the respective regression coefficients). The fourth row was obtained by multiplying the variation interval of each factor with its regression coefficient. Physically these values represent the components of the steepest ascent vector along the coordinate directions of the factor space. The choice of the size of this vector is a matter of experimental convenience. In the present case, a step corresponding to 22°C in the direction of factor x_1 was chosen and the corresponding changes in x_2, x_3 and x_4 are shown in the fifth row. These values were subsequently rounded off depending upon the accuracy with which the factor was measured in the laboratory.

The sixth row was obtained by algebraically adding the calculated values, in row 5, of changes in the levels of the variables (equivalent to unit step in that direction) to the original base levels in row 1. In other words, rows 1 and 5 were added together element by element giving the first set of values in row 6. This process was iterated giving

different sets of values in row 6, which lie in the direction of steepest ascent.

The 6^{th} column in Table 18 represents the expected yields at the combination of factor levels indicated by the corresponding row. These yields were calculated using Equation (5.14).after coding the factors in the trials using Equation (5.2).

It may be seen that, in the second trial of sixth row, the level of the factor x_1 approaches the lower bound of its experimental region given in Table 14. The movement in the direction of steepest ascent below this value was experimentally not feasible. Moreover, any future experimental investigation of the yield along this direction required that a new base level be chosen for the experimental design. The new base level chosen should be such that the upper and the lower levels of the factors used in the next experimental design should be within the region of experimentation. The factor x_1 (temperature) was constrained at a level of 428°C in trial 3, 4 and 5, so that with a variation interval of 25°C, the lower level of the same was within the experimental region. It is seen from column 6 that the yields of (butenes+ butadiene) calculated along the steepest ascent direction show an increasing trend.

The response surface strategy requires that the predicted yields along the steepest ascent direction be

experimentally verified. This, in the present case would mean that the catalysts of varying compositions (trials 1, 2, 3, ... in the steepest ascent direction) be prepared to verify the experimental yields. The experimental effort in preparing and testing a single catalyst was considerable, while the same in conducting the run was much less. Hence, one of the factor level combinations in the steepest ascent direction was chosen and a set of experiments were conducted around these base levels. The experimental design for this situation is described below.

Second Move Towards the Near-Stationary Region: The new base level was chosen on the basis of the calculations in the last row of Table 18. The factor level combinations which predicted a yield of 10.24 percent was chosen as the base level for the present experimental design. The base levels and the variation intervals of the factors so chosen are shown in Table 19. Here, the variation intervals of factors x_2 and x_4 were increased over the previous values (shown in Table 16) in order to improve the significance of the coefficients associated with these factors. The variation intervals of factors x_1 and x_3 were not changed.

The experimental design matrix, the randomised sequence of trials and the corresponding experimental yields of (butenes + butadiene) are presented in Table 20. The experimental data are given in Appendix VII under runs numbered 32 through 41. A glance at the reported yields in

Table 19. FIRST ORDER RESPONSE SURFACE STRATEGY. SECOND MOVE ON THE RESPONSE SURFACE.

$Bi_2O_3.2MoO_3$-$AlPO_4$ CATALYST.

BASE LEVELS AND VARIATION INTERVALS OF FACTORS.

Factor	Code	Base Level	Variation Interval	Factor Level -1	+1
Temperature, °C	x_1	425	25	400	450
W/F, g min/mgmol	x_2	0.8	0.4	0.4	1.2
Butane/oxygen ratio	x_3	1.5	0.25	1.25	1.75
Mol of bismuth/100 mol aluminium phosphate	x_4	13	8	5	21

Table 20. FIRST ORDER RESPONSE SURFACE STRATEGY. SECOND MOVE ON THE RESPONSE SURFACE.

$Bi_2O_3.2MoO_3$-$AlPO_4$ CATALYST. DESIGN MATRIX, EXPERIMENTAL RESULTS AND TEST FOR MODEL ADEQUACY.

Run No.	Design Trial No.	Randomised Sequence	Factor Levels x_o^*	x_1	x_2	x_3	x_4	Yield** Expt. y	Pred. y
32	1	10	+1	-1	-1	-1	-1	12.146⊕	12.511
33	2	6	+1	+1	-1	-1	+1	5.499	5.693
34	3	4	+1	-1	+1	-1	+1	6.039	4.089
35	4	3	+1	+1	+1	-1	-1	11.338	12.960
36	5	9	+1	-1	-1	+1	+1	2.278	3.870
37	6	5	+1	+1	-1	+1	-1	14.810	12.815
38	7	2	+1	-1	+1	+1	-1	10.902	11.131
39	8	1	+1	+1	+1	+1	+1	4.132	4.312
Repeat Trials									
40	9	8	+1	-1	-1	-1	-1	12.532	
41	10	7	+1	-1	-1	-1	-1	12.105	

$$s^2_{ad} = \frac{\sum_{i=1}^{N} (y_i - \hat{y}_i)^2}{N - (k+1)} = \frac{13.44}{3} = 4.48, \quad \text{d.f.} = 3$$

$$s^2_y = 0.1099, \quad \text{d.f.} = 2$$

$$F_{calc} = \frac{4.48}{0.1099} = 40.773 \qquad t_{0.05} = 2.92 \quad \text{at} \quad \text{d.f.} = 2$$

$$F_{0.05}(3, 2) = 19.164 \qquad \Delta b_j = \pm t_{0.05} \sqrt{s^2_y/N} = 0.3425$$

$F_{calc} > F_{0.05}(3, 2)$ ∴ Model is inadequate.

* x_o is a dummy variable having a constant value of +1.

** mol of (butenes + butadiene) formed/100 mol butane fed.

⊕ use average of trials 1, 9 and 10 for calculation of regression coefficients.

Tables 17 and 20 shows that the response surface methodology has been effective in achieving improved yields.

A linear model represented by Equation (5.3) was again fitted to the present set of experimental data. The coefficients were evaluated using Equation (5.7). The subregion of the response surface was therefore described by the equation,

$$\hat{y} = 8.4118 + 0.5331 x_1 - 0.3087 x_2 - 0.3184 x_3 - 3.9423 x_4 \quad (5.15)$$

Comparing this equation with Equation (5.14) of the previous subregion, it may be seen that the sign of the coefficient b_1 has changed from negative to positive and that of b_3 from positive to negative. A sign reversal implied that the optimal values of these factors lie somewhere in the region of the hyper-plane of these factors covered by the two experimental designs. This also indicated the proximity of the factors to the near-stationary region.

The experimental error variance s_y^2 reported in Table 20 has been calculated using Equation (5.8). The confidence interval of the regression coefficient b_j was calculated from Equation (5.12) as,

$$\Delta b_j = 2.92 \sqrt{0.1099/8} = 0.3425$$

Table 20 indicates that the model represented by Equation (5.15) is grossly inadequate, implying that the first order response surface assumption is no longer valid. Hence a second order strategy had to be adopted in the further experimentation (see Section 5.6).

At this juncture, it may be recalled that the phase composition of the bismuth molybdate,, namely, β- and γ-phase was used as a qualitative variable (as mentioned in Sections 5.4.1 and 5.5.1). During the course of investigation, the linear portion of the (yield) response surface of $Bi_2O_3.2MoO_3$-$AlPO_4$ and $Bi_2O_3.MoO_3$-$AlPO_4$ catalysts were investigated side-by-side in order to compare the effect of the qualitative factor on the yield. Hence, the experiments on $Bi_2O_3.MoO_3$-$AlPO_4$ catalysts which were performed in parallel with $Bi_2O_3.2MoO_3$-$AlPO_4$ are discussed in the following section. The second order response surface of (butenes+ butadiene) yield was explored only after the information regarding the qualitative variable was available.

5.5.3. Optimisation of (Butenes+ Butadiene) Yield Using $Bi_2O_3.MoO_3$-$AlPO_4$ Catalyst.

The search for the optimum was commenced by choosing a base level for the experimental design and following the procedure described in Section 5.5.1. The base levels of factors for the present catalyst were chosen to be the same as those reported in Table 16. The initial design matrix and

the corresponding response values i.e. the yields of (butenes + butadiene) are shown in Table 21. The pertinent experimental data are tabulated in Appendix VII for runs numbered 42 through 49. The experiments were conducted in a randomised sequence.

The coefficients of the linear response surface model were estimated using Equation (5.7) and the corresponding equation describing the response was,

$$\hat{y} = 4.036 - 1.7716\ x_1 - 0.376\ x_2 + 0.8919\ x_3 - 1.1515\ x_4 \qquad (5.16)$$

The experimental error variance for the present set of experiments was assumed to be the same as that of the experiments on $Bi_2O_3.2MoO_3$-$AlPO_4$ catalyst reported in Table 17 under Section 5.5.1. Then by Equations (5.11) and (5.12) the confidence interval, Δb_j of the estimated coefficient, $\hat{b}_j$ was found to be $\pm$ 0.6565. Since in Equation (5.16), the absolute value of the coefficient b_2 (0.376) was less than its confidence interval, its variation interval was purposely increased in the next set of experiments in order to check whether it was really not significant. The calculations shown in Table 21 indicated that the model of the yield response surface represented by Equation (5.16) was adequate. This indicated that the subregion of the explored response surface was away from the near-stationary region, and therefore a decision was taken to conduct another set of experiments using the first order response surface strategy.

Table 21. FIRST ORDER RESPONSE SURFACE STRATEGY. FIRST MOVE ON THE RESPONSE SURFACE.

$Bi_2O_3.MoO_3$-$AlPO_4$ CATALYST. DESIGN MATRIX, EXPERIMENTAL RESULTS AND TEST FOR MODEL ADEQUACY.

Run No.	Design Trial No.	Randomised Sequence	Factor Levels x_o*	x_1	x_2	x_3	x_4	Yield** Expt. y	Pred. y
42	1	4	+1	-1	-1	-1	-1	6.228	6.443
43	2	8	+1	+1	-1	-1	+1	2.678	0.597
44	3	6	+1	-1	+1	-1	+1	3.012	0.388
45	4	2	+1	+1	+1	-1	-1	0.608	2.148
46	5	7	+1	-1	-1	+1	+1	4.522	5.924
47	6	1	+1	+1	-1	+1	-1	3.949	4.684
48	7	3	+1	-1	+1	+1	-1	9.965	7.475
49	8	5	+1	+1	+1	+1	+1	1.325	1.629

$$s^2_{ad} = \frac{\sum_{i=1}^{N} (y - y)^2}{N - (k+1)} = \frac{15.62}{3} = 5.207, \quad \text{d.f.} = 3$$

$$s^2_y = 0.513, \quad \text{d.f.} = 2$$

$$F_{calc} = \frac{5.207}{0.513} = 10.15 \qquad t_{0.05} = 2.92 \quad \text{at d.f.} = 2$$

$$F_{0.05}(3, 2) = 19.164 \qquad \Delta b_j = \pm t_{0.05} \sqrt{s^2_y/N} = 0.6565$$

$F < F_{0.05}(3, 2)$ ∴ Model is adequate

* x_o is a dummy variable having a constant value of +1.

** mol - of (butenes + butadiene) formed per 100 mol of butane fed.

The linear nature of the response surface permits the application of steepest ascent technique to locate the next factor level combinations that produce a maximum increase in the yield on the surface. The steepest ascent direction was located, and the combination of factor levels lying in this direction were calculated according to the procedure already described in Section 5.5.2. These calculations are summarised in Table 22. It may be seen that the predicted values of the yield show an upward trend. These predicted yields were not experimentally verified for reasons described earlier in Section 5.5.2.

The first order strategy was continued by choosing a new base level that gave a higher yield of (butenes + butadiene). The next set of experiments performed are described below.

Second Move Towards the Near-Stationary Region: In the model represented by Equation (5.16), the coefficient b_2 was found to be not significant and hence the variation interval of the factor x_2 was increased to 0.6 compared to its original value of 0.3 in the previous design. The variation intervals of the factors x_3 and x_4 were also increased in order to improve the absolute numerical values of regression coefficients associated with them.

The factor levels of the experiments in design trial numbered 7 of Table 21 were chosen as the new base levels, since the observed yield at this point was more than the predicted values of the yield along the response surface.

Table 22: CALCULATION OF STEEPEST ASCENT. FIRST MOVE ON THE RESPONSE SURFACE.

$Bi_2O_3.MoO_3$-$AlPO_4$ CATALYST.

		x_1 °C	x_2 gmin / mg mol	x_3 mol / mol	x_4 mol / 100 mol	Calculated yield y
1. Basic level		450	1.3	1.0	20	
2. Variation interval (unit)		25	0.3	0.25	5	
3. Estimated slope $\hat{b}_j$ (change in yield per unit change in x_j)		-1.772	-0.376	0.892	-1.515	
4. $\hat{b}_j$ X variation interval		-44.3	-0.128	0.223	-5.756	
5. Step when x_1 changes by 22		-22	-0.064	0.112	-2.9	
Rounding off		-22	-0.06	0.11	3.0	
6. The direction of steepest ascent represented by a series of possible trials on it	1	428	1.24	1.11	17	6.76
	2	406	1.17	1.23	14	9.53
	3	428*	1.17	1.23	14	7.97
	4	428*	1.05	1.34	11	9.20

* Held stationary to accommodate variation interval for the next set.

The base levels and the variation intervals used in the present experimental design are shown in Table 23. The relevant experimental data are reported in the Appendix VII denoted by runs numbered 50 through 57. The effectiveness of the response surface methodology was established since the yields reported in Table 23 were superior to the yields reported in Table 21.

A linear response was fitted to the yield data, and the regression coefficients were estimated using the Equation (5.7). The fitted equation was,

$$\hat{y} = 7.94 - 2.644\ x_1 + 0.656\ x_2 + 1.956\ x_3 + 1.5028\ x_4 \qquad (5.17)$$

Comparing this equation with Equation (5.16), it is found that the coefficients b_2 and b_4 have reversed their sign indicating that the optimum values of the factors x_2 and x_4 lie somewhere in between the corresponding factor levels used in the previous design (Table 16) and the present design (Table 23).

The experimental error variance was assumed to be the same as that obtained in Table 20. The confidence intervals of the coefficients were given by $\Delta b_j = \pm 0.3425$. Thus all the coefficients in Equation (5.17) were found to be significant. The model adequacy test in Table 23 showed that the linear approximation of the response surface (Equation (5.17)) was no more valid. At this stage, it was decided to terminate the first order strategy.

Table 23. FIRST ORDER RESPONSE SURFACE STRATEGY. SECOND MOVE ON THE RESPONSE SURFACE.

CATALYST: $Bi_2O_3.MoO_3$-$AlPO_4$ BASE LEVEL AND VARIATION INTERVALS OF FACTORS, DESIGN MATRIX, EXPERIMENTAL RESULTS AND TEST FOR MODEL ADEQUACY.

	x_1	x_2	x_3	x_4	Yield** Expt. y	Yield** Pred. y
Basic level	425	1.6	1.25	15		
Variation interval	25	0.6	0.4	8		
Upper level	450	2.2	1.65	23		
Lower level	400	1.0	0.85	7		

Run No.	Randomised Sequence	Design Trial No.	Coded value of factors x_o^*	x_1	x_2	x_3	x_4		
50	6	1	+1	-1	-1	-1	-1	7.259	6.469
51	5	2	+1	+1	-1	-1	+1	5.829	4.187
52	7	3	+1	-1	+1	-1	+1	9.183	10.787
53	2	4	+1	+1	+1	-1	-1	1.594	2.493
54	3	5	+1	-1	-1	+1	+1	12.550	13.387
55	8	6	+1	+1	-1	+1	-1	3.551	5.093
56	4	7	+1	-1	+1	+1	-1	13.396	11.693
57	1	8	+1	+1	+1	+1	+1	10.209	9.411

$$s^2_{ad} = \frac{\sum_{i=1}^{N} (y - y^2)}{N - (k+1)} = \frac{4.4137}{0.1099} = 40.01, \quad \text{d.f.} = 3$$

$$s^2_y = 0.1099, \quad \text{d.f.} = 2$$

$$F_{calc} = \frac{4.4137}{0.1099} = 40.01 \qquad t_{0.05} = 2.92 \text{ at d.f.} = 2$$

$$F_{0.05}(3, 2) = 19.164 \qquad \Delta b_j = \pm t_{0.05} \sqrt{s^2_y/N} = 0.3425$$

$F > F_{0.05}(3, 2)$ $\therefore$ Model is inadequate.

* x_o is a dummy variable having a constant value of +1.

** mol of (butenes + butadiene) formed per 100 mol of butane fed.

Having established the best possible yields of (butenes + butadiene) in the near-stationary regions of the two response surfaces, namely, the response surfaces associated with β- and γ-phases of bismuth molybdates, the two phases were evaluated for their suitability as dehydrogenation catalyst. The second order response surface strategy was applied only to one of the above two catalysts found superior. The following section deals with the choice between the two qualitative variables and the second order methodology applied subsequently.

5.6. Second Order Response Surface Strategy. Exploration of the Response at the Near-Stationary Region.

The first order response surface strategy applied to $Bi_2O_3.2MoO_3$-$AlPO_4$ and $Bi_2O_3.MoO_3$-$AlPO_4$ led to a situation where the linear approximation of the response surface function Ø was no more valid. This suggested a curvilinear nature of the subregion of the response surface with a possibility of maximum being located close to this subregion. Therefore, the second order strategy was resorted to and a nonlinear model was employed to describe the response surface.

In the first order study, the phase composition of the bismuth molybdate was chosen as a qualitative factor. It was considered appropriate to eliminate one of the qualitative factors at this stage of experimentation, so that the better amongst the two may be used for further investigation. The choice between the phases of bismuth molybdates is discussed below.

5.6.1. Screening of the Qualitative Factors. Choice Between $Bi_2O_3.2MoO_3$ and $Bi_2O_3.MoO_3$.

Both the $Bi_2O_3.2MoO_3$ and $Bi_2O_3.MoO_3$ phases used as qualitative factors in the first order response surface methodology were found to give comparable yields of (butenes + butadiene) at the near-stationary regions of the two response surfaces (see Tables 20 and 23). The yields were slightly higher in the case of $Bi_2O_3.2MoO_3$-$AlPO_4$ catalyst when compared with the yields obtained over $Bi_2O_3.MoO_3$-$AlPO_4$ catalyst. Therefore, it was not possible to choose between the two qualitative factors on the basis of the yields obtained in the subregion of the two response surfaces.

A choice between the two qualitative factors was made by analysing process conditions at which the near-optimum yields were located. A comparison of the models describing the two response surfaces (Equations (5.14) to (5.17)) was necessary for this purpose. The values of the regression coefficients associated with the two response surfaces are shown in Table 24. The influence of the process variables on the yields of (butenes+ butadiene) were scrutinised with the help of the above table and subsequently relative merits and demerits of the two catalysts were evaluated. The influence of the process variables on the yields of (butenes+ butadiene) are as follows:

1. Temperature: (Refer Table 24).

The temperature coefficient b_1 for $Bi_2O_3.2MoO_3$-$AlPO_4$ catalyst changed its sign from minus to plus, when the region

Table 24. REGRESSION COEFFICIENTS OF THE MODELS FROM THE FIRST ORDER RESPONSE SURFACE STRATEGY*.

Qualitative Factor	Average Yield $\hat{b}_o$	Regression Coefficients of Factors $\hat{b}_1$	$\hat{b}_2$	$\hat{b}_3$	$\hat{b}_4$
1. $Bi_2O_3.2MoO_3$-$AlPO_4$ catalyst					
First move	3.625	-1.7315 (450)	-0.8930 (1.3)	1.1035 (1.0)	-0.7000 (20)
Second move	8.412	0.5331 (425)	-0.3087 (0.8)	-0.3814 (1.5)	-0.9425 (13)
2. $Bi_2O_3.MoO_3$-$AlPO_4$ catalyst					
First move	4.036	-1.7716 (450)	-0.3760 (1.3)	0.8919 (1.0)	-1.1515 (20)
Second move	7.940	-2.6440 (425)	0.6560 (1.6)	1.9560 (1.25)	1.5028 (15)

* Base levels are shown in parenthesis.

of the response surface was shifted from a base level of 450°C to 425°C. The sign reversal indicated that the optimum value of the temperature lies in between the two base levels of 450°C and 425°C. The temperature coefficient for $Bi_2O_3.MoO_3$-$AlPO_4$ catalyst was negative in both moves, and thus the optimum temperature was below 425°C.

ii. Catalyst-Feed Ratio: (Refer Table 24).

The coefficient associated with the catalyst feed ratio was b_2. The $Bi_2O_3.2MoO_3$ catalyst required a catalyst-feed ratio less than 0.8 g/(mg mol/min) as indicated by the negative values of the coefficient. However, the optimum contact time for $Bi_2O_3.MoO_3$ catalyst was existed somewhere in between a catalyst-feed ratios of 1.3 to 1.6 g/(mg mol/min).

iii. Butane-Oxygen Ratio: (Refer Table 24).

The coefficient of hydrocarbon-oxygen ratio for b_3 indicated that the optimum butane-oxygen ratio was located between 1.0 and 1.5 for $Bi_2O_3.2MoO_3$-$AlPO_4$ catalyst. In the case of $Bi_2O_3.MoO_3$-$AlPO_4$ a butane-oxygen ratios in excess of 1.5 were found beneficial.

iv. Bismuth Molybdate-Aluminium Phosphate Ratio: (Refer Table 24)

Lower proportions of bismuth molybdate to aluminium phosphates are favoured in the case of $Bi_2O_3.2MoO_3$. The regression coefficient b_4 (Equation (5.15)), associated with $Bi_2O_3.2MoO_3$, had a large negative value showing that the optimum proportion of $Bi_2O_3.2MoO_3$ to $AlPO_4$ lies far below the

value of 13 mol/100 mol. However, in the case of $Bi_2O_3.MoO_3$-$AlPO_4$ catalyst, it may be concluded that the optimum proportion lies between 15 and 20 mol/100 mol.

From Table 20 it may be seen that the $Bi_2O_3.2MoO_4$-$AlPO_4$ catalyst with a $Bi_2O_3.2MoO_3/AlPO_4$ ratio of 5 mol/100 mol has the highest activity for the yield of (butenes + butadiene), whilst the optimum proportion for $Bi_2O_3.MoO_3$-$AlPO_4$ catalyst lies somewhere in the range of 15-20 mol/100 mol. This suggested that the $Bi_2O_3.2MoO_3$ was a better catalyst, since a catalyst with a lower proportion of bismuth molybdate to aluminium phosphate would result in reduced catalyst costs.

The method of catalyst preparation also favoured the choice of $Bi_2O_3.2MoO_3$. The catalyst preparation method in the case of $Bi_2O_3.2MoO_3$ was a simple precipitation reaction followed by filtration of the precipitate, while the preparation of $Bi_2O_3.MoO_3$ involved very intricate solid state reaction between Bi_2O_3 and MoO_3 (see Section 3.2).

The expected value of the optimum temperature in the case of $Bi_2O_3.2MoO_3$ (425-450°C) further supported its choice over $Bi_2O_3.MoO_3$ since the optimum value of the temperature in the latter case was below 425°C, which could lead to a region where the reactants were partially converted to oxygenated products.

The effects of contact time as well as butane-oxygen ratios favoured the choice of $Bi_2O_3.2MoO_3$ which required a

lower contact time (0.8) and a butane to oxygen ratio of 1.0 to 1.5. However, these factors were minor compared to the above variables. The surface areas of the two catalysts reported in Chapter 4 deserve consideration at this stage. It may be seen from Table 7 (Section 4.4) that the surface area of $Bi_2O_3.MoO_3$-$AlPO_4$ catalyst is higher than the surface area of $Bi_2O_3.2MoO_3$-$AlPO_4$ catalyst. One would be tempted to favour $Bi_2O_3.MoO_3$-$AlPO_4$ on the basis of surface area data. Higher surface area would be a disadvantage in the present case since it would result in large heat generation (exothermic reaction) per unit volume of the catalyst bed. The control of the exothermic oxidative dehydrogenation reaction would be difficult in such a situation.

The above arguments strongly favour the choice of $Bi_2O_3.2MoO_3$ as an active component when compared to its competitor, $Bi_2O_3.MoO_3$, and hence it was chosen for further study of the yield-response surface. The second order strategy was applied to $Bi_2O_3.2MoO_3$-$AlPO_4$ catalyst with a view to locate the factor level combinations within the experimental region that gave highest yield of (butenes + butadiene). The second order response methodology as implemented in the present investigation is described below.

5.6.2. Quadratic Model of the Response Surface.

In the near-stationary region, the curvilinear effects dominate, and the functional form of the response function ϕ

(Equation (5.1)) will have to be suitably chosen to explain the above nonlinearity. In the present investigation, the response function was approximated by a quadratic (second degree) polynomial suggested by Box and Wilson [31]. The polynomial is given by,

$$y = b_0 + b_1x_1 + b_2x_2 + b_3x_3 + b_4x_4 + b_{11}x_1^2 + b_{22}x_2^2 + b_{33}x_3^2 + b_{44}x_4^2 + b_{12}x_1x_2 + b_{13}x_1x_3 + b_{14}x_1x_4 + b_{23}x_2x_3 + b_{24}x_2x_4 + b_{34}x_3x_4 \quad (5.18)$$

This model contains the linear terms in x_1, x_2, x_3, x_4, the squared terms in x_1^2, x_2^2, x_3^2, x_4^2 and the cross product terms in x_1x_2, x_1x_3, ..., x_3x_4.

Alternatively, the above equation can be written in the matrix notation as,

$$\underline{Y} = b_0 + \underline{b}_1\underline{x} + \underline{x}^T \underline{b}_{11}\underline{x} \quad (5.19)$$

where

$$\underline{x}^T = [\, x_1 \quad x_2 \quad x_3 \quad x_4 \,]$$

$$\underline{b}_1 = [\, b_1 \quad b_2 \quad b_3 \quad b_4 \,]$$

$$\underline{b}_{11} = \begin{bmatrix} b_{11} & b_{12} & b_{13} & b_{14} \\ b_{12} & b_{22} & b_{23} & b_{24} \\ b_{13} & b_{23} & b_{33} & b_{34} \\ b_{14} & b_{24} & b_{34} & b_{44} \end{bmatrix}$$

T denotes the transpose.

The central composite design developed by Box and Wilson [31] was employed to collect the experimental data. These data were used to estimate the coefficients in Equation (5.18). The central composite design is constructed by adding further factor level combinations to those obtained from the 2^4 factorial design. These extra factor level combinations are as follows:

$(0, 0, 0, 0)$; $(-\alpha, 0, 0, 0)$; $(+\alpha, 0, 0, 0)$;

$(0, -\alpha, 0, 0)$; $(0, +\alpha, 0, 0)$;

$(0, 0, -\alpha, 0)$; $(0, 0, +\alpha, 0)$;

$(0, 0, 0, -\alpha)$; $(0, 0, 0, +\alpha)$.

Thus the new design contained $(2^k + k + 1)$ factor level combinations with $k = 4$ in the present case. The value of α was set at 2 to make the design rotatable and the regression coefficients orthogonal to one another. The experimental design is presented in Table 25 under the heading "Design Matrix". The central point (or the base level) of the design represented by the factor level combination (0, 0, 0, 0) was repeated seven times in order to get an estimate of the experimental error variance of the optimisation parameter y as recommended by Cochran and Cox [38].

The design trial number 6 of Table 20 had the best combination of the factor levels with an experimental yield of (butenes + butadiene) equal to 14.8%. Therefore, this was

Table 25. SECOND ORDER RESPONSE SURFACE STRATEGY.

CENTRAL COMPOSITE DESIGN MATRIX AND EXPERIMENTAL RESULTS.

$Bi_2O_3.2MoO_3$-$AlPO_4$ CATALYST.

	Temp °C	Cat/Feed g/(mg mol/min)	Butane/Oxygen mol/mol	$Bi_2O_3.2MoO_3/AlPO_4$ mol/100 mol
	x_1	x_2	x_3	x_4
Base level	440	0.7	1.4	5
Variation interval	20	0.2	0.2	2

Run No.	Design Trial No.	Randomised Sequence	Design Matrix Factor Levels					Yield**	
			x_0^*	x_1	x_2	x_3	x_4	Expt. y	Pred. y
1	2	3	4	5	6	7	8	9	10
58	1	6	+1	-1	-1	-1	-1	10.458	10.839
59	2	5	+1	+1	-1	-1	-1	9.136	8.929
60	3	7	+1	-1	+1	-1	-1	10.547	10.190
61	4	2	+1	+1	+1	-1	-1	8.006	8.279
62	5	3	+1	-1	-1	+1	-1	11.302	12.299
63	6	8	+1	+1	-1	+1	-1	10.661	11.191
64	7	4	+1	-1	+1	+1	-1	11.125	11.309
65	8	1	+1	+1	+1	+1	-1	10.406	10.201

Continued...

Table 25 (continued)

1	2	3	4	5	6	7	8	9	10
66	9	5	+1	-1	-1	-1	+1	9.335	9.728
67	10	4	+1	+1	-1	-1	+1	8.521	8.486
68	11	8	+1	-1	+1	-1	+1	10.453	10.073
69	12	3	+1	+1	+1	-1	+1	9.641	8.831
70	13	6	+1	-1	-1	+1	+1	12.702	12.763
71	14	7	+1	+1	-1	+1	+1	11.961	12.323
72	15	2	+1	-1	+1	+1	+1	12.556	12.768
73	16	1	+1	+1	+1	+1	+1	12.376	12.328
74	17	3	+1	-2	0	0	0	13.022	12.444
75	18	8	+1	+2	0	0	0	9.854	10.093
76	19	5	+1	0	-2	0	0	12.528	11.456
77	20	7	+1	0	+2	0	0	10.079	10.812
78	21	9	+1	0	0	-2	0	6.415	6.955
79	22	10	+1	0	0	+2	0	12.789	11.911
80	23	-	+1	0	0	0	-2	10.995	10.291
81	24	-	+1	0	0	0	+2	11.090	11.306
82	25	6	+1	0	0	0	0	10.576	10.799
83	26	12	+1	0	0	0	0	11.383	10.799
84	27	2	+1	0	0	0	0	10.892	10.799
85	28	13	+1	0	0	0	0	10.958	10.799
86	29	11	+1	0	0	0	0	10.114	10.799
87	30	1	+1	0	0	0	0	11.401	10.799
88	31	4	+1	0	0	0	0	10.116	10.799

* x_0 is a dummy variable having a constant value of +1.

** mol (butenes + butadiene) per 100 mol butane fed.

the best choice for the base level of central composite design. Some numerical adjustments were made in the above base levels of factors to accommodate their upper and lower levels within the region of experimentation. The base levels and the variation intervals of the factors used in the present study are shown in Table 25.

The experimental data obtained were fitted to the quadratic polynomial given in Equation (5.18) and the coefficients b_0, b_1, b_2, ..., b_{34} were estimated. Unnecessary terms in Equation (5.18) were omitted through significance testing. The significance of any coefficient was evaluated as follows [58]:

The variance-covariance matrix of the regression coefficients, $\underline{s}^2(b)$ was evaluated first by

$$\underline{s}^2(b) = \frac{\underline{Y}^T\underline{Y} - \hat{\underline{b}}^T\underline{x}^T\underline{Y}}{N - p} \cdot (\underline{x}^T\underline{x})^{-1} \qquad (5.20)$$

where,

$\underline{x}$ is the matrix of the independent variables.

$\underline{y}$ is the vector of experimentally observed yields.

$\hat{\underline{b}}$ is the vector of estimated coefficients.

N is total number of experiments in the design.

p is the number of coefficients (parameters).

The "Student's t" value is calculated using the relation,

$$t_{calc} = \frac{\hat{b}_j}{s(b_j)} \tag{5.21}$$

where,

t_{calc} is the calculated value of "Student's t".

$\hat{b}_j$ is the estimated value of the j^{th} coefficient.

$s(b_j)$ is the variance of the j^{th} coefficient obtained from variance-covariance matrix $\underline{s}^2(b)$.

If $|t_{calc}| \leq t_{(1 - \alpha/2,\ N - p)}$, then the coefficient was considered as not significant. Subsequently, the coefficients of Equation (5.18) were re-estimated after setting all the non-significant coefficients to zero.

Adequacy of the model was tested as before by the F-test. The multiple correlation coefficient, R [60], was defined by the equation,

$$R = \sqrt{\frac{\sum_{i=1}^{N} (\hat{y}_i - \bar{y})^2}{\sum_{i=1}^{N} (y_i - \bar{y})^2}} \tag{5.22}$$

where $\bar{y}$ is given by the relation

$$\bar{y} = \frac{\sum_{i=1}^{N} y_i}{N} \tag{5.23}$$

The multiple correlation coefficient R is a measure of the linear association between the dependent variable y and the set of independent variables,

$x_1, \ldots, x_1^2, \ldots, x_1x_2, \ldots, x_3x_4$. R has a value close to 1 for a good fit of the data by the model.

Experimental data reported in Table 25 were used to develop a model for the yield-response surface. The coefficients of the quadratic model represented by Equation (5.18) were estimated using Equation (5.6). The variance of the experimental error was estimated from the design trials numbered 25 through 31. The various steps in the development of a correct model are as follows:

A. <u>All the Coefficients in Equation (5.18) were Assumed to be Significant</u>.

The coefficients were estimated using Equations (5.6) and (5.18). In the matrix notation these are as follows:

$$\hat{b}_o = 10.777$$

$$\underline{\hat{b}}_1 = \begin{bmatrix} -0.5876 & -0.1611 & 0.1239 & 0.2539 \end{bmatrix}$$

$$\underline{\hat{b}}_{11} = \begin{bmatrix} 0.1197 & -0.0457 & 0.2005 & 0.1672 \\ -0.0457 & 0.0861 & -0.0851 & 0.2487 \\ 0.2005 & -0.0851 & -0.3392 & 0.3938 \\ 0.1672 & 0.2487 & 0.3938 & 0.0209 \end{bmatrix}$$

<u>Model adequacy</u>:

Variance of experimental error $s_y^2 = 0.2866$,

d.f. = 6

Variance of adequacy $s^2_{ad} = 0.5151$,

d.f. = 31 - 15 = 16

$$F_{calc} = \frac{s^2_{ad}}{s^2_y} = \frac{0.5151}{0.2806} = 1.7974$$

$F_{0.05}(16, 6) = 3.9254$

$F_{calc} < F_{0.05}(16, 6)$, hence the model is adequate.

Multiple correlation coefficient using Equation (5.22):

R = 0.9341 (i.e. the fit is good).

Significance of the coefficients:

The computed "t" values of the various parameters in the matrix notation were as follows:

$t_{b_o} = 146.44$

$$\underline{t}_{b_1} = [-23.38 \quad -7.50 \quad 57.73 \quad 11.83]$$

$$\underline{t}_{b_{11}} = \begin{bmatrix} 6.65 & -1.42 & 6.23 & 5.19 \\ -1.42 & 4.78 & -2.64 & 7.73 \\ 6.23 & -2.64 & -18.83 & 12.23 \\ 5.19 & 7.73 & 12.23 & 1.16 \end{bmatrix}$$

The tabulated value of "t" at 5% significance level and 16 degrees of freedom is 2.12. It was found that the calculated "t" values of the coefficients $\hat{b}_{44}$ and $\hat{b}_{12}$ ($|t_{calc}| = 1.16$ and 1.42) were less than the tabulated "t"

value of 2.12, and hence the coefficients b_{12} and b_{44} were not significant. Their inclusion in the model may lead to undue regression of the experimental error, and hence it was considered proper to drop them from the model.

B. Elimination of Non-Significant Coefficients.

The remaining coefficients in Equation (5.18) were re-estimated, and the statistical tests were applied to this new model.

The re-estimated values of the coefficients were as follows:

$$\hat{b}_o = 10.799$$

$$\hat{\underline{b}}_1 = [-0.5876 \quad -0.1611 \quad 1.2391 \quad 0.2539]$$

$$\hat{\underline{b}}_{11} = \begin{bmatrix} 0.1175 & 0 & 0.2005 & 0.1672 \\ 0 & 0.0839 & -0.0851 & 0.2487 \\ 0.2005 & -0.0851 & -0.3414 & 0.3938 \\ 0.1672 & 0.2487 & 0.3938 & 0 \end{bmatrix} \qquad (5.24)$$

The model adequacy was tested again.

Model adequacy:

Variance of experimental error $s_y^2 = 0.2866$,
d.f. = 6

Variance of adequacy $s_{ad}^2 = 0.4604$,
d.f. = 31 - 13 = 18

$$F_{calc} = \frac{s_{ad}^2}{s_y^2} = \frac{0.4604}{0.2866} = 1.066$$

$$F_{0.05}(18, 6) = 3.8998$$

Since $F_{calc} < F_{0.05}(18, 6)$, the model is adequate.

Multiple correlation coefficient using Equation (5.22):

$R = 0.9337$ (i.e. the fit is good).

Significance of the coefficients:

The computed "t" values of various parameters in the matrix notation were as follows:

$$t_{b_o} = 220.4$$

$$\underline{t}_{b_1} = [-30.62 \quad -8.40 \quad 64.59 \quad 13.24]$$

$$\underline{t}_{b_{11}} = \begin{bmatrix} 7.38 & 0 & 6.97 & 5.81 \\ 0 & 5.27 & -2.96 & 8.64 \\ 6.97 & -2.96 & 5.27 & 13.68 \\ 5.81 & 8.64 & 13.68 & 0 \end{bmatrix}$$

The tabulated value of "t" at 5% significance level and 18 degrees of freedom is 2.10. All the coefficients in the present model were found to be significant. Hence the model of the response surface is given by,

$$\hat{y} = 10.799 - 0.5876x_1 - 0.1611x_2 + 1.2391x_3 + 0.2539x_4 + 0.1175x_1^2 + 0.0839x_2^2 - 0.3414x_3^2 + 0.2005x_1x_3 + 0.1672x_1x_4 - 0.0851x_2x_3 + 0.2487x_2x_4 + 0.3938x_3x_4 \qquad (5.25)$$

The model fitted to the subregion of the response surface was examined further to locate the factor level combinations that result in a maximum yield of (butenes + butadiene). This is discussed in the following section.

5.6.3. Analysis of the Quadratic Surface. Location of the Optimum Factor Level Combination.

The maximum of y was located by differentiating Equation (5.25) with respect to each x in turn and setting them equal to zero [10]. The resulting set of simultaneous algebraic equations were solved to obtain the optimum value of $\underline{x}$ that maximised y.

Upon differentiation with respect to x_1, Equation (5.18) yields,

$$\frac{\partial \hat{y}}{\partial x_i} = \hat{b}_i + 2\hat{b}_{11}x_1 + 2 \sum_{\substack{j=1 \\ 1 \neq j,\ i < j}}^{4} \hat{b}_{1j}x_j = 0; \quad i = 1, 2, 3, 4. \qquad (5.26)$$

Or, in the matrix notation,

$$\hat{\underline{b}}_1^T + 2\hat{\underline{b}}_{11}\,\underline{x} = 0 \qquad (5.27)$$

The solution of the above equation gave the vector $\underline{x}_{max}$, that maximised the yield y:

$$\underline{x}_{max} = -\frac{1}{2}\hat{\underline{b}}_{11}^{-1}\hat{\underline{b}}_{1}^{T} \equiv \underline{x}_{e} \qquad (5.28)$$

Substitution of $\underline{x}_e$ in Equation (5.20) would give the optimum value of yield as,

$$\hat{y}_{max} \equiv \hat{y}_e = \hat{b}_o + \hat{\underline{b}}_1 \underline{x}_e + \underline{x}_e^T \hat{\underline{b}}_{11} \underline{x}_e \qquad (5.29)$$

where, T represents the transpose of the vector. Thus, the optimum (coded) values of factor levels calculated using Equation (5.28), and the corresponding natural values are shown in Table 26. The maximum value of yield of (butenes + butadiene) was calculated using Equation (5.29).

Presence of any saddle points or ridges in the fitted response surface (Equation (5.25)) would result in the location of a false optimum. It was therefore considered worthwhile to analyse the fitted response for the presence of any saddle points or ridges within the experimental region. This analysis is as follows:

5.6.4. Simplification of the Quadratic Response Surface — Canonical Analysis [29, 60].

By suitable transformation of the coordinates, Equation (5.19) may be reduced to the form,

$$\hat{y} - \hat{y}_e = \lambda_1 X_1^2 + \lambda_2 X_2 + \lambda_3 X_3^2 + \lambda_4 X_4^2 \qquad (5.30)$$

Table 26. 'OPTIMUM' VALUES OF FACTOR LEVELS AND THE YIELD OF (BUTENES + BUTADIENE).

CATALYST: $Bi_2O_3.2MoO_3$-$AlPO_4$.

Factor	Code Name	Coded Value	Natural Value
Temperature	x_{1e}	-3.306	374°C*
Catalyst/feed ratio	x_{2e}	-1.595	0.38 mol/(mg mol/min)
Butane/oxygen ratio	x_{3e}	2.089	1.82 mol/mol
$Bi_2O_3.2MoO_3/AlPO_4$ ratio	x_{4e}	1.576	8.15 mol/100 mol

'Optimum' yield = 13.39 mol (butenes + butadiene)/ 100 mol butane fed.

* Lies outside the experimental region.

called its canonical form. This was achieved by translation and rotation of the coordinate axes as follows:

The first order terms, i.e. $\underline{b}_1\underline{x}$, in Equation (5.19) or (5.26) were eliminated by shifting the origin to the value $\underline{x}_e$ predicted by Equation (5.29). Thus, the new coordinate system (x'_1, x'_2, x'_3, x'_4) was defined by,

$$x'_i = x_i - x_{ie}$$

or

$$\underline{x}' = \underline{x} - \underline{x}_e \tag{5.31}$$

Introducing this in Equation (5.19),

$$\hat{y} = \hat{b}_o + \underline{b}_1(\underline{x}' + \underline{x}_e) + (\underline{x}' + \underline{x}_e)^T \underline{b}_{11}(\underline{x}' + \underline{x}_e) \tag{5.32}$$

Subtracting Equation (5.29) from Equation (5.32) one gets,

$$\hat{y} - \hat{y}_e = \underline{b}_1\underline{x}' + (\underline{x}'^T \underline{b}_{11} \underline{x}_e + \underline{x}_e^T \underline{b}_{11} \underline{x}') + \underline{x}'^T \underline{b}_{11} \underline{x}' \tag{5.33}$$

The expression in the brackets of Equation (5.33) is identical to zero because premultiplication of Equation (5.28) by $\underline{x}'^T \underline{b}_{11}$ results in the following equation:

$$\underline{x}'^T \underline{b}_{11} \underline{x}_e = -\frac{1}{2} (\underline{x}'^T \underline{b}_1^T)$$

while the equality,

$$\underline{x}_e^T \underline{b}_{11} \underline{x}'^T = \underline{x}'^T \underline{b}_{11} \underline{x}_e = -\frac{1}{2} (\underline{x}'^T \underline{b}_1^T)$$

is obtained by the multiplication of the elements of the respective matrices. Also observing $\underline{b}_1\underline{x}' = \underline{x}'^T \underline{b}_1^T$, we can simplify Equation (5.33) as,

$$\hat{y} - \hat{y}_e = \underline{x}'^T \underline{b}_{11} \underline{x}' \tag{5.34}$$

The translation of the coordinates of the present response surface represented by Equation (5.25) to the $\underline{x}_e$ was carried out to eliminate the linear terms namely, x_1, x_2, x_3 and x_4 in it. Hence Equation (5.25) was converted into the matrix notation using Equations (5.19) and (5.24), from which, the translation of the coordinates to $\underline{x}_e$ was affected. Hence, Equation (5.34) for the present case was

$$\hat{y} - 13.39 = \underline{x}'^T \begin{bmatrix} 0.1175 & 0 & 0.2005 & 0.1672 \\ 0 & 0.0839 & -0.0851 & 0.2487 \\ 0.2005 & -0.0851 & -0.3414 & 0.3938 \\ 0.1672 & 0.2487 & 0.3938 & 0 \end{bmatrix} \underline{x}' \tag{5.35}$$

where,

$$\underline{x}' = \begin{bmatrix} x_1 + 3.31 \\ x_2 + 1.60 \\ x_3 - 2.09 \\ x_4 - 1.58 \end{bmatrix} \tag{5.36}$$

The expansion of Equations (5.34), or (5.35) proved that the cross product terms like $x_1'x_2'$, $x_1'x_3'$ etc. were still

present in the equation. These were eliminated from the equation by rotating the coordinate axes defined by (x_1', x_2', x_3', x_4') to align it with the principal axes of the quadratic. This method, known as "reduction by orthogonal transformation" [29, 31, 40, 60], was adopted to affect such a change. In the orthogonal transformation, the new coordinate axes (X_1, X_2, X_3, X_4) are related to the old coordinates (x_1', x_2', x_3', x_4') through the transformation,

$$\underline{X} = \underline{U}^{-1} \underline{x}' = \underline{U}^{T} (\underline{x} - \underline{x}_e) \qquad (5.37)$$

where $\underline{U}$ is called the unitary matrix. The property, $\underline{U}^{-1} = \underline{U}^{T}$ of the unitary matrix was used in Equation (5.37). The component vectors of this transformation matrix were the same as the eigenvectors of the matrix $\underline{b}_{11}$. The equation of the response surface will then be reduced to the form represented by Equation (5.30), where λ_1, λ_2, λ_3 and λ_4 are the eigenvalues of $\underline{b}_{11}$.

Thus, the eigenvalues and the eigenvectors of the matrix $\underline{b}_{11}$ given in Equation (5.24) were evaluated. The determinant of this matrix was evaluated first and was found to be equal to +0.006458. It may be observed that the matrix $\underline{b}_{11}$ is real and symmetric, with positive value of the determinant. The method of Jacobi was therefore used to calculate the eigenvalues and the eigenvectors of $\underline{b}_{11}$ matrix [33]. A FORTRAN programme of this algorithm is given in

reference [33] as SUBROUTINE JCOBI. The eigenvalues and the eigenvectors of $\underline{b}_{11}$ in Equation (5.25) computed by this subroutine were,

$$\begin{aligned} \lambda_1 &= 0.49066 \\ \lambda_2 &= 0.15536 \\ \lambda_3 &= -0.66528 \\ \lambda_4 &= -0.12068 \end{aligned} \tag{5.38}$$

and

$$\underline{U} = \begin{bmatrix} 0.5222 & 0.5228 & -0.0852 & -0.6684 \\ 0.3254 & -0.8071 & 0.2709 & -0.4115 \\ 0.4109 & 0.2271 & 0.7880 & 0.3982 \\ 0.6727 & -0.1541 & -0.5463 & 0.4747 \end{bmatrix} \tag{5.39}$$

respectively. Thus, the canonical form of Equation (5.25) is given by,

$$y - 13.39 = 0.49066\, X_1^2 + 0.15536\, X_2^2 - 0.66528\, X_3^2 - 0.12068\, X_4^2 \tag{5.40}$$

where the coordinate system (X_1, X_2, X_3, X_4) is related to the original coordinates (x_1, x_2, x_3, x_4) by the following relation:

$$\begin{bmatrix} X_1 \\ X_2 \\ X_3 \\ X_4 \end{bmatrix} = \begin{bmatrix} 0.5222 & 0.3254 & 0.4109 & 0.6727 \\ 0.5228 & -0.8071 & 0.2271 & -0.1541 \\ -0.0852 & 0.2709 & 0.7880 & -0.5463 \\ -0.6684 & -0.4115 & 0.3982 & 0.4747 \end{bmatrix} \begin{bmatrix} x_1 + 3.31 \\ x_2 + 1.60 \\ x_3 - 2.09 \\ x_4 - 1.58 \end{bmatrix} \tag{5.41}$$

It is seen that the eigenvalues λ_1 and λ_2 were both positive while λ_3, λ_4 were both negative. It is evident that the yield of (butenes + butadiene) will show an increasing trend if one changes the factor levels along the positive or negative directions of X_1 and X_2 axes while any movement along X_3 and X_4 directions would decrease the yield. This established that the optimum point $\underline{x}_e$ (Table 26) computed using Equation (5.29) was not a true maximum, but a saddle point. The absolute values of the eigenvalues were comparable in magnitude. Hence, the response surface was an elliptical hyper-saddle surface. Factor level combinations, which predict yields higher than that predicted at the saddle point $\underline{x}_e$, were calculated as follows:

Since a movement along X_3 and X_4 directions resulted in a decreased yield, it was decided to constrain such a movement by setting the values of X_3 and X_4 in Equation (5.40) to zero. Equation (5.40) now becomes,

$$\hat{y} - \hat{y}_e = 0.49066\, X_1^2 + 0.15536\, X_2^2 \tag{5.42}$$

The above equation represents a plane parallel to the X_1X_2 coordinate plane passing through the saddle point $\underline{x}_e$. The constraints $X_3 = 0$ and $X_4 = 0$ result in relations,

$$X_3 = -0.0852(x_1 - x_{1e}) + 0.2709(x_2 - x_{2e}) + 0.7880(x_3 - x_{3e}) - 0.5463(x_4 - x_{4e}) = 0 \quad (5.43)$$

$$X_4 = -0.6684(x_1 - x_{1e}) - 0.4115(x_2 - x_{2e}) + 0.3982(x_3 - x_{3e}) + 0.4747(x_4 - x_{4e}) = 0 \quad (5.44)$$

In Equation (5.42), X_1 and X_2 are given by the following relations:

$$X_1 = 0.5222(x_1 - x_{1e}) + 0.3254(x_2 - x_{2e}) + 0.4109(x_3 - x_{3e}) + 0.6727(x_4 - x_{4e}) \quad (5.45)$$

$$X_2 = 0.5228(x_1 - x_{1e}) - 0.8071(x_2 - x_{2e}) + 0.2271(x_3 - x_{3e}) - 0.1541(x_4 - x_{4e}) \quad (5.46)$$

Equations (5.43) to (5.46) were obtained from Equation (5.41). Solving Equations (5.43) and (5.44) for x_3 and x_4, one gets,

$$(x_3 - x_{3e}) = 0.6856(x_1 - x_{1e}) + 0.1627(x_2 - x_{2e}) \quad (5.47)$$

$$(x_4 - x_{4e}) = 0.8329(x_1 - x_{1e}) + 0.7305(x_2 - x_{2e}) \quad (5.48)$$

Substituting Equations (5.45) to (5.48) in Equation (5.42) and simplifying, the following relationship for the yield of (butenes + butadiene) was obtained,

$$\hat{y} = \hat{y}_e + 0.9602(x_1 - x_{1e})^2 + 0.5042(x_2 - x_{2e})^2 + 1.0321(x_1 - x_{1e})(x_2 - x_{2e}) \quad (5.49)$$

The response values calculated using the above relationship within the experimental region are presented in Table 27. The factor levels were decoded using the data given in Table 25. It can be seen from the table that the hyper-plane described by Equation (5.49) lies outside the experimental range of butane to oxygen ratio. It was, therefore, decided to map (numerically) the entire response surface for various factor level combinations so that the best feasible combination of factor levels may be chosen.

The yields were calculated at different factor level combinations using Equation (5.25). The results of such calculations are presented in Appendix V.

It is apparent from these tables (in Appendix V) that an increase in the $Bi_2O_3.2MoO_3$ content of the catalyst results in an increase in the total yield of (butenes + butadiene). For example, the yield of (butenes + butadiene) predicted at a temperature of 460°C, W/F = 1.2 g catalyst/mg mol/min of feed, butane to oxygen ratio = 1.75 and bismuth molybdate to aluminium phosphate ratio of 0.1 is 16.06 percent. This value

Table 27. CANONICAL ANALYSIS OF THE RESPONSE SURFACE – LOCATION OF THE OPTIMUM FACTOR LEVEL COMBINATION FOR $Bi_2O_3 \cdot 2MoO_3$-$AlPO_4$ CATALYST.

Temperature °C	W/F g/(mg mol/min)	C_4H_{10}/O_2 mol/mol	mol $Bi_2O_3 \cdot 2MoO_3$ per 100 mol $AlPO_4$	Yield* $\hat{y}$
400	0.3	1.98	9.7	14.57
400	0.4	2.00	10.5	15.16
400	0.5	2.02	11.2	16.01
400	0.6	2.03	11.9	17.11
400	0.7	2.05	12.7	18.46
400	0.8	2.06	13.4	20.07
400	0.9	2.08	14.1	21.92
400	1.0	2.10	14.8	24.03
410	0.3	2.05	10.6	15.85
410	0.4	2.07	11.3	16.71
410	0.5	2.08	12.0	17.81
410	0.6	2.10	12.8	19.17
410	0.7	2.12	13.5	20.78
410	0.8	2.13	14.2	22.64
410	0.9	2.15	15.0	24.76
410	1.0	2.17	15.7	27.12
420	0.3	2.12	11.4	17.62
420	0.4	2.14	12.1	18.73
420	0.5	2.15	12.9	20.09
420	0.6	2.17	13.6	21.71
420	0.7	2.19	14.3	23.58
420	0.8	2.20	15.1	25.70
420	0.9	2.22	15.8	28.07
420	1.0	2.23	16.5	30.69

* Yield = mol (butenes + butadiene) formed per 100 mol of butane fed.

needs to be experimentally verified so as to check its validity since these factor level combinations lie on the boundaries of the range of experimental variables covered in the second order design (see Table 25).

It can be seen from the design trial 8 of both Tables 17 and 19 that similar combinations of factor levels resulted in poor experimental yields of (butenes + butadiene) of 4.17 and 4.13 percent respectively. Therefore, 16.06 percent yield predicted by Equation (5.25) at the above-mentioned factor level combinations is erroneous and hence it was not considered to be the best value.

Next the predicted yield at catalyst compositions of less than 7.5 mol $Bi_2O_3.2MoO_3$/100 mol $AlPO_4$ were examined. At this stage, it may be pointed out that a very high butane to oxygen ratio (1.5 or larger)is not desirable since the long term activity of the bismuth molybdate will be reduced drastically. The catalyst has the best long term activity when it is operated at a butane to oxygen ratio of 1.0 to 1.5. Hence, a catalyst composition which has reasonably uniform yield over a wide range of butane to oxygen ratio would be the best from an industrial point of view. From a comparison of the two catalysts at composition levels of 5.0 and 7.5 mol $Bi_2O_3.2MoO_3$/100 mol $AlPO_4$, it can be seen that at a temperature of 420°C and a butane to oxygen ratio of 1.0 or less the yield for the former is better. From a comparison of the

catalysts at composition levels of 2.5 and 5.0 mol $Bi_2O_3.2MoO_3$/100 mol $AlPO_4$, it is seen that the latter catalyst gives better yield of (butenes + butadiene) at butane to oxygen ratios of 1.25 and higher. From these arguments, the best catalyst composition was assumed to be 5.0 mol $Bi_2O_3.2MoO_3$/100 mol $AlPO_4$.

Effect of temperature on the yield of (butenes + butadiene) on the 5.0 mol $Bi_2O_3.2MoO_3$/100 mol $AlPO_4$ catalyst was examined next. It can be seen that for the butane to oxygen ratios between 0.75 to 1.75, the yield of (butenes + butadiene) decreases with an increase in the temperature. A temperature of 420°C was chosen to be the best value in preference to 400°C in order to avoid the formation of oxygenated compounds during the oxidative dehydrogenation reaction.

Having chosen a temperature of 420°C, and a catalyst composition of 5.0 mol $Bi_2O_3.2MoO_3$/100 mol $AlPO_4$ experiments were conducted on this catalyst at various catalyst to feed ratios and butane to oxygen ratios in order to verify experimentally the predicted values of (butenes + butadiene) yields. These experiments (discussed in the following chapter) are reported in Appendix VII as runs numbered 89 through 106. A comparison of these experimental yields with the yields predicted by the second order model (Appendix VI) supports the conclusions drawn in the above analysis.

5.7. Conclusions.

The response surface methodology has been successful in establishing the best conditions for the oxidative dehydrogenation of butane to butenes and butadiene over bismuth molybdate – aluminium phosphate catalysts. The first order approximation of the response surface, and the subsequent application of the steepest ascent technique to the fitted response surface gradually increased the yield of (butenes + butadiene). The first order strategy also led the process conditions like temperature, catalyst-feed ratio, butane-oxygen ratio, catalyst composition to their near-optimum conditions.

The lack of fit of the linear model to the response surface indicated that the curvature effects could no more be neglected. This indicated the nearness of the stationary region of the response surface.

At this stage, a decision was taken regarding the qualitative variable, i.e. the type of bismuth molybdate phase used in the preparation of the catalysts. The two phases, namely, $Bi_2O_3.2MoO_3$ and $Bi_2O_3.MoO_3$ were found to be equally active in the conversion of butane to butenes and butadiene. However, $Bi_2O_3.2MoO_3$ was preferred to $Bi_2O_3.MoO_3$ since the former was stable at higher temperatures, and also its proportion in the catalyst (compared to $AlPO_4$) was less. Therefore, the near-stationary region of only $Bi_2O_3.2MoO_3$-$AlPO_4$ catalyst was

studied by making use of central composite design and subsequently, a quadratic model was fitted to the experimental data. A canonical analysis of this quadratic polynomial indicated that the response surface was not a multidimensional hill, instead, it was an elliptical hyper-saddle surface.

Exploration for the optimum factor level combination along the rising section of the hyper-saddle proved futile, since better yields were predicted only at butane to oxygen ratios above 2.0. Such an optimum was not feasible, since, the bismuth molybdate catalyst would deactivate rapidly at high butane to oxygen ratios.

As an alternate step, the yield of (butenes + butadiene) was evaluated at all possible combinations of factor levels in the experimental range. From an observation of these values, a temperature of 420°C and a catalyst composition of 5.0 mol $Bi_2O_3.2MoO_3$/100 mol $AlPO_4$ were chosen to be the best values since at these factor level combinations, the yields of (butenes + butadiene) were uniformly better at various butane to oxygen ratios.

CHAPTER 6

MODELLING OF OXIDATIVE DEHYDROGENATION REACTION

6.1. Introduction.

In the yield studies using response surface methodology, the oxidative dehydrogenation of butane was investigated without any prior knowledge of the mathematical model describing the dehydrogenation process. A black-box approach was used and the localised regions of the response surface were approximated using simple algebraic expressions which do not give any insight into the physical nature of the dehydrogenation reaction. In the present chapter, an attempt has been made to arrive at a most plausible mechanism based on the physical nature of the system and the experimental observations. An understanding, in the microscopic level, of the possible steps involved in the oxidative dehydrogenation reaction aids in the development of a mathematical model describing the oxidative dehydrogenation process.

In heterogeneous reactions, one or more of the reactants are chemisorbed on the solid surface of the catalyst prior to their conversion to the final products. Some possible modes of butane adsorption on the solid catalysts are discussed b low.

6.2. Mechanism of Butane Adsorption.

Studies of exchange reactions of alkanes with deuterium (Parshall et.al. [92]) indicated that the adsorption of alkanes on the metal oxides is dissociative, i.e.,

$$RCH_3 + 2S \longrightarrow \begin{matrix} RCH_2 & H \\ | & \vdots \\ S & S \end{matrix} \qquad (6.1)$$

where S is an adsorption site on the catalyst and R is an alkyl group. An alternate formulation suggested by the same authors involved the adsorption of alkane on a site, given by,

$$RH + S \longrightarrow \begin{matrix} R & H \\ \diagdown & \diagup \\ & S \end{matrix} \qquad (6.2)$$

followed by migration of hydrogen atom.

Mobile lattice oxygen present in bismuth molybdates suggest a redox mechanism (proposed by Mars and Van Krevelen [85]) for oxidative dehydrogenation of butane. In this scheme, the interaction of the butane molecule with lattice oxygen in the catalyst leads to the formation of butene and water which on further reaction with lattice oxygen forms butadiene.

On the basis of reaction mechanisms discussed above, various plausible models have been developed in the following section.

6.3. Reaction Rate Models.

In the derivations given below,

r is the rate of reaction,

p is the partial pressure of reactant, and

K is the adsorption equilibrium constant,

with subscripts A, B, C, O and W representing butane, butene, butadiene, oxygen and water respectively.

6.3.1. Redox Model.

The oxidative dehydrogenation of butane to butadiene is represented by the following reaction scheme:

$$A + Cat(ox) \xrightarrow{k_1} B + Cat(red) \qquad (6.3)$$

$$B + Cat(ox) \xrightarrow{k_2} C + Cat(red) \qquad (6.4)$$

$$Cat(red) + \tfrac{1}{2}O_2 \xrightarrow{k_3} Cat(ox) \qquad (6.5)$$

where Cat(ox) represents the oxidised state of the catalyst and Cat(red) denotes the reduced state of the catalyst.

Let, θ be the fraction of oxidised sites in the catalyst. Then, by using the above reaction scheme, one can write the reaction rates as,

$$r_A = - k_1 p_A^a \theta$$

$$r_B = (k_1 p_A^a - k_2 p_B^b)\theta$$

$$r_C = k_2 p_B^b \theta$$

$$r_{ox} = k_3 p_O^q (1 - \theta)$$

By a balance for oxygen, i.e., $r_{Cat(ox)} = r_{Cat(red)}$, the following equation is obtained,

$$\theta = \frac{k_3 p_O^q}{(k_1 p_A^a + k_2 p_B^b + k_3 p_O^q)}$$

Hence, the reaction rates are now given by,

$$r_A = - \frac{k_1 k_3 p_A^a p_O^q}{k_1 p_A^a + k_2 p_B^b + k_3 p_O^q} \qquad (6.6)$$

$$r_B = \frac{(k_1 p_A^a - k_2 p_B^b) k_3 p_O^q}{k_1 p_A^a + k_2 p_B^b + k_3 p_O^q} \qquad (6.7)$$

$$r_C = \frac{k_2 p_B^b k_3 p_O^q}{k_1 p_A^a + k_2 p_B^b + k_3 p_O^q} \qquad (6.8)$$

The rate of consumption of oxygen and the rate of generation of water can be calculated from the equations,

$$r_O = \frac{r_A - r_C}{2} \qquad (6.9)$$

$$r_W = - r_A + r_C \qquad (6.10)$$

6.3.2. Langmuir-Hinshelwood Model.

Assuming irreversible surface reactions, viz.,

$$A^* + O^* \xrightarrow{k_1} B^* + H_2O^* \qquad (6.11)$$

$$B^* + O^* \xrightarrow{k_2} C^* + H_2O^* \qquad (6.12)$$

(* represents adsorbed species),

the following expressions may be derived when surface reactions are rate controlling,

$$r_A = - \frac{k_1 K_A p_A \sqrt{K_O p_O}}{(1 + K_A p_A + K_B p_B + K_C p_C + \sqrt{K_O p_O} + K_W p_W)^2} \qquad (6.13)$$

$$r_B = \frac{(k_1 K_A p_A - k_2 K_B p_B) \sqrt{K_O p_O}}{(1 + K_A p_A + K_B p_B + K_C p_C + \sqrt{K_O p_O} + K_W p_W)^2} \qquad (6.14)$$

$$r_C = \frac{k_2 K_B p_B \sqrt{K_O p_O}}{(1 + K_A p_A + K_B p_B + K_C p_C + \sqrt{K_O p_O} + K_W p_W)^2} \qquad (6.15)$$

The oxygen consumption and water generation rates can be calculated using Equations (6.9) and (6.10).

6.3.3. Rideal-Eley Mechanism.

It is possible that only one of the two reactants (either butane or oxygen) is adsorbed, and the other reacts from the gas phase. In a situation, where butane is adsorbed, and

oxygen is in the gas phase, the surface reactions are given by

$$A^* + \tfrac{1}{2}O_2 \xrightarrow{k_1} B^* + H_2O \qquad (6.16)$$

$$B^* + \tfrac{1}{2}O_2 \xrightarrow{k_2} C^* + H_2O \qquad (6.17)$$

Assuming irreversible surface reactions to be rate controlling, the following rate expressions can be obtained,

$$r_A = -\frac{k_1 K_A p_A p_O^q}{1 + K_A p_A + K_B p_B + K_C p_C} \qquad (6.18)$$

$$r_B = \frac{(k_1 K_A p_A - k_2 K_B p_B) p_O^q}{1 + K_A p_A + K_B p_B + K_C p_C} \qquad (6.19)$$

$$r_C = \frac{k_2 K_B p_B p_O^q}{1 + K_A p_A + K_B p_B + K_C p_C} \qquad (6.20)$$

Rates of oxygen consumption and water generation are again given by Equations (6.9) and (6.10).

Similar expressions can be derived for the case where the reaction takes place between adsorbed oxygen species and butane in gas phase. Such a mechanism involving butane in gas phase is very unlikely.

Experimental data obtained in the laboratory, were used to test if one or more of the above models are plausible.

6.4. Experimental Observations.

The analysis of the response surface of (butenes + butadiene) yield reported in Section 5.8 indicated a catalyst composition of 5 mol $Bi_2O_3.2MoO_3$/100 mol $AlPO_4$ to be the most suitable one. Experiments were conducted in a randomised order on this catalyst at 420°C and at various levels of catalyst to feed ratio and butane to oxygen ratio. These data are reported in Appendix VII as runs numbered 89 through 106.

The partial pressures of butene and butadiene measured at different catalyst-feed ratios and butane to oxygen ratios are shown in Figs. 22 and 23. It can be visualised from Fig. 22 that the partial pressure of butene has a possible maximum in the range of catalyst to feed ratios employed. This is because butene is an intermediate product of two consecutive reactions. The partial pressure of butadiene (Fig. 23) reached a plateau at high values of catalyst to feed ratios, which is possibly due to cracking.

Point selectivity, defined as the ratio of the rates of formation of any two species [99], was used to identify the plausible models describing the oxidative dehydrogenation process. Results and discussion of these aspects are given in the following sections.

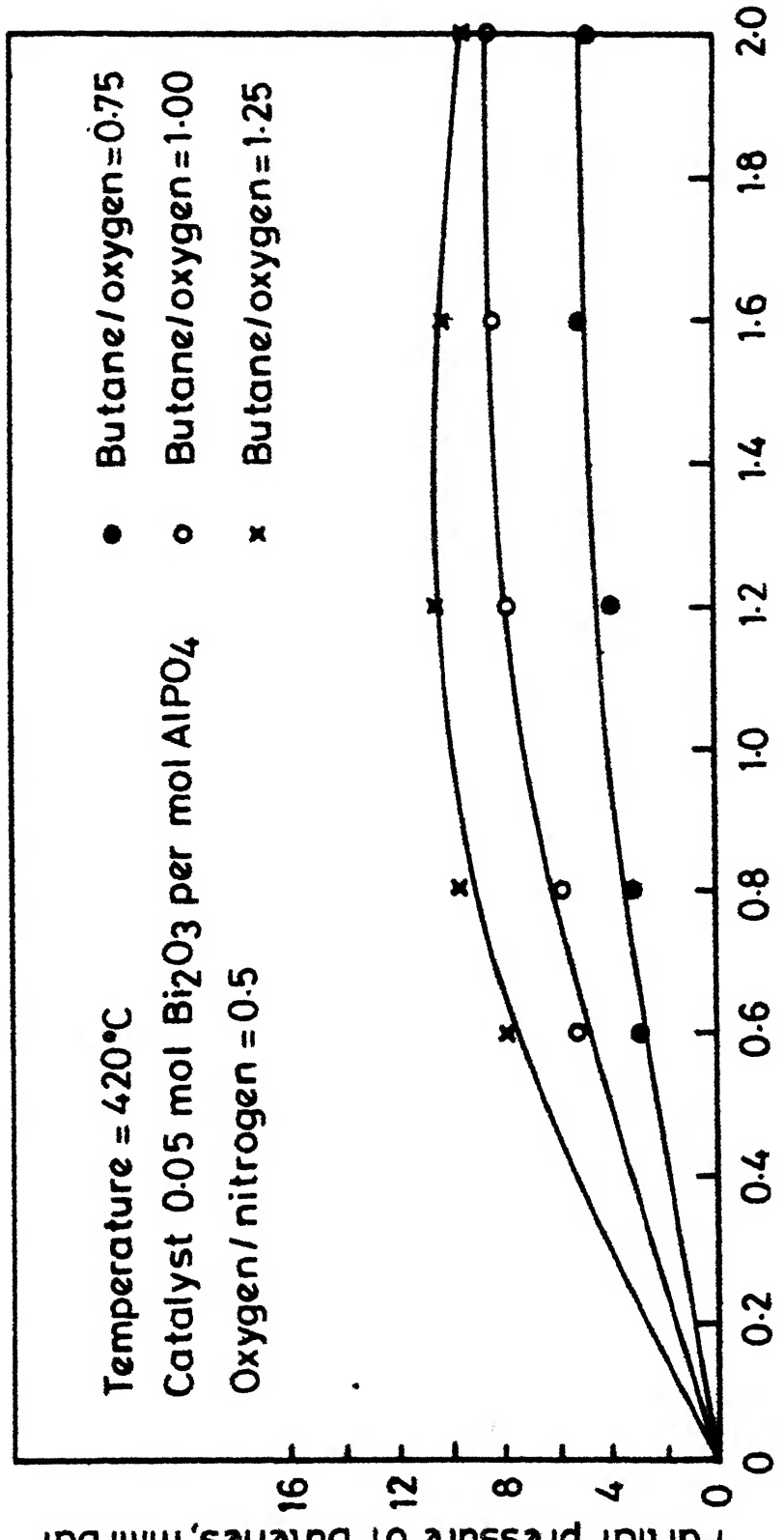

Fig. 22 : Partial pressure of butenes vs. W/F ratio for $Bi_2O_3.2MoO_3$-$AlPO_4$ catalyst.

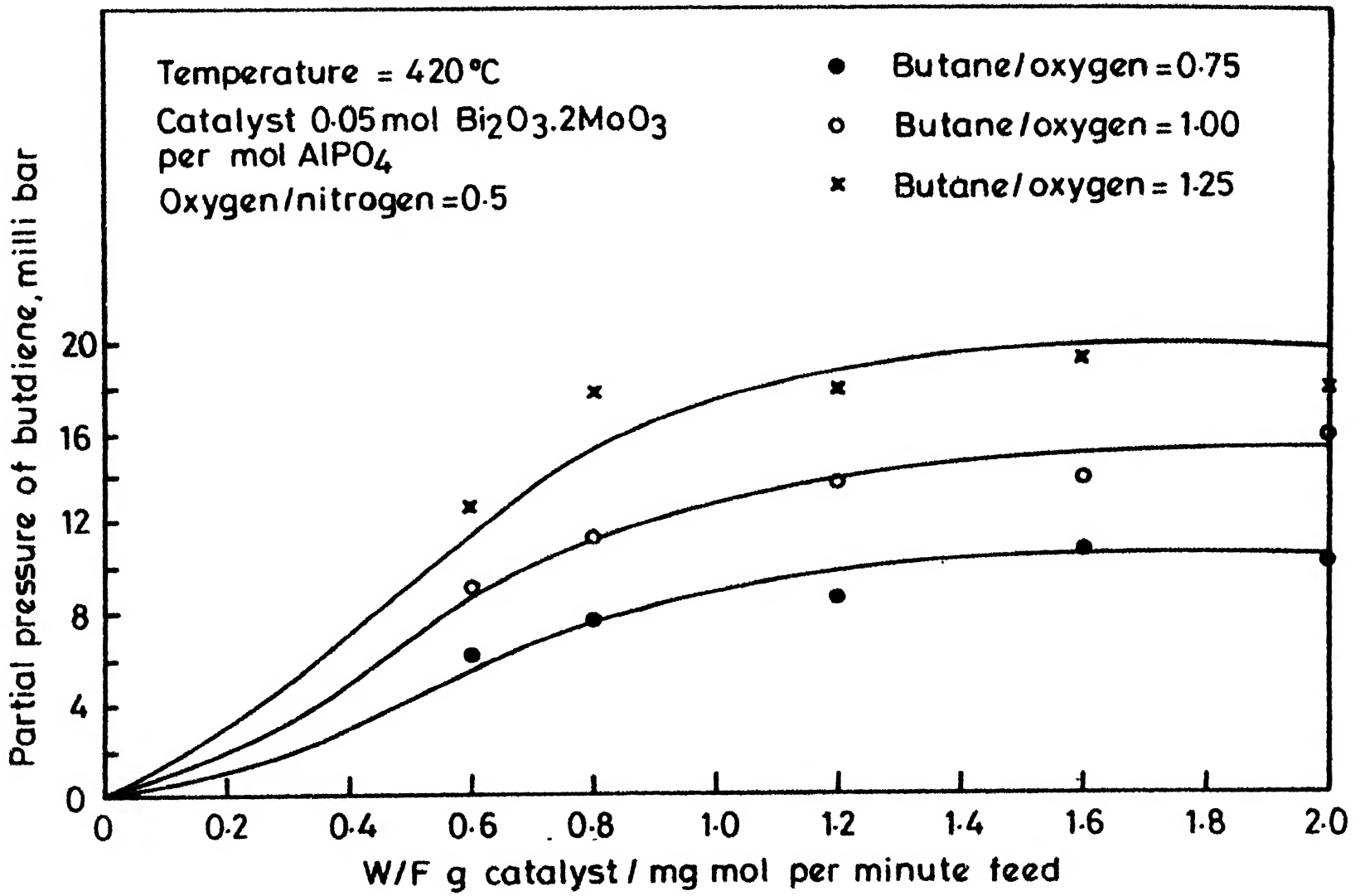

Fig. 23 : Partial pressure of butadiene vs. W/F ratio for $Bi_2O_3.2MoO_3$-$AlPO_4$ catalyst.

6.5. Identification of Plausible Models – Method of Point Selectivity.

Point selectivity was defined as the ratio of the rate of formation of butene to that of butadiene. These ratios for the various models proposed in Section 6.3 are as follows:

Redox Model

$$\frac{r_B}{r_C} = \frac{k_3}{k_2} p_A^a p_B^b - 1 \qquad (6.21)$$

Langmuir-Hinshelwood Model

$$\frac{r_B}{r_C} = \frac{k_1 K_A}{k_2 K_B} \cdot \frac{p_A}{p_B} - 1 \qquad (6.22)$$

Rideal-Eley Mechanism

$$\frac{r_B}{r_C} = \frac{k_1 K_A}{k_2 K_B} \cdot \frac{p_A}{p_B} - 1 \qquad (6.23)$$

These equations can be reduced to the form,

$$\frac{r_B}{r_C} = k' p_A^a p_B^{-b} - 1 \qquad (6.24)$$

where k' is a constant and a = b = 1 for both Langmuir-Hinshelwood and Rideal-Eley models. Thus all the models describe the response (point selectivity) for the situation when a = b = 1. However, discrimination is possible when the exponents are different from unity.

The rates of formation of butene and butadiene were obtained by graphical differentiation of partial pressure Vs. catalyst to feed ratio curves which are shown in Figs. 22 and 23. The parameter k' in Equation (6.24) was evaluated at different values of a (= 0.5 to 2) and b (= 0.5 to 1) by linear

regression and the confidence limits [60] of the same are presented in Table 28. It can be inferred from the table that, since the parameter k' is positive for all cases it is not possible to reject any models. The combination (a = 0.5, b = 0.5) has the least estimate of error variance. Taking this as the best model (in the least squares sense), the plausibility of most of the combinations of a and b cannot be ruled out. Hence, in order to achieve better understanding about the models, a multiresponse technique has been proposed as a scope for future study.

6.6. Parameter Estimation – Multiresponse Situation.

Models constructed in Section 6.3 on the basis of redox, Langmuir-Hinshelwood and Rideal-Eley mechanisms, in each of the cases were a set of nonlinear ordinary differential equations. The two step nature of the oxidative dehydrogenation reaction required that all the reliable responses be considered in evaluating the parameters [62]. In the present investigation, butene and butadiene measurements were found to be most reliable and hence they were used in the parameter estimation.

Bard [15] analysed the problem of parameter estimation in systems of nonlinear ordinary differential equations and concluded that the use of surface minimisation methods (such as Davidon-Fletcher-Powell method given in subroutine DFMP and Fletcher-Reeves conjugate gradient method given as subroutine

Table 28. POINT SELECTIVITY METHOD OF MODEL DISCRIMINATION.

PARAMETER ESTIMATES AND THEIR CONFIDENCE INTERVAL.

S.No.	Exponents		Parameter k' ± Confidence Interval	Estimate of Variance	Total Residue
	a	b			
1	0.5	0.5	0.195 ± 0.059	0.559	4.84
2	0.5	1.0	0.194 ± 0.102	1.155	10.43
3	1.0	0.5	0.016 ± 0.006	0.827	7.32
4	1.0	1.0	0.014 ± 0.009	1.365	12.37
5	1.5	0.5	0.0012 ± 0.0007	1.069	9.57
6	1.5	1.0	0.0011 ± 0.0008	1.534	13.93
7	2.0	0.5	0.00009 ± 0.00005	4.466	11.49
8	2.0	1.0	0.00008 ± 0.00006	1.669	15.17

FMCG in IBM Scientific Subroutine Package [117]) would lead to poor convergence of the parameters. This was confirmed in the present investigation when using the determinant minimisation criterion suggested by Box and Draper [30, 62]. Hence a simpler criterion suggested by Lapidus and Peterson [76, 95, 107] given as,

$$\sum_{i=1}^{N} (p_{B_i} - \hat{p}_{B_i})^2 + \sum_{i=1}^{N} (p_{C_i} - \hat{p}_{C_i})^2 = \text{minimum} \qquad (6.21)$$

was used instead.

The algorithm used in the parameter estimation is presented in the form of a flow diagram in Fig. 24. Marquardt's nonlinear least squares algorithm [84], as implemented by Ball and Groenweghe [13, 14], was used for the minimisation of sum of squares. A listing of this subroutine is found in Kuester and Mize [72] as SUBROUTINE BSOLVE. The system of ordinary differential equations describing the model was integrated using the method suggested by Gil [67b]. A computer programme for the same has been developed by Krishnamurthy and Sen [67a].

The derivative matrix, $\underline{\Delta}$ required in the Marquardt's algorithm may be computed as the solution of the sensitivity equations [101, 107], with initial conditions as given below:

$$\dot{\lambda}_{ij} = \sum_{l=1}^{n} \left(\frac{\partial \phi_i}{\partial p_l}\right) \lambda_{lj} + \left(\frac{\partial \phi_l}{\partial k_j}\right) \qquad (6.22)$$

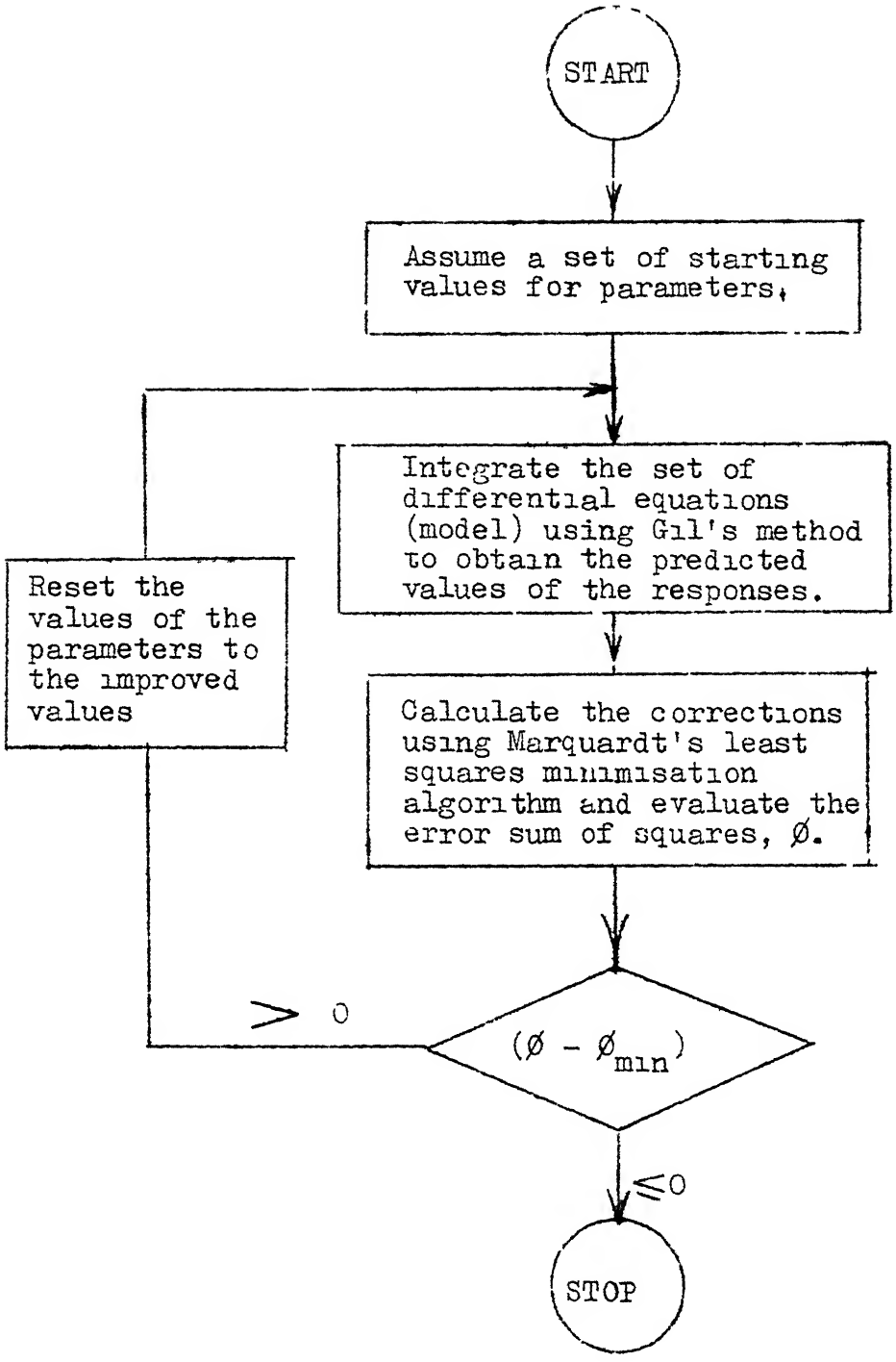

Fig. 24. Flow Diagram of the Algorithm Used in Multiresponse Parameter Estimation.

with initial conditions,

$$\lambda_{ij}(0) = 0$$

$$i = 1, 2, \ldots, n$$

$$j = 1, 2, \ldots, P \qquad (6.23)$$

where,

$\dot{\lambda} = \frac{d\lambda}{dt}$, derivative with respect to time, t,

λ_{ij} is the derivative of the response with respect to the various parameters given as $\lambda_{ij} = \frac{\partial p_i}{\partial k_j}$

ϕ_i is the function defining the i-th response (model)

p_i is response, p_A, p_B, etc.

k_j is the parameters to be estimated

n is the number of responses in the model (Five in the present study, viz., the partial pressure of butane, butene, butadiene, oxygen and water)

P is the total number of parameters to be estimated.

In the matrix form Equation (6.22) may be represented as,

$$\dot{\underline{\Lambda}} = \underline{A}\,\underline{\Lambda} + \underline{B} \qquad (6.23)$$

where,

$$\underline{A} = \left\{ \frac{\partial \phi_l}{\partial p_\nu} \right\}_{k^*} \qquad \begin{matrix} l = 1, 2, \ldots, n \\ \nu = 1, 2, \ldots, n \end{matrix} \qquad (6.24)$$

$$\underline{B} = \left\{ \frac{\partial \phi_l}{\partial k_\nu} \right\}_{k^*} \qquad \begin{matrix} l = 1, 2, \ldots, n \\ \nu = 1, 2, \ldots, P \end{matrix} \qquad (6.25)$$

The details regarding the construction of these sensitivity equations have been described in Appendix VI. For n responses and P parameters to be estimated, n(P+1) sensitivity equations (a set of simultaneous differential equations) have to be solved in order to evaluate the derivative matrix analytically. The effort required in the numerical evaluation of the derivative matrix is even more.

The algorithm described above and shown by a flow diagram in Fig. 24 can be used for obtaining the parameters of the multiresponse model. An attempt has been made in this direction. However due to the limitations of the computer speed (IBM 7044) and time, it could not be pursued at the present time.

6.7. Conclusions.

Using point selectivity ratio, defined as the ratio of the rate of formation of butene to that of butadiene, an attempt has been made to screen the various reaction models represented by sets of ordinary differential equations. In view of the acceptable nature of the parameter k' (that it should be positive in the confidence region) and a small ratio of the error variances between the best (in the least squares sense) and the poor model, barring the model represented by S.No. 7 of Table 28 for which the error variance was usually large, it was deemed not possible to discriminate amongst the various models.

A suggestion for future work has been included in Section 6.6 for estimating the parameters for multiresponse situation which hopefully gives better discrimination amongst the various models.

CHAPTER 7

SUMMARY AND CONCLUSIONS

7.1. Summary and Conclusions.

The present work was started with a feasibility investigation of the oxidative dehydrogenation of n-butane on a molybdic oxide catalyst. Though the yield of (butenes + butadiene) on this catalyst was low, the feasibility of one step dehydrogenation of butane to butadiene was established.

In order to improve the yield of (butenes + butadiene), bismuth, which has a promoter effect in the oxidative dehydrogenation of butenes, was incorporated in the catalyst in the form of bismuth molybdate. Three phases of bismuth molybdates, namely, α, β and γ with chemical compositions $Bi_2O_3.3MoO_3$, $Bi_2O_3.2MoO_3$ and $Bi_2O_3.MoO_3$ were used in the present investigation. The dehydrogenation catalysts were prepared by mixing them physically with ortho-aluminium phosphate in varying proportions.

The physical and chemical characteristics of the prepared catalysts were investigated first in order to understand their structure and thermal stabilities. The X-ray and infrared analyses of the bismuth molybdates established that the α-phase was likely to be inactive since it had a monoclinic structure with edge shared octahedra. The presence of corner-shared octahedral molybdenum in β- and γ-bismuth molybdates

(as inferred from infrared and X-ray analyses) indicated that they were promising active materials for the dehydrogenation catalyst. The calcination of these β- and γ- forms with o-$AlPO_4$ did not indicate any structural changes in them. In the case of β-bismuth molybdate, calcination with o-$AlPO_4$ inhibited, partially, the decomposition of the former, while the calcination of γ-bismuth molybdate with o-$AlPO_4$ indicated a tendency towards preferred orientations of certain crystal planes.

An investigation of the thermal stabilities of β- and γ-bismuth molybdates indicated that the β-bismuth molybdate underwent a reversible decomposition at temperatures close to its melting point (about 700°C), while the γ-form underwent an irreversible transition γ — γ' (at temperatures above 600°C), γ' being a poor catalyst active material. Both these transformations occurred beyond the range of temperatures 400-500°C used in the oxidative dehydrogenation reaction. Hence the β- and γ-bismuth molybdates catalysts on o-$AlPO_4$, prepared by the above procedure, were used.

Response surface methodology was applied to optimise the yield of (butenes + butadiene). 2^{4-1} fractional factorial experiments were used to explore the linear region of the yield-response surface using temperature, catalyst to feed ratio, butane to oxygen ratio and proportion of the bismuth molybdate in aluminium phosphate support, as variables.

In addition, the phase of bismuth molybdate was used as a qualitative variable. Simultaneous exploration of the response surface with two qualitative variables indicated that they had similar activity for oxidative dehydrogenation of butane, the maximum experimental yields being 12.6% and 14.8% for γ- and β-bismuth molybdate aluminium phosphate catalysts respectively.

The near-stationary region of the yield response surface was explored for β-bismuth molybdate-aluminium phosphate catalyst only. This catalyst was preferred to γ-bismuth molybdate-aluminium phosphate, since all the thermal (phase) transitions of β-bismuth molybdate were reversible while those of γ-bismuth molybdate were irreversible. Simplicity of preparation of β-bismuth molybdate also favoured its choice over γ-bismuth molybdate.

The near-stationary region of yield-response surface using β-bismuth molybdate-aluminium phosphate catalyst was explored by employing a central composite design. The experimental data, fitted to a quadratic (second degree) polynomial, was found to represent the data adequately. A canonical analysis of the fitted response surface indicated that the surface was an elliptical hyper-saddle with the rising section of saddle passing through the principal planes (of the quadratic) lying outside the region of experimentation. Hence, the response surface was mapped numerically and a region where the predicted yields of (butenes + butadiene) were

uniformly good (about 10-12%) in the commonly employed range of butene to oxygen ratios (0.5-1.5) was chosen for modelling the oxidative dehydrogenation reaction.

Models based on point selectivity (defined as the ratio of rate of formation of butenes to that of butadiene) indicated that the redox, Langmuir-Hinshelwood and Rideal-Eley models were all equally plausible.

7.2. Suggestions for Future Work.

On the basis of the present investigation, the following aspects are recommended for future work:

1. Catalysts prepared by coprecipitation of Bi_2O_3, MoO_3 and $AlPO_4$ could be studied.
2. In the present study it was observed that γ-bismuth molybdate exhibits preferred orientation in crystal planes and the decomposition of β-bismuth molybdate is partially inhibited, in the presence of aluminium phosphate. Hence, the thermal stability of the bismuth molybdates in the presence of aluminium phosphate provides an interesting area for research.
3. Discrimination amongst various models based on redox Langmuir-Hinshelwood and Rideal-Eley mechanisms was not achieved in the present study using point selectivity ratios. Estimation of parameters in these models using

multiresponse techniques and discrimination of these models based on the estimates of parameters are suggested for future study.

4. The canonical analysis of the response surface of (butenes + butadiene) yield indicated that better yields are obtained at higher butane to oxygen ratios (>2). The stability of the catalyst under such high butane-oxygen ratios needs to be investigated.

5. The bismuth molybdates undergo structural transformations (participation of lattice oxygen) during oxidative dehydrogenation, which may lead to a slow change in the structure of a freshly prepared catalyst. Hence, a study of the aging of the bismuth molybdate-aluminium phosphates will be important from an industrial viewpoint.

LIST OF REFERENCES

1. Adams, C.R., in "Proceedings of the Third International Congress on Catalysis Amsterdam 1964", Sachtler, W.M.H., Schmit, G.C.A., Zwietering, P., Eds., Vol. 1, p. 240, North-Holland Publishing Co., Amsterdam, 1965.

2. Adams, C.R., Voge, H.H., Morgan, C.Z., and Armstrong, W.E., J. Catalysis, 3, 379 (1964).

3. Adler, Yu. P., Markova, E.V., and Granovsky, Yu. V., "The Design of Experiments to Find Optimal Conditions", Mir Publishers, Moscow, 1975.

4. Ai, M., and Ikawa, T., J. Catalysis, 40, 203 (1975).

5. Ai, M., and Suzuki, S., J. Catalysis, 26, 202 (1972).

6. Ai, M., and Suzuki, S., J. Catalysis, 30, 362 (1973).

7. Akayan, K., J. Catalysis, 12, 281 (1968).

8. Akimoto, M., and Echigoya, E., J. Catalysis, 29, 191 (1973).

9. Akimoto, M., and Echigoya, E., J. Catalysis, 35, 278 (1974).

10. Appleby, W.G., Avery, W.H., Meerbott, W.K., and Sartor, A.F., J. Am. Chem. Soc., 75, 1809 (1953).

11. Appleton, A.A., J. Inst. Petrol., 46, 367 (1964).

12. Bakshi, Yu. M., Gur'yanova, R.N., and Gelbstein, A.I., Kinet. Katal. (Eng. Transl.). 16, 374 (1976).

13. Ball, W.E., Ind. Eng. Chem. Fundamentals, 6, 475 (1967).

14. Ball, W.E., and Groenweghe, L.C.D., Ind. Eng. Chem. Fundamentals, 5, 181 (1966).

15. Bard, Y., SIAM J. Numer. Anal., 7, 157 (1970).

16. Batist, Ph. A., Bouwens, J.F.H., and Matsuura, I., J. Catalysis, 32, 362 (1974).

17. Batist, Ph. A., Bouwens, J.F.H., and Schuit, G.C.A., J. Catalysis, 25, 1 (1972).

18. Batist, Ph. A., Der Kinderen, A.H.W.M., Leeuwenburgh, Y., Metz, F.A.M.G., and Schuit, G.C.A., J. Catalysis, 12, 45 (1968).

19. Batist, Ph. A., Kapteijns, C.J., Lippens, B.C., and Schuit, G.C.A., J. Catalysis, 7, 33 (1967).

20. Batist, Ph. A., Lippens, B.C., and Schuit, G.C.A., J. Catalysis, 5, 55 (1966).

21. Batist, Ph. A., Prettre, H.J., and Schuit, G.C.A., J. Catalysis, 15, 267 (1969).

22. Beckberger, L.H., and Watson, K.M., Chem. Eng. Progr., 44(3), 229 (1948).

23. Begley, J.W., Hydrocarb. Process, 44(7), 149 (1965).

24. Beres, J., Brueckman, K., Haber, J., and Janas, J., Bull. Acad. Pol. Sci. Ser. Sci. Chim., 20, 813 (1972).

25. Bleyenberg, A.C.A., Lippens, B.C., and Schuit, G.C.A., J. Catalysis, 4, 581 (1965).

26. Blue, R.W., Holm, V.C.F., Fast, E., and Heckelsberg, L.F., Ind. Eng. Chem., 44, 2710 (1962).

27. Boreskov, G.K., Ven'yaminov, S.A., Dzis'ko, V.A., Tarsova, D.V., Dindoin, V.M., Sazonova, N.N., Olen'kova, I.P., and Kafeli, L.M., Kinet. Kal. (Eng. transl.), 70, 1350 (1969).

28. Boutry, P., Dumas, J., and Montarnal, R., C. R. Acad. Sc. Paris Series-C, 264, 81 (1967).

29. Box, G.E.P., Biometrics, 10, 16 (1954).

30. Box, G.E.P., and Draper, N.R., Biometrika, 52, 355 (1965).

31. Box, G.E.P., and Wilson, K.B., J. Royal Stat. Soc., B13, 1 (1951).

32. Box, G.E.P., and Youle, P.V., Biometrics, 11, 287 (1955).

33. Carnahan, B., Luther, H.A., and Wilkes, J.O., "Applied Numerical Methods", John Wiley & Sons Inc., New York, 1969.

34. Carra, S., Forni, L., and Vintani, C., J. Catalysis, 9, 154 (1967).

35. Chemical Weekly, p. 41, Aug. 9, 1977; p. 45, Sept. 13, 1977.

36. Chemical Weekly, p. 43, July 19, 1977; p. 41, July 26, 1977; p. 37, Sept. 20, 1977.

37. Clark, G.M., and Doyle, W.P., Spectrochim. Acta, 22, 1441 (1966).

38. Cochran, W.G., and Cox, G.M., "Experimental Designs", 2nd ed., John Wiley Inc., New York, 1957.

39. Corson, B.B., Jones, H.E., Welding, C.E., Hinkley, J.A., and Stahly, E.E., Ind. Eng. Chem., 42, 359 (1951).

40. Davies, O.L., "Design and Analysis of Industrial Experiments", Hafner Publ. Co., New York, 1956.

41. Dodd, R.H., and Watson, K.M., Trans. A.I.Ch.E., 42, 263 (1946).

42. Duck, E.W., and Timms, D.G., in "Production of Polymer and Plastics Intermediates from Petroleum", R. Long, Ed., pp. 18-39, Butterworth & Co., London, 1967.

43. Elwell, N.T., and Wood, D.F., "Analytical Chemistry of Molybdenum and Tungsten", p. 41, Pergamon Press, Oxford, 1971.

44. Emig, G., Chemie. Ing. Tech., 49, 865 (1977).

45. Eraman, L. Ya., Gal'perin, E.L., Russ. J. Inorg. Chem., 11, 122 (1966); 13, 487 (1968).

46. Erman, L. Ya., Gal'perin, E.L., Kolchin, I.K., Dobrzhanskii, G.F., and Chernyshev, K.S., Russ. J. Inorg. Chem., 9, 1174 (1964).

47. Ettre, L.S., and Zlatkis, A., "The Practice of Gas Chromatography", Interscience Publ., New York, 1963.

48. Frey, E.E., and Hupke, W.F., Ind. Eng. Chem., 25, 54 (1933).

49. Frondel, C., Am. Min., 28, 536 (1943); "Powder Diffraction File", File Number 7-401, Am. Soc. for Testing and Materials, Philadelphia, 1966.

50. Gaspar, N.J., and Pasternak, I.S., U.S. Patent 3,320,331 (1967); Chem. Abstr., 68, 39068g.

51. Gaspar, N.J., Pasternak, I.S., and Vadekar, M., Can. J. Chem. Eng., 52, 793 (1974).

52. Grzybowska, B., Haber, J., and Komorek, J., J. Catalysis, 25, 25 (1972).

53. Haber, J., International Chem. Eng., 15, 21 (1975).

54. Haber, J., and Grzybowska, B., J. Catalysis, 28, 489 (1973).

55. Happel, J., Black, H., and Hamill, T.D., Ind. Eng. Chem. Fundamentals, 5, 289 (1966).

56. Happel, J., Hnatow, M.A., and Mezaki, R., Advances Chem. Series No. 97, pp. 102-109, Am. Chem. Soc. Publications, 1970.

57. Harber, R.U., Petroleum, 22(10), 348 (1958).

58. Hemmerle, W.J., "Statistical Computations on Digital Computer", Blaisdell Publ. Co., Waltham, Massachusetts, 1967.

59. Hill, W.J., and Hunter, W.G., Technometrics, 8, 571 (1966).

60. Himmelblau, D.M., "Process Analysis by Statistical Methods", John Wiley & Sons Inc., New York, 1968.

61. Hucknall, D.J., "Selective Oxidation of Hydrocarbons", Academic Press Inc., London, 1974.

62. Hunter, W.G., Ind. Eng. Chem. Fundamentals, 6, 461 (1967).

63. Keizer, K., Batist, Ph. A., and Schuit, G.C.A., J. Catalysis, 15, 256 (1969).

64. Keulemans, A.I.M., "Gas Chromatography", Reinhold Publishing Corp., New York, 1957.

65. Keulks, G.W., J. Catalysis, 19, 232 (1971).

66. Khabibuleva, O.K., Lavrovoskii, K.P., and Rozenthal, A.L., Bull. Acad. Sci. USSR (Div. Chem. Sci.), p. 1164 (1968).

67a. Krishnamurthy, E.V., and Sen, S.K., "Computer Based Numerical Algorithms", Affiliated East-West Press Ltd., New Delhi, 1976.

67b. Gil, S., Proc. Camb. Phil. Soc., 47, 96 (1951).

68. Kodama, K., "Methods of Quantitative Inorganic Analysis", p. 166, Interscience Publishers, London, 1963.

69. Komarovskii, N.A., Tsailingol'd, M.E., Basner, M.E., Pilipenko, F.S., and Slin'ko, M.G., Kinet. Katal. (Eng. transl.), 14, 1313 (1974).

70. Konings, A.J.A., Creemers, H.J.M., and Batist, Ph. A., J. Catalysis, 41, 333 (1976).

71. Kovaleva, I.N., and Tulupov, V.A., Russian J. Phys. Chem., 48, 110 (1974).

72. Kuester, J.L., and Mize, J.H., "Optimisation Techniques with Fortran", McGraw Hill Book Co., New York, 1973.

73. Kunigita, E., Suga, K., and Otake, T., J. Chem. Eng. Japan, 2, 75 (1969).

74. Kuz'michev, S.P., and Skarachenko, V.K., Kinet. Katal. (Eng. transl.), 11, 531 (1970).

75. Kwic Guide to the Powder Diffraction File; and "Powder Diffraction File", File Number 10-423, Soc. for Testing and Materials, Philadelphia, 1966.

76. Lapidus, L., and Peterson, T.I., A.I.Ch.E. Journal, 11, 891 (1965).

77. Lavrovskii, K.P., Rozenthal, A.L., and Khabibuleva, O.K., International Chem. Eng., 9, 75 (1969).

78. Lavrovskii, K.P., Rozenthal, A.L., and Khabibuleva, O.K., Kinet. Katal. (Eng. transl.), 10, 102 (1969).

79. Lavrovskii, K.P., Rozenthal, A.L., Khabibuleva, O.K., and Verkotina, L.V., International Chem. Eng., 8, 573 (1968).

80. Lester, G.R., U.S. Patent 3,361,839 (1968).

81. Levin, V.A., Vernova, T.V., and Tsailingol'd, A.L., Kinet. Katal. (Eng. transl.), 13, 454 (1972).

82. McDonald, W.R., and McIntyre, A.D., U.S. Patent 3,119,111 (1964); Chem. Abstr., 60, 9088a.

83. McNair, T.M., and Bonelli, E.J., "Basic Gas Chromatography Varian Aerograph Inc., Walnut Creek, Calif., 1969.

84. Marquardt, D.M., J. Soc. Indust. Appl. Math., 11, 431 (1963).

85. Mars, P., and van Krevelen, D.W., Chem. Eng. Sci., Suppl., 3, 41 (1954).

86. "Matheson Gas Data Book", Matheson Gas Company Inc., East Rutherford, New Jersey, 1961.

87. Matsuura, I., and Schuit, G.C.A., J. Catalysis, 20, 19 (1971).

88. Meites, L., "Handbook of Analytical Chemistry", McGraw Hill Book Co., New York, 1963.

89. Mellor, J.W., "A Comprehensive Treatise on Inorganic and Theoretical Chemistry", Vol. 9, p. 709, Longmans Green & Co., London, 1957.

90a. Mitchell, P.C.H., and Trifiro, F., J. Chem. Soc. (A), 3183 (1970).

90b. Nakamoto, K., "Infrared Spectra of Inorganic and Coordination Compounds", John Wiley and Sons, New York, 1963.

91. Noda, S., Hudgins, R.R., and Silveston, P.L., Can. J. Chem. Eng., 45, 294 (1967).

92. Parshall, G.W., Green, M.L.H., Caderrazo, F., Dowden, G.A., Gault, F.G., Halpern, G.A., Hamilton, G.A., Kemball, C., Teichner, S.J., and Volger, H.C., in "Proceedings of the NATO Science Committee Conference on Catalysis held at Santa Margherita di Pula, December 1972", Baslo, F., and Burwell, D.L., Eds., Plenum Press, New York, 1973.

93. Pasternak, I.S., and Vadekar, M., Can. J. Chem. Eng., 48, 216 (1970).

94. Paul, R.E., and Marek, L.F., Ind. Eng. Chem., 26, 454 (1934).

95. Peterson, T.I., and Lapidus, L., Chem. Eng. Sci., 21, 655 (1966).

96. Polataiko, R.L., Shapovalova, L.P., and Musienko, V.P., Neft. Gazov. Prom., p. 38 (6), (1968); Chem. Abstr., 70, 77204x.

97. Pribil, R., and Malat, M., Collection Czechoslov. Chem. Commun, 15, 120 (1950).

98. Raley, J.H., Mullineauk, R.D., and Bittner, C.W., J. Am. Chem. Soc., 85, 3174 (1963).

99. Rao, M.S., "Identification of Rate Controlling Steps in Pentene-2 Hydrogenation from Selectivity – A Likelihood-Ratio Approach", Ph.D. Thesis in Chemical Engineering, University of Waterloo, Ontario, Canada, January, 1969.

100. Rasmussen, H.E., Hansford, R.C., and Sachanen, A.N., Ind. Eng. Chem., 38, 376 (1946).

101. Rosenbrock, H.H., and Storey, C., "Computational Techniques for Chemical Engineers", Pergamon Press, London, 1966.

102. Rossner, Wm. F., and Wensel, H.T., in "Temperature, Its Measurement and Control in Science and Industry", Am. Inst. Physics, Vol. I, p. 284, Reinhold Publishing Corp., New York, 1941.

103. Russel, R.P., Murphree, E.V., and Asbury, W.C., Trans. A.I.Ch.E., 42, 1 (1946).

104. Sachtler,W.M.H.,Catal. Rev., 4, 27 (1970).

105. Sachtler, W.M.H., and DeBoer, N.H., in "Proceedings of the Third International Congress on Catalysis, Amsterdam, 1964", W.M.H. Sachtler, G.C.A. Schuit, and P. Zwietering, Eds., Vol. I, p. 252, North-Holland Publishing Co., Amsterdam, 1965.

106. Sala, F., and Triforo, F., J. Catalysis, 34, 68 (1974).

107. Seinfeld, J.H., and Lapidus, L., "Mathematical Methods in Chemical Engineering, Vol. 3, Process Modelling, Estimation and Identification", Prentice Hall, Inc., Englewood Cliffs., New Jersy, 1974.

108. Shchukin, V.P., Ven'yaminov, S.A., and Boreskov, G.K., Kinet. Katal. (Eng. transl.), 11, 1236 (1970).

109. Shchukin, V.P., Ven'yaminov, S.A., and Boreskov, G.K., Kinet. Katal. (Eng. transl.), 12, 547 (1970).

110. Shchukin, V.P., Boreskov, G.K., Ven'yaminov, S.A., and Tarasova, D.V., Kinet. Katal. (Eng. transl.), 11, 153 (1970).

111. Shell Internat. Res. Maatsch. N.V., Brit. Patent 911,212; Chem. Abstr., 59, 11166f.

112. Shenoy, S.C., "Oxidative Dehydrogenation of Butane Over Doped Bismuth Molybdate Catalysts", M.Tech. Thesis in Chemical Engineering, I.I.T. Kanpur, February 1974.

113. Sitnikov, V.G., Andrushkevich, M.M., Buyanov, R.A., Plyasova, L.M., Babenko, V.S., Kustova, G.N., and Klimik, I.N., Kinet. Katal. (Eng. transl.), 15, 841 (1974).

114. Sittig, M., "Combine Hydrocarbons and Oxygen for Profit", Noyes Development Corporation, New Jersey, U.S.A. (1968).

115. Skarachenko, V.I., International Chem. Eng., 9, 1 (1969).

116. Steacie, E.W.R., and Puddington, I.E., Canad. J. Res., 163, 176 (1938).

117. "System/360 Scientific Subroutine Package Version III", International Business Machines, White Plains, N.Y., 1971.

118. Tarasova, G.A., and Solomatina, Z.A., Bull. Acad. Sci. USSR (Div. Chem. Sci.), p. 1164 (1968).

119. Tarasova, G.A., Solomatina, Z.A., and Roitberg, S. Ya., Neftekhimiya, 13, 382 (1973).

120. Timoshenko, V.I., and Buyanov, R.A., International Chem. Eng., 12, 314 (1972).

121. Trim, D.L., and Gabbay, D.S., Trans. Faraday Soc., 67, 2782 (1971).

122. Tsailingol'd, A.L., Philipenko, F.S., Stepanov, G.A., and Turyayev, I. Ya., Neftekhimiya, 6, 367 (1966); Chem. Abstr., 65, 13484e.

123. Vadekar, M., and Pasternak, V.I., Can. J. Chem. Eng., 48, 212 (1970).

124. Voge, H.H., and Adams, C.R., Adv. Catalysis, 17, 151 (1967).

125. Voge, H.H., and Morgan, C.Z., Ind. Eng. Chem., Proc. Design Develop., 11, 454 (1972).

126. Vogel, A.I., "A Text-Book of Quantitative Inorganic Analysis", 3rd ed., Longmans Green & Co. Ltd., London, 1971.

127. Van Wazer, J.R., "Phosphorous and Its Compounds", Vol. I, Interscience Publishers, New York, 1958.

128. Weast, R.C., "Handbook of Chemistry and Physics", 45th ed., p. E-48, The Chemical Rubber Publishing Co., Cleveland, Ohio, 1964.

129. Williams, E.J., "Regression Analysis", John Wiley & Sons Inc., New York, 1959.

130. Wragg, R.D., Ashmore, P.G., and Hockey, J.A., J. Catalysis 22, 49 (1971).

A P P E N D I C E S

APPENDIX I

CHEMICAL ANALYSIS OF CATALYSTS

A. Analysis of Bismuth Nitrate $Bi(NO_3)_3.5H_2O$ and Bismuthyl Nitrate $BiONO_3.H_2O$ [126].

EDTA solution: 0.05 M. Dissolve 18.613 g of disodium-dihydrogen-ethylenediaminetetra-acetate dihydrate (BDH Analar) in 1 liter of water.

Bismuth ion solution: 0.05 M. About 6.06 g of bismuth nitrat was dissolved in about 25 ml concentrated nitric acid and made to 250 ml with water.

Xylenol orange indicator: 0.05 g in 10 ml of water.

Procedure: 25 ml of bismuth ion solution were diluted to about 150 ml with water. pH was adjusted to 2 to 3 by cautious addition of dilute ammonia. 3-4 drops of xylenol orange indicator solution were added, and the solution was titrated against standard EDTA solution. Titrant was introduced slowly when the red colour of the original solution started fading. At the end point the colour changed sharply, from red to orange yellow.

1 ml EDTA ≡ 10.4500 mg Bi

Purity of bismuth compounds estimated as per above procedure are given below:

Bismuth nitrate (BDH Analar) - 98.97%

Bismuthyl nitrate 81.09% Bi_2O_3

B. Analysis of Molybdic Acid [68, 126].

Oxine solution (acid): 4 g oxine (8, hydroxyquinoline, Ward Blenkinsop & Co., London, A.R. Grade) were dissolved in 8.5 ml of warm glacial acetic acid. It was poured into 80 ml of wate and diluted to 100 ml.

Oxine solution (alcoholic): 2 g of A.R. grade oxine were dissolved in 100 ml of ethyl alcohol.

Procedure: 0.1 g of molybdic acid were dissolved in dilute ammonia. A few drops of methyl red indicator were added to get yellow coluration. The solution was acidified with 2 N sulphuric acid to methyl red colour (neutral). A few drops of 2 N sulphuric acid were then added in excess. Further, 5 ml of ammonium acetate solution were added and diluted with water to 50-100 ml. Solution was heated to gentle boiling and acetic acid solution of oxine was added until supernatant liquid becomes perceptibly yellow. The suspension was simmered for 5 minutes while stirring. The precipitate was filtered through a G3 sintered glass crucible and was washed with hot water to free t from the oxine reagent. It was dried in an oven at 130-140°C to constant weight, and weighed as $MoO_2(C_9H_6ON)_2$.

Molybdic oxide content of molybdic acid (Reachim U.S.S.R.) = 86.934 wt % (88.874% as per chemical formula).

C. MoO_3 Content of β- and γ-Bismuth Molybdates [43, 97].

The bismuth molybdate to be analysed was dissolved in nitric acid, and a few drops of methyl red indicator were added. Mix about 15 ml of 2 wt % EDTA solution, and 5 ml of buffer solution (120 ml of 50 wt % ammonium acetate solution with 80 ml acetic acid and 80 ml water), then dilute to 100 ml. The solution was brought to boiling, oxine solution (in acetic acid as prepared in Section B) was added in slight excess, and the suspension was simmered for 2-3 minutes. The suspension was filtered through a G3 sintered glass crucible; precipitate was washed with hot water until the washings were colourless. The precipitate was dried at 130-140°C to constant weight, and weighed as $MoO_2(C_9H_6ON)_2$.

wt % MoO_3 found in the β-bismuth molybdate prepared ($Bi_2O_3.2MoO_3$)	=	38.35% (38.19 as per the chemical formula).
wt % MoO_3 found in the γ-bismuth molybdate prepared ($Bi_2O_3.MoO_3$)	=	23.89% (23.6% as per the chemical formula).

APPENDIX II

CALIBRATION OF THERMOCOUPLES

Chromel-alumel thermocouples were fabricated from 20 and 24 BS gage thermocouple wires. Thermocouple beads were made by twisting the wires and fusing them over a oxyacetylene flame with borax as the flux. The length of the thermocouples was about 50 cm. Thermocouples made from 24 gage wires were placed in stainless steel sheath of about 4 mm I.D. and were aged by heating them in a tubular furnace at 550-600°C for a period of two days.

Thermocouples were calibrated by measuring the e.m.f. generated across the thermocouple at the boiling points of water, naphthalene, mercury and sulphur. Boiling tubes for determining boiling points of naphthalene, mercury and sulphur were constructed according to N.B.S. specifications [102]. The results of e.m.f. measurement at different boiling points are given below:

Naphthalene : Pure, white, sublimed grade from Riedel, Germany.

Mercury : Tripple distilled quality from City Chemical Corporation, New York.

Sulphur : Resublimed grade.

Table 29. CALIBRATION OF THERMOCOUPLES.

Compound	B.P. °C	Chromel-Alumel Standard e.m.f. [128] mV	E.m.f. Generated by Thermocouples - mV					
			1	2	3	4	5	6
Water	100	4.10	4.05	3.85	4.05	4.00	3.95	4.05
Naphthalene	217.96	8.86	8.90	8.50	8.55	8.75	8.75	8.80
Mercury	356.8	14.59	14.50	14.35	14.55	14.40	14.35	14.35
Sulphur	444.6	18.28	18.20	18.18	18.25	18.19	18.10	18.10

The e.m.f.s were measured using a Honeywell Model 2720 Portable Test Set potentiometer.

Thermocouples 1, 3 and 6 were used for the measurement of temperatures in the reactor. The e.m.f. generated by these thermocouples were close to the standard values and hence the standard tables [128] were used for e.m.f.-temperature conversion.

Thermocouple (1) was used for controlling the temperature of reactor furnace and thermocouples (3) and (6) were used to measure the catalyst bed temperature.

APPENDIX III

ORSAT ANALYSIS

Orsat analysis was employed to analyse carbon dioxide, oxygen and carbon monoxide in the gas mixture. Reagents employed in different cases are given below:

Carbon dioxide.

A 25-30 wt % aqueous solution of Analar potassium hydroxide was used [126].

Oxygen.

Sodium dithionite solution was used. This reagent was preferred to alkaline pyragallol reagent for the following reasons [126]: The absorption of oxygen though slow, takes place at lower temperatures also. No carbon monoxide is evolved, and the reagent is unaffected by the unsaturated hydrocarbons. The absorption reaction is,

$$Na_2S_2O_4 + O_2 + H_2O \longrightarrow NaHSO_3 + NaHSO_4$$

The reagent is prepared by dissolving 80 g L.R. grade sodium dithionite in 400 cm^3 of distilled water and 48 g Analar potassium hydroxide in 64 cm^3 distilled water. The two solutions are mixed and stored in a tightly stoppered bottle.

Carbon monoxide.

Acid cuprous chloride solution was used to avoid the absorption of ethylene [88, 126]. The solution was prepared by dissolving 100 g of L.R. grade cuprous chloride in 500 cm^3 of concentrated L.R. grade hydrochloric acid, and diluting it to 1 liter. The solution was stored in a stoppered bottle containing copper tubes, extending through the entire depth of the solution. The reaction is

$$CuCl + 2H_2O + CO \longrightarrow CuCl.2H_2O.CO$$

The absorption is never entirely complete. For this reason, the gas was always contacted with a fresh solution to remove traces of unabsorbed carbon monoxide. The gas mixture after the absorption of CO was passed over KOH solution to remove HCl vapours.

The gas absorption pipette in which the solution was used, also contained copper strips to avoid the formation of cupric ions.

Confining liquid.

Saturated aqueous sodium sulphate solution containing a little of sulphuric acid was used. The solution was prepared by dissolving 200 g anhydrous sodium sulphate in 800 cm^3 water and 40 cm^3 of concentrated sulphuric acid [88]. This reduces the solubility of the gases in the confining liquid.

APPENDIX IV

PROCESS CALCULATIONS

Carbon, hydrogen, oxygen and nitrogen atomic balances were used to calculate the yield from the experimental observations recorded by the gas chromatograms and Orsat analysis. The calculation procedure is as follows:

Basis of calculation: A gas mixture containing hydrocarbons in the same proportions as the proportions obtained in the gas chromatogram i.e.

C_1 moles of ethane,
C_2 moles of ethylene,
C_3 moles of propane,
C_4 moles of propylene,
C_5 moles of n-butane,
C_6 moles of 1-butene,
C_7 moles of trsns-2-butene,
C_8 moles of cis-2-butene, and
C_9 moles of 1, 3-butadiene.

$C_1 : C_2 : \ldots : C_9$ are chosen in the same proportion as in the chromatogram.

The peak areas calculated from the chromatograms were multiplied by their respective response factors (Chapter 4, Table 5), and the resulting value or a suitable multiple thereof were chosen as the values of C_1, C_2, ..., C_9.

Calculation procedure.

Let,

C_0 moles of methane,

C_{10} moles of carbon dioxide,

C_{11} moles of carbon monoxide,

C_{12} moles of oxygen,

N moles of nitrogen, and

W moles of water vapour

be present in the total moles of gas chosen in the basis of calculation.

A carbon, hydrogen and oxygen atomic balances lead to the following relations:

$$CARB = 2(C_1 + C_2) + 3(C_3 + C_4) + 4(C_5 + C_6 + C_7 + C_8 + C_9) + C_{10} + C_{11} + C_0 \quad \text{(A.IV-1)}$$

$$HYD = 6(C_1 + C_4 + C_9) + 4C_2 + 8(C_3 + C_6 + C_7 + C_8) + 10C_5 + 2W + 4C_0 \quad \text{(A.IV-2)}$$

$$OXY = 2C_{10} + C_{11} + 2C_{12} + W \quad \text{(A.IV-3)}$$

The carbon to hydrogen ratio is fixed by the type of hydrocarbon used. Therefore, for butane gas,

$$HYD = 10\ (CARB) \qquad (A.IV-4)$$

The butane to oxygen ratio (HYOX) is known, since its value is fixed during the experiments. Hence, for butane gas used,

$$4\ (CARB) = 2\ (OXY)\ .\ HYOX \qquad (A.IV-5)$$

The nitrogen to oxygen ratio (RNITROX) is also fixed during the experiments. Therefore,

$$N = (OXY)\ .\ (RNITOX) \qquad (A.IV-6)$$

Thus we have six equations and nine unknowns (CARB, HYDG, OXY, C_0, C_{10}, C_{11}, C_{12}, N and W). The three more relations required, can be derived from the results of the Orsat analysis.

Let ORS1, ORS2 and ORS3 be the volumes of carbon dioxide, oxygen and carbon monoxide gases measured per 100 volumes of gas drawn into the Orsat apparatus. With the water vapour pressure (at temperature of analysis) represented as VP, the following relationships may be obtained.

$$\frac{\text{mol } CO_2}{\text{mol unabsorbable gas}} = \frac{ORS1}{100 - \left(ORS1 + ORS2 + ORS3 + \frac{100}{760}\ .\ VP\right)} \qquad (A.IV-7)$$

$$\frac{\text{mol } O_2}{\text{mol unabsorbable gas}} = \frac{ORS2}{100 - \left(ORS1 + ORS2 + ORS3 + \frac{100}{760}\ .\ VP\right)} \qquad (A.IV-8)$$

$$\frac{\text{mol CO}}{\text{mol unabsorbable gas}} = \frac{\text{ORS3}}{100 - (\text{ORS1} + \text{ORS2} + \text{ORS3} + \frac{100}{760} \cdot \text{VP})} \qquad \text{(A.IV-9)}$$

In the basis of calculation chosen, the total moles of gases that are not absorbed by the Orsat reagents are given by,

$$\text{moles of unabsorbable gas} = C_1 + C_2 + C_3 + C_4 + C_5 + C_6 + C_7 + C_8 + C_9 + C_0 + N$$

$$= \text{TOTMOL} + C_0 + N \qquad \text{(A.IV-10)}$$

Substituting the above equation in Equations (A.IV-7) to (A.IV-9), one gets,

$$C_{10} = \frac{(\text{ORS1}) \cdot (\text{TOTMOL} + C_0 + N)}{(\text{ORSHYC})} \qquad \text{(A.IV-11)}$$

$$C_{12} = \frac{(\text{ORS2}) \cdot (\text{TOTMOL} + C_0 + N)}{(\text{ORSHYC})} \qquad \text{(A.IV-12)}$$

$$C_{11} = \frac{(\text{ORS3}) \cdot (\text{TOTMOL} + C_0 + N)}{(\text{ORSHYC})} \qquad \text{(A.IV-13)}$$

where,

$$(\text{TOTMOL}) = C_1 + C_2 + C_3 + C_4 + C_5 + C_6 + C_7 + C_8 + C_9 \qquad \text{(A.IV-14)}$$

and

$$(\text{ORSHYC}) = 100 - (\text{ORS1} + \text{ORS2} + \text{ORS3} + \frac{100}{760} \cdot \text{VP}) \qquad \text{(A.IV-15)}$$

Equations (A.IV-1) through (A.IV-6) and (A.IV-11) through (A.IV-15) now consist of eleven equations with CARB, HYD, OXY, C_0, C_{10}, C_{11}, C_{12}, N, W, TOTMOL, ORSHYC as the unknowns, and hence they may be solved.

Algebraic manipulation of the above equation give the following equations:

$$\left[1 + \frac{ORS1 + ORS2}{ORSHYC}\right] C_0 + \left[\frac{(ORS1 + ORS3) \cdot (RNITOX)}{4(ORSHYC) \cdot (HYOX)} - 1\right] \cdot (CARB)$$

$$= - (CARBON) - \frac{(TOTMOL)}{(ORSHYC)} \cdot (ORS1 + ORS3) \qquad (A.IV-16)$$

$$4.C_0 - 10\ (CARB) + 2.W = - (HYDGEN) \qquad (A.IV-17)$$

$$\left[\frac{2(ORS1 + ORS2) + ORS3}{(ORSHYC)}\right] \cdot C_0$$

$$+ \left[\frac{2(ORS1 + ORS2) + (ORS3).(RNITOX)}{4(HYOX).(ORSHYC)} - \frac{1}{2(HYOX)}\right] \cdot (CARB) + W$$

$$= - \frac{(TOTMOL)}{(ORSHYC)} \cdot (2(ORS1 + ORS2) + ORS3) \qquad (A.IV-18)$$

where,

$$CARBON = 2(C_1 + C_2) + 3(C_3 + C_4) + 4(C_5 + C_6 + C_7 + C_8 + C_9) \qquad (A.IV-19)$$

and

$$HYDGEN = 6(C_1 + C_4 + C_9) + 4C_2 + 8(C_3 + C_6 + C_7 + C_8) + 10C_5 \qquad (A.IV-20)$$

The computational algorithm is as follows:

1. Obtain the values C_1 through C_9 from the chromatogram.
2. Obtain the values ORS1, ORS2 and ORS3 from Orsat analysis. Find the vapour pressure of water, VP, at the temperature of Orsat analysis.
3. Calculate (TOTMOL) from Equation (A.IV-14).
4. Calculate (ORSHYC) from Equation (A.IV-15).
5. Calculate (CARBON) from Equation (A.IV-19).
7. Calculate (HYDGEN) from Equation (A.IV-20).
8. RNITOX and HYOX are the nitrogen to oxygen and butane to oxygen ratios respectively, used in the experiments.
9. Solve Equations (A.IV-16) through (A.IV-18) for (CARB), W and C_0.
10. Compute (OXY) from Equation (A.IV-5).
11. Compute N from Equation (A.IV-6).
12. Compute C_{10}, C_{12} and C_{11} from Equations (A.IV-11) through (A.IV-13).
13. Compute (HYD) from Equation (A.IV-4).

The yields of the various products were calculated from the following definition.

$$\% \text{ yield} = \frac{\text{mol products formed}}{\text{100 mol butane fed}}$$

The above algorithm was implemented on a IBM 7044 computer.

APPENDIX V

MAP OF RESPONSE SURFACE

Table 30. LOCATION OF OPTIMUM FACTOR LEVEL COMBINATION. SECOND ORDER RESPONSE SURFACE. $Bi_2O_3.2MoO_3$-$AlPO_4$ CATALYST.

LOCATION OF OPTIMUM FACTOR LEVEL COMBINATION
SECOND ORDER RESPONSE SURFACE

CATALYST .. BETA-BISMUTH MOLYBDATE - ALUMINIUM PHOSPHATE
YIELD = MOL BUTENES+BUTADIENE FORMED PER 100 MOL BUTANE FED

TEMPER C	W/F G/(NGMOL/MIN)	BUTANE/OXY MOL/MOL	MOL BISMOLY/ 100 MOL ALPO4	YIELD Y
4 .0	0.6	0.50	2.5	3.96
4 .0	0.8	0.50	2.5	3.88
4 .0	1.0	0.50	2.5	3.95
4 .0	1.2	0.50	2.5	4.20
4 .0	0.6	0.75	2.5	7.76
4 .0	0.8	0.75	2.5	7.56
4 .0	1.0	0.75	2.5	7.53
4 .0	1.2	0.75	2.5	7.67
4 .0	0.6	1.00	2.5	10.48
4 .0	0.8	1.00	2.5	10.18
4 .0	1.0	1.00	2.5	10.05
4 .0	1.2	1.00	2.5	10.08
42 .0	0.6	0.50	2.5	2.12
42 .0	0.8	0.50	2.5	2.03
42 .0	1.0	0.50	2.5	2.11
42 .0	1.2	0.50	2.5	2.36
42 .0	0.6	0.75	2.5	6.16
42 .0	0.8	0.75	2.5	5.97
42 .0	1.0	0.75	2.5	5.94
42 .0	1.2	0.75	2.5	6.08
42 .0	0.6	1.00	2.5	9.14
42 .0	0.8	1.00	2.5	8.84
42 .0	1.0	1.00	2.5	8.70
42 .0	1.2	1.00	2.5	8.74
44 .0	0.6	0.50	2.5	0.27
44 .0	0.8	0.50	2.5	0.18
44 .0	1.0	0.50	2.5	0.26
44 .0	1.2	0.50	2.5	0.51
44 .0	0.6	0.75	2.5	4.57
44 .0	0.8	0.75	2.5	4.37
44 .0	1.0	0.75	2.5	4.34
44 .0	1.2	0.75	2.5	4.48
44 .0	0.6	1.00	2.5	7.79
44 .0	0.8	1.00	2.5	7.49
44 .0	1.0	1.00	2.5	7.36
44 .0	1.2	1.00	2.5	7.39
46 .0	0.6	0.50	2.5	-1.57
46 .0	0.8	0.50	2.5	-1.66
46 .0	1.0	0.50	2.5	-1.58
46 .0	1.2	0.50	2.5	-1.34
46 .0	0.6	0.75	2.5	2.97
46 .0	0.8	0.75	2.5	2.78
46 .0	1.0	0.75	2.5	2.75
46 .0	1.2	0.75	2.5	2.89
46 .0	0.6	1.00	2.5	6.45
46 .0	0.8	1.00	2.5	6.15
46 .0	1.0	1.00	2.5	6.01
46 .0	1.2	1.00	2.5	6.05

LOCATION OF OPTIMUM FACTOR LEVEL COMBINATION
SECOND ORDER RESPONSE SURFACE .. CONTD

CATALYST .. BETA-BISMUTH MOLYBDATE - ALUMINIUM PHOSPHATE
YIELD = MOL BUTENES+BUTADIENE FORMED PER 100 MOL BUTANE FED

TEMPR C	W/F G/(MGMOL/MIN)	BUTANE/OXY MOL/MOL	MOL BISMOLY/ 100 MOL ALPO4	YIELD Y
40[illegible]	1.6	[illegible].75	5.0	6.[illegible]8
4[illegible]	[illegible].8	[illegible].75	5.0	6.19
4[illegible]	1.[illegible]	[illegible].75	5.0	6.48
4[illegible]	1.2	0.75	5.0	6.93
4[illegible]	[illegible].6	1.25	5.0	11.69
4[illegible]	[illegible].8	1.25	5.0	11.60
4[illegible]	1.[illegible]	1.25	5.0	11.67
4[illegible]	1.2	1.25	5.0	11.90
4[illegible]	[illegible].6	1.75	5.0	13.04
4[illegible]	[illegible].8	1.75	5.0	12.73
4[illegible]	1.[illegible]	1.75	5.0	12.59
4[illegible]	1.2	1.75	5.0	12.61
42[illegible]	[illegible].6	[illegible].75	5.0	4.49
42[illegible]	1.8	[illegible].75	5.0	4.60
42[illegible]	1.[illegible]	[illegible].75	5.0	4.88
42[illegible]	1.2	[illegible].75	5.0	5.34
42[illegible]	[illegible].6	1.25	5.0	10.66
42[illegible]	[illegible].8	1.25	5.0	10.51
42[illegible]	1.[illegible]	1.25	5.0	10.58
42[illegible]	1.2	1.25	5.0	10.61
42[illegible]	[illegible].6	1.75	5.0	12.45
42[illegible]	[illegible].8	1.75	5.0	12.14
42[illegible]	1.[illegible]	1.75	5.0	12.00
42[illegible]	1.2	1.75	5.0	12.[illegible]3
44[illegible]	[illegible].6	[illegible].75	5.0	3.13
44[illegible]	[illegible].8	[illegible].75	5.0	3.24
44[illegible]	1.[illegible]	[illegible].75	5.0	3.53
44[illegible]	1.2	[illegible].75	5.0	3.98
44[illegible]	[illegible].6	1.25	5.0	9.75
44[illegible]	[illegible].8	1.25	5.0	9.65
44[illegible]	1.[illegible]	1.25	5.0	9.72
44[illegible]	1.2	1.25	5.0	9.96
44[illegible]	[illegible].6	1.75	5.0	12.10
44[illegible]	[illegible].8	1.75	5.0	11.79
44[illegible]	1.[illegible]	1.75	5.0	11.65
44[illegible]	1.2	1.75	5.0	11.67
46[illegible]	[illegible].6	[illegible].75	5.0	2.[illegible]1
46[illegible]	[illegible].8	[illegible].75	5.0	2.12
46[illegible]	1.[illegible]	[illegible].75	5.0	2.41
46[illegible]	1.2	[illegible].75	5.0	2.86
46[illegible]	[illegible].6	1.25	5.0	9.13
46[illegible]	[illegible].8	1.25	5.0	9.03
46[illegible]	1.[illegible]	1.25	5.0	9.10
46[illegible]	1.2	1.25	5.0	9.34
46[illegible]	[illegible].6	1.75	5.0	11.98
46[illegible]	[illegible].8	1.75	5.0	11.67
46[illegible]	1.[illegible]	1.75	5.0	11.53
46[illegible]	1.2	1.75	5.0	11.55

LOCATION OF OPTIMUM FACTOR LEVEL COMBINATION
SECOND ORDER RESPONSE SURFACE .. CONTD

CATALYST .. BETA-BISMUTH MOLYBDATE - ALUMINIUM PHOSPHATE
YIELD = MOL BUTADIENE FORMED PER 100 MOL BUTANE FED

TEMPR C	W/F G/(MGMOL/MIN)	BUTANE/OXY MOL/MOL	MOL BISMOLY/ 100 MOL ALPO4	YIELD Y
400.0	0.6	0.75	7.5	4.22
400.0	0.8	0.75	7.5	4.65
400.0	1.0	0.75	7.5	5.24
400.0	1.2	0.75	7.5	6.00
400.0	0.6	1.25	7.5	11.07
400.0	0.8	1.25	7.5	11.28
400.0	1.0	1.25	7.5	11.66
400.0	1.2	1.25	7.5	12.21
400.0	0.6	1.75	7.5	13.65
400.0	0.8	1.75	7.5	13.65
400.0	1.0	1.75	7.5	13.82
400.0	1.2	1.75	7.5	14.15
420.0	0.6	0.75	7.5	2.84
420.0	0.8	0.75	7.5	3.27
420.0	1.0	0.75	7.5	3.86
420.0	1.2	0.75	7.5	4.62
420.0	0.6	1.25	7.5	10.19
420.0	0.8	1.25	7.5	10.40
420.0	1.0	1.25	7.5	10.78
420.0	1.2	1.25	7.5	11.33
420.0	0.6	1.75	7.5	13.27
420.0	0.8	1.75	7.5	13.27
420.0	1.0	1.75	7.5	13.44
420.0	1.2	1.75	7.5	13.77
440.0	0.6	0.75	7.5	1.69
440.0	0.8	0.75	7.5	2.12
440.0	1.0	0.75	7.5	2.71
440.0	1.2	0.75	7.5	3.47
440.0	0.6	1.25	7.5	9.54
440.0	0.8	1.25	7.5	9.75
440.0	1.0	1.25	7.5	10.14
440.0	1.2	1.25	7.5	10.68
440.0	0.6	1.75	7.5	13.12
440.0	0.8	1.75	7.5	13.12
440.0	1.0	1.75	7.5	13.29
440.0	1.2	1.75	7.5	13.63
460.0	0.6	0.75	7.5	0.78
460.0	0.8	0.75	7.5	1.21
460.0	1.0	0.75	7.5	1.80
460.0	1.2	0.75	7.5	2.56
460.0	0.6	1.25	7.5	9.13
460.0	0.8	1.25	7.5	9.34
460.0	1.0	1.25	7.5	9.72
460.0	1.2	1.25	7.5	10.27
460.0	0.6	1.75	7.5	13.21
460.0	0.8	1.75	7.5	13.21
460.0	1.0	1.75	7.5	13.38
460.0	1.2	1.75	7.5	13.72

LOCATION OF OPTIMUM FACTOR LEVEL COMBINATION
SECOND ORDER RESPONSE SURFACE .. CONTD

CATALYST .. BETA-BISMUTH MOLYBDATE - ALUMINIUM PHOSPHATE
YIELD = MOL BUTENES+BUTADIENE FORMED PER 100 MOL BUTANE FED

TEMPR C	W/F G/(MGMOL/MIN)	BUTANE/OXY MOL/MOL	MOL BISMOLY/ 100 MOL ALPO4	YIELD Y
40[illegible]0	[illegible].6	[illegible].75	10.00	2.37
40[illegible]0	[illegible].8	[illegible].75	10.00	3.10
40[illegible]0	1.0	0.75	10.00	4.[illegible]1
40[illegible]0	1.2	[illegible].75	10.00	5.[illegible]8
40[illegible]0	[illegible].6	1.25	10.00	10.44
40[illegible]0	[illegible].8	1.25	10.00	10.97
40[illegible]0	1.0	1.25	10.00	11.66
40[illegible]0	1.2	1.25	10.00	12.52
40[illegible]0	[illegible].6	1.75	10.00	14.25
40[illegible]0	[illegible].8	1.75	10.00	14.56
40[illegible]0	1.0	1.75	10.00	15. 4
40[illegible]0	1.2	1.75	10.00	15.69
42[illegible]0	0.6	0.75	10.00	1.19
42[illegible]0	0.8	[illegible].75	10.00	1.93
42[illegible]0	1.0	0.75	10.00	2.83
42[illegible]0	1.2	0.75	10.00	3.91
42[illegible]0	0.6	1.25	10.00	9.77
42[illegible]0	0.8	1.25	10.00	10.29
42[illegible]0	1.0	1.25	10.00	10.99
42[illegible]0	1.2	1.25	10.00	11.85
42[illegible]0	0.6	1.75	10.00	14.08
42[illegible]0	0.8	1.75	10.00	14.39
42[illegible]0	1.0	1.75	10.00	14.87
42[illegible]0	1.2	1.75	10.00	15.52
44[illegible]0	0.6	0.75	10.00	0.25
44[illegible]0	0.8	0.75	10.00	0.99
44[illegible]0	1.0	[illegible].75	10.00	1.96
44[illegible]0	1.2	[illegible].75	10.00	2.97
44[illegible]0	0.6	1.25	10.00	9.33
44[illegible]0	0.8	1.25	10.00	9.86
44[illegible]0	1.0	1.25	10.00	10.55
44[illegible]0	1.2	1.25	10.00	11.41
44[illegible]0	0.6	1.75	10.00	14.14
44[illegible]0	0.8	1.75	10.00	14.46
44[illegible]0	1.0	1.75	10.00	14.94
44[illegible]0	1.2	1.75	10.00	15.58
46[illegible]0	0.6	[illegible].75	10.00	-0.45
46[illegible]0	0.8	[illegible].75	10.00	0.29
46[illegible]0	1.0	[illegible].75	10.00	1.19
46[illegible]0	1.2	[illegible].75	10.00	2.27
46[illegible]0	0.6	1.25	10.00	9.13
46[illegible]0	0.8	1.25	10.00	9.65
46[illegible]0	1.0	1.25	10.00	10.35
46[illegible]0	1.2	1.25	10.00	11.21
46[illegible]0	0.6	1.75	10.00	14.44
46[illegible]0	0.8	1.75	10.00	14.75
46[illegible]0	1.0	1.75	10.00	15.23
46[illegible]0	1.2	1.75	10.00	15.88

APPENDIX VI

SENSITIVITY EQUATIONS OF ORDINARY DIFFERENTIAL EQUATIONS

The differential equations representing the reaction scheme can be written as,

$$\frac{dp_A}{dt} = \phi_A(t, \underline{p}(t), \underline{k}) \qquad p_A(t = 0) = p_{A_o} \qquad \text{(A.VI-1)}$$

$$\frac{dp_B}{dt} = \phi_B(t, \underline{p}(t), \underline{k}) \qquad p_B(t = 0) = 0 \qquad \text{(A.VI-2)}$$

$$\frac{dp_C}{dt} = \phi_C(t, \underline{p}(t), \underline{k}) \qquad p_C(t = 0) = 0 \qquad \text{(A.VI-3)}$$

$$\frac{dp_O}{dt} = \phi_O(t, \underline{p}(t), \underline{k}) \qquad p_O(t = 0) = p_o \qquad \text{(A.VI-4)}$$

$$\frac{dp_W}{dt} = \phi_W(t, \underline{p}(t), \underline{k}) \qquad p_W(t = 0) = 0 \qquad \text{(A.VI-5)}$$

The number of responses in the present case are, n = 5. These are the partial pressures of butane, butene, butadiene, oxygen and water.

Let the number of parameters to be estimated be P and let the data be obtained at r discrete values of time. The sensitivity equations for the above set of differential equations are given by the relations:

$$\dot{\lambda}_{ij} = \sum_{l=1}^{n} \frac{\partial \phi_l}{\partial p_l} \cdot \lambda_{ij} + \frac{\partial \phi_l}{\partial k_j}, \qquad \lambda_{ij}(0) = 0 \tag{A.VI-6}$$

$$i = 1, 2, \ldots, n$$

$$j = 1, 2, \ldots, P.$$

where,

$$\lambda_{ij} = \frac{\partial p_i}{\partial k_j} \tag{A.VI-7}$$

The above set of equations can be represented in the matrix form as,

$$\dot{\underline{\Lambda}} = \underline{A}\underline{\Lambda} + \underline{B}, \qquad \underline{\Lambda}(0) = 0 \tag{A.VI-8}$$

where,

$$\underline{A} = \left\{ \frac{\partial \phi_l}{\partial p_\nu} \right\}_{\underline{k}^*} \qquad l = 1,2,\ldots,n, \quad \nu = 1,2,\ldots,n \tag{A.VI-9}$$

$$\underline{B} = \left\{ \frac{\partial \phi_l}{\partial k_\nu} \right\}_{\underline{k}^*} \qquad l = 1,2,\ldots,n, \quad \nu = 1,2,\ldots,P \tag{A.VI-10}$$

Hence the sensitivity equations in the present case can be written as follows:

$$\frac{d}{dt}\left(\frac{\partial p_A}{\partial k_j}\right) = \frac{\partial \phi_A}{\partial p_A} \cdot \left(\frac{\partial p_A}{\partial k_j}\right) + \frac{\partial \phi_A}{\partial p_B} \cdot \left(\frac{\partial p_B}{\partial k_j}\right) + \frac{\partial \phi_A}{\partial p_C} \cdot \left(\frac{\partial p_C}{\partial k_j}\right) +$$

$$\frac{\partial \phi_A}{\partial p_O} \cdot \left(\frac{\partial p_O}{\partial k_j}\right) + \frac{\partial \phi_A}{\partial p_W} \cdot \left(\frac{\partial p_W}{\partial k_j}\right) + \frac{\partial \phi_A}{\partial k_j}$$

$$j = 1, 2, \ldots, P \tag{A.VI-11}$$

$$\frac{d}{dt}\left(\frac{\partial p_B}{\partial k_J}\right) = \frac{\partial \phi_B}{\partial p_A} \cdot \left(\frac{\partial p_A}{\partial k_J}\right) + \frac{\partial \phi_B}{\partial p_B} \cdot \left(\frac{\partial p_B}{\partial k_j}\right) + \frac{\partial \phi_B}{\partial p_C} \cdot \left(\frac{\partial p_C}{\partial k_j}\right) +$$

$$\frac{\partial \phi_B}{\partial p_O} \cdot \left(\frac{\partial p_O}{\partial k_J}\right) + \frac{\partial \phi_B}{\partial p_W} \cdot \left(\frac{\partial p_W}{\partial k_j}\right) + \frac{\partial \phi_B}{\partial k_J}$$

$$J = 1, 2, \ldots, P \qquad \text{(A.VI-12)}$$

$$\frac{d}{dt}\left(\frac{\partial p_C}{\partial k_J}\right) = \frac{\partial \phi_C}{\partial p_A} \cdot \left(\frac{\partial p_A}{\partial k_J}\right) + \frac{\partial \phi_C}{\partial p_B} \cdot \left(\frac{\partial p_B}{\partial k_j}\right) + \frac{\partial \phi_C}{\partial p_C} \cdot \left(\frac{\partial p_C}{\partial k_J}\right) +$$

$$\frac{\partial \phi_C}{\partial p_O} \cdot \left(\frac{\partial p_O}{\partial k_J}\right) + \frac{\partial \phi_C}{\partial p_W} \cdot \left(\frac{\partial p_W}{\partial k_j}\right) + \frac{\partial \phi_C}{\partial k_J}$$

$$J = 1, 2, \ldots, P \qquad \text{(A.VI-13)}$$

$$\frac{d}{dt}\left(\frac{\partial p_O}{\partial k_J}\right) = \frac{\partial \phi_O}{\partial p_A} \cdot \left(\frac{\partial p_A}{\partial k_J}\right) + \frac{\partial \phi_O}{\partial p_B} \cdot \left(\frac{\partial p_B}{\partial k_J}\right) + \frac{\partial \phi_O}{\partial p_C} \cdot \left(\frac{\partial p_C}{\partial k_J}\right) +$$

$$\frac{\partial \phi_O}{\partial p_O} \cdot \left(\frac{\partial p_O}{\partial k_J}\right) + \frac{\partial \phi_O}{\partial p_W} \cdot \left(\frac{\partial p_W}{\partial k_J}\right) + \frac{\partial \phi_O}{\partial k_J}$$

$$j = 1, 2, \ldots, P \qquad \text{(A.VI-14)}$$

$$\frac{d}{dt}\left(\frac{\partial p_W}{\partial k_J}\right) = \frac{\partial \phi_W}{\partial p_A} \cdot \left(\frac{\partial p_A}{\partial k_J}\right) + \frac{\partial \phi_W}{\partial p_B} \cdot \left(\frac{\partial p_B}{\partial k_J}\right) + \frac{\partial \phi_W}{\partial p_C} \cdot \left(\frac{\partial p_C}{\partial k_J}\right) +$$

$$\frac{\partial \phi_W}{\partial p_O} \cdot \left(\frac{\partial p_O}{\partial k_J}\right) + \frac{\partial \phi_W}{\partial p_W} \cdot \left(\frac{\partial p_W}{\partial k_J}\right) + \frac{\partial \phi_W}{\partial k_J}$$

$$j = 1, 2, \ldots, P \qquad \text{(A.VI-15)}$$

The partial derivative in the above equations can be evaluated from the Equations (A.VI-1) to (A.VI-5) defining the model. The Equations (A.VI-11) to (A.VI-16) will have to be solved together with the Equations (A.VI-1) to (A.VI-5) in order to obtain the elements in the derivative matrix, $\underline{\Delta}$. Hence, in the present case, which has five responses, a total of 5(1+P) number of equations will have to be solved to obtain the elements in the matrices $\underline{A}$ and $\underline{B}$ given in Equation (A.VI-8).

APPENDIX VII

EXPERIMENTAL DATA

In the following tables, experimental data have bee reported on dry basis. In these:

Conversion is defined as moles of butane reacted per 100 mol of butane fed,

Yield is the moles of product formed per 100 moles of butane reacted (bute = butenes, bdn = butadiene).

1.	Run number	1	2	3	4	5	6	7	8	1
2.	Catalyst weight, g	6.1	6.1	6.1	6.1	5.3	5.3	5.3	5.3	2
3.	Active component	MoO_3	MoO_3	MoO_3	MoO_3	MoO_3	MoO_3	MoO_3	MoO_3	3
4.	Catalyst composition (mol/100 mol $AlPO_4$)	10	10	10	10	5	5	5	5	4
5.	Temperature, °C	550	550	600	600	550	550	600	600	5
6.	W/F, g/(mg mol/min)	1.25	0.75	0.75	1.25	0.75	1.25	1.25	0.75	6
7.	Butane : oxygen	1.0	1.0	1.0	1.0	1.0	1.0	1.0	1.0	7
8.	Oxygen : nitrogen	-	-	-	-	-	-	-	-	8
9.	Conversion, %	52.9	48.7	48.3	50.1	35.5	76.9	74.3	41.98	9
10.	Yield of butadiene, %	0.23	0.73	0.31	0.21	0.42	0.00	0.01	0.69	10
11.	Yield, (bute + bdn), %	8.89	5.64	6.93	3.89	5.34	0.98	1.52	2.46	11
	Reactor Effluent Gas Analysis on Dry and Nitrogen Free Basis:									
12.	Ethylene	8.274	31.308	24.617	6.056	5.322	0.519	0.734	1.351	12
13.	Propylene	9.497	24.396	29.440	11.597	5.045	0.623	5.139	3.706	13
14.	n-Butane	47.032	51.296	51.687	49.909	57.080	23.000	25.654	58.018	14
15.	1-Butene	2.812	3.285	3.685	2.017	1.566	0.369	0.624	0.903	15
16.	trans-2-Butene	3.103	1.052	1.758	1.029	1.774	0.314	0.496	0.808	16
17.	cis-2-Butene	2.750	0.569	1.177	0.632	1.569	0.301	0.392	0.056	17
18.	1, 3-Butadiene	0.227	0.738	0.310	0.215	0.427	0.000	0.006	0.697	18
19.	Methane	12.448	0.183	0.145	11.826	7.021	93.260	79.112	13.712	19
20.	Carbon dioxide	8.958	19.524	19.288	9.892	14.498	2.871	0.034	8.571	20
21.	Oxygen	0.498	0.312	1.071	0.471	0.359	0.261	0.000	0.238	21
22.	Carbon monoxide	21.524	67.399	74.268	16.723	18.093	2.094	4.045	23.927	22

1.	Run number	9	10	11	12	13	14	15	16	1
2.	Catalyst weight, g	5.9	5.9	5.9	5.9	6.1	6.1	6.1	6.1	2
3.	Active component	MoO_3	MoO_3	MoO_3	MoO_3	MoO_3	MoO_3	MoO_3	MoO_3	3
4.	Catalyst composition (mol/100 mol $AlPO_4$)	15	15	15	15	25	25	25	25	4
5.	Temperature, °C	550	550	600	600	550	550	600	600	5
6.	W/F, g/(mg mol/min)	0.75	1.25	1.25	0.75	0.75	1.25	1.25	0.75	6
7.	Butane : oxygen	1.0	1.0	1.0	1.0	1.0	1.0	1.0	1.0	7
8.	Nitrogen : oxygen	-	-	-	-	-	-	-	-	8
9.	Conversion, %	49.0	39.2	58.1	55.4	38.4	52.7	48.0	55.7	9
10.	Yield (butadiene), %	0.91	0.38	0.13	0.25	0.84	0.56	0.60	2.14	10
11.	Yield (bute + bdn), %	8.39	3.63	2.41	7.73	5.30	5.12	4.23	8.60	11
	Reactor Effluent Gas Analysis on Dry and Nitrogen Free Basis:									
12.	Ethylene	7.011	0.907	3.039	19.941	6.512	2.501	1.682	15.983	12
13.	Propylene	13.936	2.947	5.730	22.720	7.911	3.492	6.088	16.689	13
14.	n-Butane	50.941	60.820	41.842	44.563	61.536	47.294	51.984	46.716	14
15.	1-Butene	3.060	1.198	0.826	3.261	1.613	1.500	1.320	2.450	15
16.	trans-2-Butene	2.356	1.218	0.836	2.345	1.655	1.633	1.332	1.960	16
17.	cis-2-Butene	2.063	0.833	0.621	1.880	1.187	1.413	0.972	1.994	17
18.	1, 3-Butadiene	0.913	0.382	0.128	0.249	0.847	0.570	0.606	2.141	18
19.	Methane	7.384	14.555	37.994	3.311	3.578	25.181	18.199	7.172	19
20.	Carbon dioxide	10.135	6.559	4.388	7.746	14.860	5.710	7.070	7.294	20
21.	Oxygen	0.579	0.285	0.112	0.516	0.606	0.528	1.622	0.972	21
22.	Carbon monoxide	37.646	44.491	10.127	54.741	42.154	9.729	1.966	48.465	22

1.	Run number	17	18	19	20	21	22	23	24	1
2.	Catalyst weight, g	6.6	6.6	6.6	6.6	Blank	16.2	19.7	19.7	2
3.	Active component	MoO_3	MoO_3	MoO_3	MoO_3	reactor	Beta	Beta	Beta	3
4.	Catalyst composition (mol/100 mol $AlPO_4$)	30	30	30	30	tube	15	25	25	4
5.	Temperature, °C	550	550	600	600	550	425	475	425	5
6.	W/F, g/(mg mol/min)	0.75	1.25	1.25	0.75	-	1.0	1.0	1.6	6
7.	Butane : oxygen	1.0	1.0	1.0	1.0	1.0	0.75	0.75	0.75	7
8.	Nitrogen : oxygen	-	-	-		-	2.0	2.0	2.0	8
9.	Conversion	39.4	50.0	54.7	50.3	10.0	51.5	66.1	28.1	9
10.	Yield (butadiene), %	0.67	0.41	1.31	1.73	0.0	3.601	0.293	0.198	10
11.	Yield (bute + bdn), %	5.57	2.52	4.42	8.49	1.67	5.751	0.503	3.298	11
	Reactor Effluent Gas Analysis on Dry and Nitrogen Free Basis:									
12.	Ethylene	7.097	0.201	1.404	15.587	5.168	28.179	0.111	0.807	12
13.	Propylene	8.746	2.419	6.151	20.130	5.931	4.720	0.136	0.359	13
14.	n-Butane	60.625	49.990	45.219	49.644	89.032	38.445	18.950	41.154	14
15.	1-Butene	1.267	0.621	0.941	2.953	0.806	0.741	0.071	0.767	15
16.	trans-2-Butene	1.633	0.893	1.110	2.175	0.603	0.794	0.888	1.394	16
17.	cis-2-Butene	1.990	0.596	1.060	1.633	0.262	0.615	0.051	0.938	17
18.	1, 3-Butadiene	0.680	0.418	1.311	1.732	0.000	3.601	0.293	0.198	18
19.	Methane	3.804	27.999	31.881	0.952	2.775	11.682	105.290	21.057	19
20.	Carbon dioxide	13.271	5.319	4.768	8.060	71.270	10.889	3.426	7.849	20
21.	Oxygen	0.925	0.957	0.476	0.700	0.642	0.311	11.180	3.389	21
22.	Carbon monoxide	45.062	10.746	17.404	59.929	30.819	49.779	5.139	7.760	22

1.	Run number	25	26	27	28	29	30	31	32	1
2.	Catalyst weight, %	16.2	19.7	16.2	16.2	19.7	19.7	19.7	11.9	2
3.	Active component	Beta	Beta	Beta	Beta	Beta	Beta	Beta	Beta	3
4.	Catalyst composition (mol/100 mol $AlPO_4$)	15	25	15	15	25	25	25	5	4
5.	Temperature, °C	475	425	475	425	475	425	425	400	5
6.	W/F, g/(mg mol/min)	1.6	1.0	1.0	1.6	1.6	1.6	1.6	0.4	6
7.	Butane : oxygen	0.75	1.25	1.25	1.25	1.25	0.75	0.75	1.25	7
8.	Nitrogen : oxygen	2.0	2.0	2.0	2.0	2.0	2.0	2.0	2.0	8
9.	Conversion, %	46.7	34.7	32.4	21.6	17.1	32.7	25.93	49.9	9
10.	Yield (butadiene), %	0.953	1.396	1.469	2.704	2.952	1.144	0.516	6.035	10
11.	Yield (bute + bdn), %	1.152	4.346	1.746	5.305	4.171	2.707	2.029	6.112	11
	Reactor Effluent Gas Analysis on Dry and Nitrogen Free Basis:									
12.	Ethylene	0.219	1.437	0.285	7.707	2.082	0.623	1.113	32.333	12
13.	Propylene	0.101	1.286	0.227	2.470	0.486	0.284	1.736	10.774	13
14.	n-Butane	26.735	65.287	48.680	63.103	66.310	40.190	39.333	47.550	14
15.	1-Butene	0.046	1.059	0.073	0.700	0.559	0.357	0.331	2.358	15
16.	trans-2-Butene	0.103	1.184	0.171	1.127	0.389	0.624	0.628	2.049	16
17.	cis-2-Butene	0.050	0.707	0.034	0.775	0.271	0.581	0.556	1.705	17
18.	1, 3-Butadiene	0.953	1.396	1.468	2.704	2.952	1.145	0.516	6.035	18
19.	Methane	80.556	16.730	87.455	8.758	16.264	26.399	25.230	4.935	19
20.	Carbon dioxide	3.741	6.138	2.279	9.522	6.188	6.682	6.847	5.933	20
21.	Oxygen	26.790	12.159	38.364	0.464	12.258	6.589	4.685	0.456	21
22.	Carbon monoxide	4.789	6.020	3.798	14.399	6.545	5.661	5.766	34.381	22

1.	Run number	33	34	35	36	37	38	39	40	1
2.	Catalyst weight, g	18.69	18.69	11.9	18.69	11.9	11.9	18.69	11.9	2
3.	Active component	Beta	Beta	Beta	Beta	Beta	Beta	Beta	Beta	3
4.	Catalyst composition (mol/100 mol $AlPO_4$)	21	21	5	21	5	5	21	5	4
5.	Temperature, °C	450	400	450	400	450	400	450	400	5
6.	W/F, g/(mg mol/min)	0.4	1.2	1.2	0.4	0.4	1.2	1.2	0.4	6
7.	Butane : oxygen	1.25	1.25	1.25	1.75	1.75	1.75	1.75	1.25	7
8.	Nitrogen : oxygen	2.0	2.0	2.0	2.0	2.0	2.0	2.0	2.0	8
9.	Conversion, %		29.1	34.9	48..1	41.1	25.4	29.2	51.1	9
10.	Yield (butadiene), %		3.127	6.529	0.580	8.106	4.693	2.787	6.628	10
11.	Yield (bute + bdn), %		6.040	11.338	2.278	14.810	10.902	4.132	12.532	11
	Reactor Effluent Gas Analysis on Dry and Nitrogen Free Basis:									
12.	Ethylene		14.506	12.855	0.381	33.544	3.235	0.511	33.469	12
13.	Propylene		3.731	3.139	0.429	12.367	2.410	0.411	10.427	13
14.	n-Butane		57.675	56.845	26.958	58.878	70.514	54.551	47.811	14
15.	1-Butene		0.810	1.625	0.494	2.472	1.841	0.397	2.802	15
16.	trans-2-Butene		1.231	1.885	0.696	2.371	2.574	0.560	1.801	16
17.	cis-2-Butene		0.872	1.299	0.508	1.862	1.794	0.388	1.302	17
18.	1, 3-Butadiene		3.127	6.529	0.580	8.106	4.698	2.787	6.627	18
19.	Methane		10.215	8.899	84.072	9.786	4.939	61.703	3.767	19
20.	Carbon dioxide		8.502	7.816	1.802	3.942	8.321	2.138	6.288	20
21.	Oxygen		0.232	0.124	10.410	2.274	0.231	7.698	0.306	21
22.	Carbon monoxide		12.576	20.099	3.378	31.994	12.250	7.698	35.123	22

1.	Run number	41	42	43	44	45	46	47	48	1
2.	Catalyst weight, g	11.9	15.3	18.6	18.6	15.3	18.6	15.3	15.3	2
3.	Active component	Beta	Gamma	Gamma	Gamma	Gamma	Gamma	Gamma	Gamma	3
4.	Catalyst composition (mol/100 mol $AlPO_4$)	5	15	25	25	15	25	15	15	4
5.	Temperature, °C	400	425	475	425	475	425	475	425	5
6.	W/F, g/(mg mol/min)	0.4	1.0	1.0	1.6	1.6	1.0	1.0	1.6	6
7.	Butane : oxygen	1.25	1.25	1.25	1.25	1.25	0.75	0.75	0.75	7
8.	Nitrogen : oxygen	2.0	2.0	2.0	2.0	2.0	2.0	2.0	2.0	8
9.	Conversion, %	46.3	36.5		47.2		31.3	28.19	27.2	9
10.	Yield (butadiene), %	6.636	3.428		1.927		2.469	3.079	7.255	10
11.	Yield (bute + bdn), %	12.105	6.228		3.012		4.522	3.949	9.965	11
	Reactor Effluent Gas Analysis on Dry and Nitrogen Free Basis:									
12.	Ethylene	28.643	1.400		0.166		0.858	0.699	3.510	12
13.	Propylene	9.019	0.959		0.412		0.757	0.328	1.648	13
14.	n-Butane	49.542	35.480		26.937		48.785	57.803	63.723	14
15.	1-Butene	2.538	0.658		0.158		0.616	0.294	0.701	15
16.	trans-2-Butene	1.628	1.292		0.568		0.661	0.334	1.274	16
17.	cis-2-Butene	1.304	0.849		0.360		0.776	0.243	0.761	17
18.	1, 3-Butadiene	6.636	3.428		1.927		2.469	3.079	7.255	18
19.	Methane	5.645	40.471		49.695		53.866	51.237	17.138	19
20.	Carbon dioxide	6.741	5.181		3.706		2.409	2.800	10.394	20
21.	Oxygen	0.293	7.783		9.190		3.985	7.694	2.512	21
22.	Carbon monoxide	31.068	6.241		16.641		14.475	15.601	11.650	22

1.	Run number	49	50	51	52	53	54	55	56	1
2.	Catalyst weight, g	18.6	12.9	15.6	15.6	12.9	15.6	12.9	12.9	2
3.	Active component	Gamma	Gamma	Gamma	Gamma	Gamma	Gamma	Gamma	Gamma	3
4.	Catalyst composition (mol/100 mol $AlPO_4$)	25	7	23	23	7	23	7	7	4
5.	Temperature, °C	475	400	450	400	450	400	450	400	5
6.	W/F, g/(mg mol/min)	1.6	1.0	1.0	2.2	2.2	1.0	1.0	2.2	6
7.	Butane : oxygen	0.75	0.85	0.85	0.85	0.85	1.65	1.65	1.65	7
8.	Nitrogen : oxygen	2.0	2.0	2.0	2.0	2.0	2.0	2.0	2.0	8
9.	Conversion, %	36.3	31.8	22.4	51.2	49.6	34.2	26.5	33.5	9
10.	Yield (butadiene), %	0.944	4.471	2.781	5.777	1.382	7.092	2.948	3.414	10
11.	Yield (bute + bdn), %	1.325	6.988	5.829	9.183	1.594	12.550	3.55	13.396	11
	Reactor Effluent Gas Analysis on Dry and Nitrogen Free Basis:									
12.	Ethylene	0.156	5.576	33.905	12.190	0.956	10.454	0.894	3.474	12
13.	Propylene	0.139	1.077	6.725	2.615	0.147	3.946	0.349	2.929	13
14.	n-Butane	31.797	43.700	31.454	45.199	48.308	65.765	73.424	66.475	14
15.	1-Butene	0.111	0.775	1.088	1.012	0.038	1.749	0.116	2.666	15
16.	trans-2-Butene	0.159	1.074	1.033	1.344	0.086	2.131	0.299	4.326	16
17.	cis-2-Butene	0.111	0.669	0.928	1.050	0.087	1.579	0.188	2.990	17
18.	1, 3-Butadiene	0.941	4.471	2.781	5.777	1.382	7.092	2.948	3.414	18
19.	Methane	46.082	18.778	12.674	9.808	26.978	14.054	13.333	5.106	19
20.	Carbon dioxide	1.978	7.653	7.582	12.647	6.103	7.431	5.530	8.913	20
21.	Oxygen	4.409	0.099	0.133	0.114	2.375	0.125	6.747	0.228	21
22.	Carbon monoxide	18.462	13.716	25.007	20.006	15.187	18.892	9.535	11.427	22

1.	Run number	57	58	59	60	61	62	63	64	1
2.	Catalyst weight, g	15.6	11.2	11.2	11.2	11.2	11.2	11.2	11.2	2
3.	Active component	Gamma	Beta	Beta	Beta	Beta	Beta	Beta	Beta	3
4.	Catalyst composition (mol/100 mol $AlPO_4$)	23	3	3	3	3	3	3	3	4
5.	Temperature, °C	450	420	460	420	460	420	460	420	5
6.	W/F, g/(mg mol/min)	2.2	0.5	0.5	0.9	0.9	0.5	0.5	0.9	6
7.	Butane : oxygen	1.65	1.2	1.2	1.2	1.2	1.6	1.6	1.6	7
8.	Nitrogen : oxygen	2.0	2.0	2.0	2.0	2.0	2.0	2.0	2.0	8
9.	Conversion, %	30.8	47.9	45.5	30.72	34.07	28.0	39.5	26.6	9
10.	Yield (butadiene), %	5.241	6.869	5.065	7.093	4.580	9.020	5.993	6.970	10
11.	Yield (bute + bdn), %	10.209	10.458	9.136	10.547	8.006	11.302	10.661	11.124	11
	Reactor Effluent Gas Analysis on Dry Nitrogen Free Basis:									
12.	Ethylene	6.525	22.591	25.504	9.489	11.207	10.004	20.977	8.245	12
13.	Propylene	2.410	6.315	9.374	1.864	5.700	2.932	9.654	1.844	13
14.	n-Butane	69.139	52.501	48.315	58.122	53.127	66.792	58.002	67.116	14
15.	1-Butene	1.473	1.654	2.109	1.177	1.250	0.815	2.119	1.289	15
16.	trans-2-Butene	2.098	1.146	1.178	1.353	1.327	0.741	1.497	1.698	16
17.	cis-2-Butene	1.398	0.789	0.785	0.924	0.849	0.726	1.052	1.166	17
18.	1, 3-Butadiene	5.241	6.869	5.065	7.093	4.581	9.020	5.993	6.970	18
19.	Methane	4.542	7.659	5.149	9.407	9.232	5.155	2.186	5.951	19
20.	Carbon dioxide	9.690	7.448	7.304	8.224	8.139	6.550	6.494	7.253	20
21.	Oxygen	0.817	0.275	0.152	0.119	0.129	0.251	0.147	0.483	21
22.	Carbon monoxide	10.858	28.137	34.240	19.071	21.187	20.658	28.928	16.561	22

1.	Run number	65	66	67	68	69	70	71	72	1
2.	Catalyst weight	11.2	12.8	12.8	12.8	12.8	12.8	12.8	12.8	2
3.	Active component	Beta	Beta	Beta	Beta	Beta	Beta	Beta	Beta	3
4.	Catalyst composition (mol/100 mol $AlPO_4$)	3	7	7	7	7	7	7	7	4
5.	Temperature, °C	460	420	460	420	460	420	460	420	5
6.	W/F, g/(mg mol/min)	0.9	0.5	0.5	0.9	0.9	0.5	0.5	0.9	6
7.	Butane : oxygen	1.6	1.2	1.2	1.2	1.2	1.6	1.6	1.6	7
8.	Nitrogen : oxygen	2.0	2.0	2.0	2.0	2.0	2.0	2.0	2.0	8
9.	Conversion, %	33.0	39.4	49.2	31.5	42.3	34.4	41.8	26.2	9
10.	Yield (butadiene), %	5.874	6.457	4.656	8.094	6.729	9.053	5.664	9.434	10
11.	Yield (bute + bdn), %	10.406	9.335	8.521	10.453	9.641	12.702	11.961	12.556	11
	Reactor Effluent Gas Analysis on Dry and Nitrogen Free Basis:									
12.	Ethylene	17.430	20.129	31.219	11.015	27.535	17.819	22.751	6.459	12
13.	Propylene	5.574	5.219	11.128	1.489	5.513	4.666	11.051	1.362	13
14.	n-Butane	63.171	52.118	45.672	57.600	51.722	63.101	57.126	67.819	14
15.	1-Butene	1.551	1.208	1.583	0.775	1.123	1.438	2.467	1.023	15
16.	trans-2-Butene	1.771	0.971	1.409	0.933	1.018	1.261	2.261	1.227	16
17.	cis-2-Butene	1.210	0.699	0.874	0.652	0.772	0.951	1.569	0.872	17
18.	1, 3-Butadiene	5.874	6.457	4.656	8.094	6.729	9.053	2.952	9.434	18
19.	Methane	3.841	11.773	4.724	10.352	7.205	2.833	5.963	7.873	19
20.	Carbon dioxide	7.725	6.333	6.924	7.506	8.070	6.719	5.963	7.873	20
21.	Oxygen	0.130	0.263	0.314	0.242	0.278	0.268	0.152	0.238	21
22.	Carbon monoxide	20.165	24.409	35.254	20.097	26.438	23.617	33.334	15.746	22

Run number	73	74	75	76	77	78	79	80	1
Catalyst weight, g	12.8	10.5	10.5	10.5	10.5	10.5	10.5	9.9	2
Active component	Beta	Beta	Beta	Beta	Beta	Beta	Beta	Beta	3
Catalyst composition (mol/100 mol $AlPO_4$)	7	5	5	5	5	5	5	1	4
Temperature, °C	460	400	480	440	440	440	440	440	5
W/F, g/(mg mol/min)	0.9	0.7	0.7	0.3	1.1	0.7	0.7	0.7	6
Butane : oxygen	1.6	1.4	1.4	1.4	1.4	1.0	1.8	1.0	7
Nitrogen : oxygen	2.0	2.0	2.0	2.0	2.0	2.0	2.0	2.0	8
Conversion, %	33.8	37.2	40.4	45.2	36.0	43.6	31.0	42.9	9
Yield (butadiene), %	8.806	8.316	6.239	6.834	5.561	3.502	8.254	5.093	10
Yield (bute + bdn), %	12.376	13.029	9.854	12.529	10.079	6.415	12.789	10.996	11
Reactor Effluent Gas Analysis on Dry and Nitrogen Free Basis:									
Ethylene	17.955	6.017	16.544	17.154	8.530	24.696	10.166	15.686	12
Propylene	3.204	1.536	4.179	12.622	1.920	5.506	2.134	8.049	13
n-Butane	64.139	62.790	59.593	54.722	63.935	34.629	68.999	57.016	14
1-Butene	1.364	1.640	1.478	2.985	1.533	1.127	1.725	1.618	15
trans-2-Butene	1.262	1.778	1.257	1.659	1.805	1.133	1.632	2.568	16
cis-2-Butene	0.944	1.288	0.881	1.050	1.179	0.654	1.178	1.716	17
1, 3-Butadiene	8.806	8.316	6.239	6.834	5.561	3.502	8.254	5.093	18
Methane	2.889	7.260	7.579	4.414	6.854	14.067	3.229	6.591	19
Carbon dioxide	7.327	8.140	7.161	6.269	8.692	7.896	7.460	7.696	20
Oxygen	0.266	0.465	0.255	0.139	0.119	0.129	0.497	0.513	21
Carbon monoxide	22.514	14.535	19.950	28.280	16.193	23.300	16.289	19.112	22

1.	Run number	81	82	83	84	85	86	87	88	1
2.	Catalyst weight, g	12.0	10.5	10.5	10.5	10.5	10.5	10.5	10.5	2
3.	Active component	Beta	Beta	Beta	Beta	Beta	Beta	Beta	Beta	3
4.	Catalyst composition (mol/100 mol $AlPO_4$)	9	5	5	5	5	5	5	5	4
5.	Temperature, °C	440	440	440	440	440	440	440	440	5
6.	W/F, g/(mg mol/min)	0.7	0.7	0.7	0.7	0.7	0.7	0.7	0.7	6
7.	Butane : oxygen	1.4	1.4	1.4	1.4	1.4	1.4	1.4	1.4	7
8.	Nitrogen : oxygen	2.0	2.0	2.0	2.0	2.0	2.0	2.0	2.0	8
9.	Conversion, %	44.0	43.5	43.7	41.4	39.7	41.3	41.5	40.5	9
10.	Yield (butadiene), %	5.714	5.412	5.507	5.676	5.927	5.430	6.686	6.271	10
11.	Yield (bute + bdn), %	11.090	10.577	11.382	10.892	10.958	10.114	11.401	10.116	11
	Reactor Effluent Gas Analysis on Dry and Nitrogen Free Basis:									
12.	Ethylene	23.397	22.756	21.418	17.826	16.766	17.034	15.868	14.888	12
13.	Propylene	6.507	6.463	5.679	5.051	4.403	6.827	5.034	0.806	13
14.	n-Butane	55.976	56.402	56.290	58.572	60.224	58.683	58.413	59.402	14
15.	1-Butene	1.757	1.702	1.760	1.818	1.785	1.687	1.771	1.875	15
16.	trans-2-Butene	2.122	2.153	2.489	2.048	1.984	1.776	1.767	0.887	16
17.	cis-2-Butene	1.496	1.309	1.627	1.350	1.263	1.221	1.177	1.083	17
18.	1, 3-Butadiene	5.714	5.412	5.507	5.676	5.927	5.430	6.686	6.271	18
19.	Methane	5.594	5.471	6.268	6.165	5.312	5.867	7.438	8.986	19
20.	Carbon dioxide	7.232	8.030	7.428	7.818	8.270	7.988	6.748	6.468	20
21.	Oxygen	0.545	0.133	0.397	0.130	0.393	0.261	0.259	0.126	21
22.	Carbon monoxide	23.333	21.380	21.092	20.849	21.924	21.085	21.543	20.040	22

Run number	89	90	91	92	93	94	95	96	1
Catalyst weight, g	12.3	12.3	12.3	12.3	12.3	12.3	12.3	12.3	2
Active component	Beta	Beta	Beta	Beta	Beta	Beta	Beta	Beta	3
Catalyst composition (mol/100 mol $AlPO_4$)	5	5	5	5	5	5	5	5	4
Temperature, °C	420	420	420	420	420	420	420	420	5
W/F, g/(mg mol/min)	0.6	0.8	1.2	1.6	2.0	0.6	0.8	0.8	6
Butane : oxygen	0.75	0.75	0.75	0.75	0.75	1.0	1.0	1.0	7
Nitrogen : oxygen	2.0	2.0	2.0	2.0	2.0	2.0	2.0	2.0	8
Conversion, %	41.9	52.6	60.3	62.3	63.1	39.7	49.4	51.2	9
Yield (bute + bdn), %	7.030	5.019	6.236	7.595	7.070	8.440	7.847	4.765	10
Reactor Effluent Gas Analysis, Partial Pressures in mm Mercury:									
Ethylene	17.411	20.318	15.501	9.296	7.942	26.674	16.159	30.013	11
Propylene	4.592	3.129	1.250	1.068	1.132	7.913	5.356	5.556	12
n-Butane	54.260	54.113	57.071	57.169	61.175	70.463	78.921	84.824	13
1-Butene	0.704	1.041	0.971	1.290	1.189	1.606	1.960	1.785	14
trans-2-Butene	0.878	0.764	1.030	1.454	1.311	1.472	2.611	1.608	15
cis-2-Butene	0.609	0.562	0.870	1.131	1.091	0.894	1.830	1.082	16
1, 3-Butadiene	4.618	5.796	7.404	7.981	7.550	6.730	7.155	8.364	17
Methane	45.745	43.425	40.959	32.749	27.025	20.280	27.698	29.278	18
Carbon dioxide	12.270	11.363	11.835	12.461	14.628	14.567	12.654	13.048	19
Oxygen	0.408	0.183	0.174	0.155	0.149	0.741	0.222	0.221	20
Carbon monoxide	36.413	31.253	27.326	23.053	18.597	48.887	39.072	37.654	21
Water	261.957	268.469	243.264	268.069	271.734	268.963	250.717	255.859	22
Nitrogen	339.583	319.305	352.339	344.117	346.110	287.500	299.698	292.745	23

1.	Run number	105	106
2.	Catalyst weight, g	12.3	12.3
3.	Active component	Beta	Beta
4.	Catalyst composition (mol/100 mol $AlPO_4$)	5	5
5.	Temperature, °C	420	420
6.	W/F, g/(mg mol/min)	1.6	2.0
7.	Butane : oxygen	1.25	1.25
8.	Nitrogen . oxygen	2.0	2.0
9.	Conversion, %	40.9	42.3
10.	Yield (bute + bdn), %	10.843	10.064
	Reactor Effluent Gas Analysis, Partial Pressures in mm Mercury:		
11.	Ethylene	15.192	5.346
12.	Propylene	6.147	1.795
13.	n-Butane	115.390	123.703
14.	1-Butene	2.543	2.584
15.	trans-2-Butene	2.331	2.966
16.	cis-2-Butene	1.804	2.083
17.	1, 3-Butadiene	13.246	14.325
18.	Methane	11.724	19.491
19.	Carbon dioxide	21.331	16.081
20.	Oxygen	0.520	0.217
21.	Carbon monoxide	36.418	38.351
22.	Water	236.671	253.019
23.	Nitrogen	296.374	280.057